Performance of Weathering Steel Bridge under Atmospheric Corrosion in Myanmar

WINT THANDAR

2021

Performance of Weathering Steel Bridge under Atmospheric Corrosion in Myanmar

A Thesis Submitted to

The Graduate School of Engineering

of

Kyoto University

by

WINT THANDAR

In Partial Fulfilment of the

Requirements for the Degree

of

Doctor of Engineering

2021

ACKNOWLEDGEMENT

The author would like to express her deepest gratitude to her supervisor, Professor Kunitomo Sugiura, Structural Mechanics Laboratory, Department of Civil and Earth Resources Engineering, for his outstanding guidance. The words cannot express enough her appreciation to her supervisor for his kindness.

The author thanks to Professor Junji Kiyono from Laboratory of Earthquake and Lifeline Engineering and Professor Tomomi Yagi from Laboratory of Bridge Engineering for her being co-supervisors and giving their precious comments for her research. The author also would like to extend her appreciation to Associate Professor Yasuo Kitane, Structural Mechanics Laboratory, Department of Civil and Earth Resources Engineering, for his precious advices and comments. The author acknowledges Assistant Professor Yoshinao Goi of Structural Mechanic Lab for sharing his knowledge and kind advices on her research.

The author would express her gratitude to Professor Mashide Matsumura from the Center for Water Cycle, Marine Environment and Disaster Management of Kumamoto University and Professor Yasuo Suzuki from the Department of Civil Engineering of University of Toyama for their kind supports for measurement data in Myanmar. The author would express her heartfelt thanks to Professor Thinzar Khaing from the Department of Civil Engineering of Yangon Technological University (Myanmar) for her continuous supports since her master's degree.

The author deeply thanks to Dr. Itaru Nishizaki, Leader of Materials Resources Research Group of PWRI and Dr. Tomonori Tomiyama, Senior Researcher of PWRI for their valuable advices on experiment and research. The author would also offer her acknowledgements to JFE Steel and JFE Engineering for providing test pieces for her experiment.

The author contributes her special thanks to Mrs. Namie Kawano for her endless help during the stay in Japan. Last but not least, the author expresses her deeply thanks to all friends in this laboratory, especially Mr. Oshiro Yuki, Mr. Shinya Watanabe, Mr. Akihiko Sato and Mr. Eitaro Horisawa for their encouragements in research and help in both experimental and daily life problems during her doctoral student life.

ABSTRACT

The corrosion evaluation in Myanmar was taken by measuring outdoor exposure tests at the eight test sites. The measurement results observed that he low and medium levels of corrosion were measured at the present locations in Myanmar. The calculation of acceleration coefficients at the current test locations are determined by performing the relation between laboratory test and field exposure test results. The results of calculated factors are showing that the time frame correlation within the chamber and outdoor environments. According to the finding, the factors decreased with increasing coastal distance and flying salt content. The prediction equation was also formulated by using the acceleration coefficients and the amount of salts. This equation can help to predict the long-term thickness loss at the locations with known flying salt amount.

As a comparison of carbon and weathering steel corrosion performances in shelter and un-shelter environments, the weathering steel can produce its own protective layer faster in outdoor exposure than shelter exposure. It is realized that the use of weathering steel under shelter may take long time for developing protective layer than direct contact to the environment. The prediction equations are formulated for long-term corrosion based on 3 years data in Myanmar. By reviewing the data from past researches, characterization of steel corrosion in Asia region was also discussed. According to finding, temperature is an influential effect on corrosion in Asia's environment. Two different ways were found in temperature effect. It may increase the corrosion rate to some extent of temperature level, however, the corrosion rate will decrease with higher temperature. This study also define the threshold temperature for the corrosion development in Asia's environment.

The practical approach of bridge washing evaluation with appropriate time interval was pointed out to find out as an effective way of countermeasure for corrosion in weathering steel bridges. The measured data approved that the washing with normal water can help to reduce the corrosion degradation. The time necessary for the washing in different environments were specified by the experimental results.

The bridge reliability analysis was conducted to find out the degradation of bridge performance by understanding the variation of corrosion effects. The system can perform its reliability above the target value specified by AASHTO at the end of service life, however, the individual member reliability index falls under the target value after the 60 years of corrosion intensity. According to the finding, 23% and 42% in moment and shear of the bridge performances were reduced after 100 years of exposure time. Moreover, the corrosion can also reduce the redundancy of the structure. The calculation of reliability on system is more economical rather than the member approach. The performance of bridge under regular wash program show higher value than the target one till the end of predefined service life. In contrast, reliability in serviceability and ultimate shear state without washing maintenance show lower value at 60 years and 80 years respectively. The redundancy was also considered as a parameter which can tolerate by the corrosion effect. The system redundancy indicators in ULS decrease with corrosion propagation. The value decrease from 2.7 in moment and 1.9 in shear at the initial state to 2.4 in moment and 1.38 in shear at 100 years of service life. Comparing of costs for different painting systems (as a referenced to past study of painting system in Myanmar) and bare weathering steel with regular washing program, the results show that the cost of weathering steel can save a lot more money than conventional painting.

TABLE OF CONTENTS

LIST OF FIGURES

LIST OF TABLES

Chapter 1

INTRODUCTION

1.1 General

Corrosion is a very important problem for all steel superstructures since structures are contact with environment. Studying about the performances of various steel structures under corrosive environment is vital not only for public safety but also for economics. Steel material such as carbon and weathering steel, have high deal about corrosion, are popular materials for construction of bridges and other superstructures.

The major deficiencies of structures are contributed by age, inadequate maintenance, increasing load spectra and environmental contamination. Financial losses due to corrosion shows that the cost has been varied from 1-5% of GNP (Corrosion-Doctor, 2012). Fifty percent of these financial losses correspond to the atmospheric corrosion. The devastating range due to atmospheric corrosion extends from small articles, such as bolts, nuts and fasteners to industrial plants and equipment and megastructures, such as skyscrapers, towers and bridges. Therefore, it is important to understand the relation between the materials and the environments for both economical and safety measures.

1.2 Problem statement

According to the data from the Ministry of Construction (2013), a total of 528 long span bridges (span longer than 180 ft or 54 m) have been constructed in various region of Myanmar. Most of the bridges are located in the delta and coastal regions due to the presence of several rivers flowing within these areas. Among these 528 bridges, 198 bridges were constructed before year of 1988 and 330 bridges were built after 1988. The total number of steel bridges over four major rivers (the Ayeyarwaddy, the Chindwin, the Sittaung, and the Thanlwin) were also increasing from 5 to 28 bridges within 1988 to 2013. Due to this rapid development of bridge construction within two

decades, there has some drawbacks in bridge construction techniques and maintenance. Therefore, the government of Myanmar planned to check the situation of bridges in Myanmar with the collaboration with Japan Infrastructure Partners (JIP) in 2011. The team inspected total of 77 bridges including 43 concrete bridges, 13 steel truss bridges, 9 cable-stayed/suspension bridges and 12 bailey bridges in Yangon and Ayeyarwaddy Regions.

The report from the survey of "Current Situation and Issues of Myanmar's Bridge Work" in 2012 mentioned that most of the surveyed bridges were mainly damaged by corrosion and fatigue. A survey team also found out that Myaungmya Bridge in Ayeyarwaddy Region has been corroded at the connection between the main cable and hanger. Moreover, the inclination of main tower were observed during the survey, and it was also confirmed that the bridge has been reduced its capacity from the two-lane flow traffic to one-lane traffic by the explanation of bridge manager. Unfortunately, this bridge was failed in the 1st April of 2018. Although the main reason of failure has not been approved yet, the survey before the failure approve that the problem might be due to the successive penetration of corrosion at the area between cable and hanger. The failure of Myaungmya Bridge called for attention on the problem of corrosion in Myanmar's infrastructures. Furthermore, the experts from JICA also investigated 54 bridges along Yangon-Mandalay railway track, which is under the control of Myanmar Railway (MR) of the Ministry of Transport and Communications, for the rehabilitation of the railway track between Yangon and Mandalay. According to the report by JICA (2013), most of the steel truss bridge and the girder bridge in delta and coastal regions were suffering from serious corrosion.

There has no referenced data of corrosion measurements in Myanmar till 2015. In 2016, a research group of "Corrosion and Deterioration of Construction Materials and Strategic Maintenance of Infrastructures on Southeast Asia" from Kyoto University and Yangon Technological University started to measure corrosion rates in major cities in Myanmar. The measurements have been started in some major cities of Myanmar and carried out by the doctoral student from Yangon Technological University (Y. Yu, 2017). This student measured the corrosion rates at two major cities (i.e. Yangon and Mandalay), and classified the atmosphere corrosivity of the cities.

Due to the nature of corrosion process which is based on the environmental parameter and atmosphere parameters, the corrosion rates vary according to the climatic and geographical conditions of exposure sites. Myanmar has long coast line which is

about 2300 km and the climate varies from the south to the north. The classification with respect to meteorological aspects has been taken as the coastal area, the deltaic area, the central dry area and the northern highland area. The present study shows the results of measured corrosion rates at the exposure sites located along the coast line, the delta area and the central dry area. Two types of exposure conditions are considered in this study such as direct contact with atmosphere (outdoor exposure) including rain effect and allowing direct attach of aerosol particles and indirect contact with environments (shelter exposure) in which the specimen's surface is shielded from direct precipitation and solar radiation. Moreover, the shelter also prevents windblown sea salt or soil dust from reaching out the corroded surface. Two kinds of structural steel; carbon steel (SM) and weathering steel (SMA); supplied by Japanese steel makers were used for the measurement similar with previous measurement by the student from YTU. The variation of corrosion rates under direct and indirect contacts with atmosphere in SM and SMA steels are also considerable to see how the exposure condition influences on corrosion losses of SM and SMA steels.

In addition, the determination of prediction equation for future corrosion losses is also necessary to countermeasure the cost of corrosion. In order to reduce the corrosion in steel bridges, the two most common alternatives can be achieved. One is the application of a coating system to the surfaces of the carbon steel or the use of weathering steel. The proper maintenance system can save the cost of corrosion in both safety and economy measures. Nevertheless, the failure in protection system can cause the accumulation of chloride compounds on the surface of the steel and shorten the structure service life.

The use of weathering steel is one of the best solution to solve corrosion problem at the location where the atmosphere is satisfactory for weathering steel. It can not only save for life-cycle cost but also provide ecofriendly color visualization. Moreover, the weathering steel can produce the protective rust layer by itself under conditions of alternative wetting and drying in the environments. This protective layer effectively withstands corrosion caused by exhaust gases and sulfur-containing fuels. The research discusses about the use of weathering steel (SMA steel) in bridge construction in Myanmar based on corrosion measurements and economic assessments. The benefits of life-cycle cost reductions in application of weathering steel is also presented in comparison with the costs consumed by traditional painting methods. The present study

opens up the beneficial application of weathering steel in bridge construction in Myanmar.

1.3 Literature review

1.3.1 Atmospheric corrosion

Atmospheric corrosion is the degradation of materials caused by air and the pollutants contained in the air. It can be precisely defined as an electrochemical process which depends upon the presence of electrolyte which may be rain, dew, humidity or melting snow. Atmospheric corrosion commonly takes place under humid conditions, where the atmospheric relative humidity exceeds the equilibrium relative humidity over any saturated solution which is present on the metal surface (usually NaCl solution). The corrosion rate is controlled by time of wetness, temperature and the electrolyte composition (Z. Ahamad, 2006).

It can further be classified atmospheric corrosion into dry, damp and wet categories. Dry oxidation takes place in the atmosphere with all metals that have a negative free energy of oxide formation. The damp moisture films are created at a certain critical humidity level, while wet films are associated with dew, ocean spray, rainwater, and other forms of water splashing. By the nature of atmospheric corrosion, it has been reported to account for more failures in terms of cost and tonnage than any other form of corrosion (S. Syed, 2006). The deterioration rate by atmospheric corrosion varies according to its contact environments. The atmospheric environments can be classified as rural, urban, industrial, marine or combinations of these. Rural environments are usually free of aggressive agents and it is generally the least corrosive and free from chemical pollutants. Urban atmosphere is similar to rural, however, there has a little industrial activity such as sulfur dioxide (SO_x) and nitrogen oxide (NO_x) pollutants. Industrial and marine environments have very severe pollutants such as intense amount of sulfur dioxide (SO_x) and nitrogen oxide (NO_x) contain in the former environment and heavy salt contamination (NaCl) by marine fog and wind-blown spray droplets occur in later one.

1.3.2 Factors affecting atmospheric corrosion

Atmospheric corrosion is the visible kind of corrosion when metals exposed to corrosive environment. The materials will be corroded when the damp moisture film occurs on their surfaces. The formation of corrosion products on meal surfaces depend on presence of surface contamination, moisture, either in the form of rain, dew, condensation, or high relative humidity (RH). The important practical variables in atmospheric corrosion are shown as follows.

1.3.2.1 Temperature

Temperature, T, affects on the atmospheric corrosion in two different ways. An increase in temperature leads to simulate corrosion attack by increasing the rate of electrochemical reaction and diffusion processes under constant humidity. However, raising the temperature tends to a decrease in relative humidity and more rapid evaporation of surface electrolyte which causes to decrease in corrosion rate (Roberge, P.R. 2008).

1.3.2.2 Relative humidity

The increase of relative humidity, RH, has been found to increase the corrosion rate. Many studies observed that there is almost no atmospheric corrosion of carbon steel when the relative humidity is below 80%-85% (Lapuerta S. & et al., 2008). This is due to the present of film electrolyte formed on metallic surfaces is the fundamental basis to proceed atmospheric corrosion with anodic and cathodic reactions. Therefore, this value is defined as threshold value denoted as critical relative humidity (CRH).

1.3.2.3 Time of wetness

The time of wetness (TOW) is a key parameter, determining the duration of electrochemical corrosion processes. TOW is basically dependent on the critical relative humidity, associated with clean surfaces. It refers to the length of time during which the metal surface is covered by a film of water that renders significant atmospheric corrosion possible.

The actual time of wetness will vary with climatic conditions at the location and it can be calculated based on the relative humidity and temperature in total numbers

of hours when the material is covered by the electrolyte. To calculate TOW, the average monthly data of temperature and relative humidity are used to count the total numbers of hours that the test probes are at a temperature above 0°C with a relative humidity greater than or equal to 80%. This parameter is expressed as a percentage. The geographical location and seasonal changes of the stations are greatly influence on TOW measure because of the temperature and relative humidity differences for each station.

1.3.2.4 Atmosphere contaminants

The formation of corrosion products on metal surfaces rely on not only the environmental conditions but also the contaminants present in the atmosphere. One of the major air contaminants which promote the atmospheric corrosion is chloride. Chloride ions is the most common and important atmospheric corrosive agent. In marine environment, chloride deposition is in the form of droplets or crystals formed by evaporation of spray that has been carried by wind from the sea (P. R. Roberge, 2017). The deposition of chloride ions in the air decrease when the distance from the offshore increase. The most severe cases can be observe in marine environments.

Sulfur dioxide plays important role in urban and industrial atmospheric corrosion. This is a product of sulfur containing fossil fuels. For iron and steel, the presence of sulfate ions ultimately leads to the formation of iron sulfate (FeSO4) which leads the stimulating of corrosion reaction and this can be found in layers at the metal surface. At very high levels of sulfur dioxide, dissolution of protective layers and the formation of more soluble corrosion products is associated with higher corrosion rates. Other forms of atmospheric contaminants such as hydrogen sulfide, hydrogen chloride, and chlorine are also intensify as the air contaminants which promote atmospheric corrosion damage.

1.3.3 Atmospheric corrosion in carbon and weathering steels

Carbon steel is the most widely used materials for superstructure construction and also large quantities of galvanized steel, stainless steel, aluminum, brass and copper are also used for same purpose nowadays.

Weathering steel is also one of the famous material used for infrastructures construction due to its advantages in economical facts such as reducing maintenance cost by eliminating the need for the initial painting and periodic repainting of the entire superstructure as it is required for ordinary steels. The performances of these steels under corrosive environments are also different. The current study emphasizes on the corrosion rate measurements of carbon and weathering steels. The anti-corrosive performances of these two materials are as follows.

1.3.3.1 Carbon steel (hot and cold rolled)

In polluted atmospheres, chlorides and SO2 are the common pollutants influencing metallic corrosion. Though chlorides come from natural airborne salinity, they are considered to be a significant pollutant as a consequence of their strong action on metals during atmospheric exposure. Particulate matter present in the atmosphere also plays a vital role in undermining materials resistance to atmospheric corrosion. Aggressive anions such as Cl^- and SO_2 are renowned culprits for introducing localized attack. Sea-salt is a further important atmospheric contaminant, especially for the corrosion of carbon steel structures. The primary sources of sea-salt in the atmosphere are the oceans. Ericsson (1978) showed that the presence of sodium chloride particles on a carbon steel surface can cause corrosion at relative humidities which have been considered too low to start SO_2 induced corrosion. According to his report, the synergistic effect of sodium chloride and SO_2 at 90% RH increased the corrosion rate of carbon steel by about 14 times than caused by sodium chloride alone. Moreover, the most widely reported climatic factors by Evans (1972), Brown (1982) and Masters, Morcillo et al. (1999) and Feliu et al. (1993) are time of wetness (TOW), temperature and rainfall. Not only these presented factors but also the properties of the material such as chemical composition, the design and types of the structures and joins are also influenced the corrosion of the structures under corrosive environment.

The corrosion rate after 1 year of exposure supplies critical information about the interaction between the metallic surface and environmental parameters. The wide range of values obtained is a sequence of the exposure of the base metal in atmospheres representing different combinations of corrosive agents, depending on the location of the site and the time of year. The weight losses of metals after longer exposure times provide information about the protective character of the carbon steel corrosion

protective layers (SCPLs), which once sufficiently developed, attenuate the effects of meteorological and pollution variables. The barrier effect of SCPLs depends on their thickness, uniformity, porosity, solubility, adhesion and other characteristics, and can significantly, adhesion and other characteristics, and significantly affect the carbon steel corrosion rate and attack morphology through different mechanisms. The lowest corrosion rate can be found in rural atmospheres, where corrosion products also usually present relatively smaller structures. However, as atmospheric corrosion nucleation depends on the time of wetness (TOW) of metallic surfaces, soil pollution and background atmospheric pollution, corrosion rates in rural atmospheres present a relatively wide range of values for each metal (Goodwin F.E, 1990).

1.3.3.2 Weathering steel

Weathering steel is composed of 1-25% of alloying elements (Cr, Cu, Si and P) and has a tendency to form rust at a rate depending on the accesses of oxygen in the presence of moisture and air. When the structural details are properly designed and the bridge is located in a suitable environment, weathering steel forms a protective oxide coating that inhabits the steel's tendency to continuously rust in the atmosphere. However, weathering steel is resistant only to specific types of atmospheric corrosion in a limited range of environments. Therefore, the proper design of weathering steel structures must be based on an understanding of the material's corrosion resistant characteristics under desired environment.

In weathering steels, the rusting process is initiated in the same process with carbon steels, but the alloying elements help to produce less porous and more adherent rust film. This rust system develops with time, becomes protective by impeding further access of oxygen and moisture to the metal surface, and hence reduces considerably the rate of the rust growth. The rust color and its characteristics of weathering steel depend upon the nature of the environment and exposure time. In an industrial atmosphere, the weathering process will generally be more rapid and the final color becomes darker. In the rural environment, the oxide formation is usually forms over a period of 18 months to 3 years. However, it takes about 8 years for the promoting of adherent rust layer formation in industrial atmosphere. The presence of relatively high airborne sea salt (such as coastal environment) cannot formed the protective layer. The favorable atmospheric conditions to promote the protective layer on weathering steel are the

atmospheres where air borne chloride is less than 0.5 mg/100cm2/day, average wetness time is less than 60% and industrial pollutants SO2 is less than 2.1mg/100 cm2/day (T. Ohtsuk, 1996).

1.3.4 Atmospheric corrosivity classification

The classification of atmospheric corrosion has been carried by the European standard and the ISO standard. The European standard EN 12500-2000 (BSI 2000) defines five categories of outdoor environment on the basis of the presence of corrosive agents. According to the standard, the atmosphere is defined as rural where the location is countryside and there has low level of minor corrosive agent contamination (carbon dioxide, chlorides and artificial fertilizers). Urban atmosphere is a densely populated area and has few industrial activities. A medium contamination of corrosive agent (such as sulfur dioxides) also includes in urban atmosphere. The standard specifies the atmosphere as a marine atmosphere in which the areas close to the sea and strongly effected by airborne salinity. Corrosion in that atmosphere is mainly influenced by topographic conditions and prevailing wind direction. Another environment classifies by the standard is a marine industrial atmosphere. This atmosphere is a complex environment which is an area close to both the sea and industrial districts or internal zone located in the prevalent wind direction with medium or high corrosive agent contamination (sulfur dioxides, chlorides). The atmospheric corrosion classification by this standard is very simple, however, it still has some drawback in defining clear boundary to distinguish each environment.

An atmospheric corrosion classification method introduced by International Standard Organization (ISO) based on atmospheric variables. The standard describe a method to determine class of each atmospheric variables and respective corrosion rate. The classification of corrosive environments mainly depends on the categorization of sulfur dioxide and chloride deposition rates and time of wetness (TOW). The standard also describes the one year corrosion rates of different metals in relevant with corrosivity class. The standard limited in its accuracy and precision since the corrosivity classification does not include the effects of potentially important corrosive pollutants and impurities such as NO_x, hydrogen sulfide, carbon dioxide, temperature, rainfall, wind speed etc. (N. Munasinghe & et. Al., 2014). Corrosivity of atmosphere is specified by using the ISO standard in this study.

1.3.5 Accelerated corrosion tests

Accelerated corrosion tests are used with the aim to develop corrosion in the laboratory in a reduced time (Guthrie, 2002; Lin, 2005). Field tests are usually offer an excellent results on producing corrosion, however, the tests consume a lots of time and it may also have some trouble in measurement due to unfavorable environmental condition (such as Typhoon and seasonal Cyclones). Hence, accelerated corrosion tests are an outstanding alternative to create an appropriate corrosion in a very short time period (Guthrie, 2002). Carlsson (2016) mentioned that accelerated tests are always good to approach an approximation to reality. The oldest method for laboratory accelerated corrosion testing is the continuous neutral salt spray test by ASTM B117. This procedure has been used for many years for all types of applications (Cremer, 1996). Due to several variations are considered in corrosion process, other standardized accelerated tests have been developed and implemented, with the aim to approach specific nature of corrosion (Guthire, 2002).

At the present, numerous accelerated tests conditions, such as SS, S6, DS, JASO, NS, seawater-NS, ASTM-cycles, etc. are available, (Fujiwara and Tahara 1997). Fujiwara and Tahara (1997) performed accelerated exposure tests on painted steel plates for two months, which included the seven sets of the accelerated corrosion tests conditions (SS; JIS Z2371, JASO cycle; JASO M609-91, ASTM cycle; ASTM D2933-74, DS cycle; PWRI in 1980, S6 cycle; JIS K5621, NS1 cycle and NS2 cycle. After all the tests were done, the authors compared the accelerated test data with the field test data at five sites in Japan for three years. The result showed that S6 cycle test condition (JIS K5621) can simulate the corrosion which is the most similar to the result of outdoor exposure tests. Therefore, the S6 cycle condition (JIS K 5621) is used to simulate corrosion on proposed specimens in this study.

1.3.6 Reliability of corroded bridge

Yasser (2009) studied the environmental effects on ultimate strength reliability of corroded steel box girder bridges. This study presented that the environmental conditions have a great effect on the load-carrying capacity and reliability of steel box girder bridges. The safety of box girder deteriorated suddenly during its service life although the remaining ultimate moment may exhibit little decrease in the same period.

Effects of corrosion attack to structural members and to structural systems safety were studied by several researcher. Nowak (2001) studied the reliability profiles of typical girder bridges with regards to corrosion and fatigue. The study examined that the loss of load carrying capacity due to corrosion is higher in shear than in moment. However, the study only based on the reliability index of individual member.

Eamon (2008) highlighted the potential benefit of secondary elements on the system reliability of girder bridges. The author mentioned that secondary elements such as barriers, sidewalks, and diaphragms may increase the load carrying capacity of girder bridges. Nowak (2004) mentioned that component-based design is very conservative due to the effect of redundancy and ductility in system measure. When the load in a critical component approaches the ultimate value, the other components can take additional loads and prevent a failure. The author also pointed out that the quantification of this load sharing within the system requires a special approach using the system reliability models. According to this study, the coefficient of correlation between each member can decrease or increase the system reliability in a range between 15% and 30%.

The research conducted by Czanecki (2006) analyzed the performances of composite girder bridges under corrosion. The study considered the analysis into account the variation in bridge parameters. According to the author, the corroded steel girders produce a reduction in the structure strength and intending to increase the probability of failure.

1.3.7 Research in bridge maintenance activities

Effective inspections and bridge maintenance activities are required to make sure that a bridge can maintain its capacity till the end of service life (ITD, 2008). Moreover, Czarnecki (2006) indicated that "if a steel highway bridge is not maintained properly (such as regular cleaning, inspection, repainting, and repair), steel corrosion occurs." The Federal Highway Administration sponsored a Weathering Steel Forum in 1989. As a result from that event, some of the guidelines are presented to achieve the potential of the product. One recommendation of this guidelines mainly focused on maintenance actions which indicates that the effective inspection and maintenance programs are essential to ensure all bridges reach their intended service lives. This recommendation is especially proposed for the case of uncoated weathering steel

bridges (FHWA, 1989). Some specific maintenance activities recommend to remove dirt, debris and other deposits that hold moisture and maintain wet surface condition on the steel. Furthermore, it is also pointed out hosting down a bridge to remove debris and contaminants is practical and effective in some situation.

A study from the Rhode Island Department of Transportation (RIDOT, 2002) demonstrated the effectiveness of bridge washing on highway bridges. The study considered two alternatives program in which one is performing the Do Nothing program during the proposed time of eight years period. The other alternative is the implementation of a regular bridge cleaning and washing with performing in each two years during eight years period. According to the predicted conditions and results from an economic analysis for the total cost of the bridges for both alternatives, the research group can summarize the bridge maintenance plan consisting of cleaning and washing would be more cost-effective than the Do Nothing alternative.

1.4 Objectives of the study

The objective of this research is to understand the characterization and classification of atmospheric corrosion in Myanmar. Field exposure tests were carried out at the outdoor exposure sites. Corrosion models were developed to estimate the loss of thickness with aging through the exposure time. The laboratory test was performed to estimate the long-term deterioration of steel inside the simulated environment. The corrosion models were developed to determine the loss of mass and reduction of section thickness with aging.

A series of accelerated testes were also conducted with intermittent washing to find out the appropriate frequency for bridge washing effect on corrosion degradation. From the accelerated test, a curve relating to the aging time and corrosion penetration was established. Choosing a proper maintenance method is also a major issue for extending lifetime of weathering steel bridge. Bridge washing practice considering on real experimental corrosion data was introduced as a maintenance plan. Proper time interval for bridge washing was also determined to be more effective to enhance corrosion losses by bridge washing.

Based on the section thickness reduction by corrosion, the structural capacity reduction of real steel bridge was evaluated with the aging time. The structural capacity reduction was checked by performing the nonlinear structural analysis on the composite

steel bridge model by using finite element software. The reduction of bending, shear and deflection capacity of bridge with thickness reduction due to corrosion was estimated, and respective reliability calculation through the exposure time has been performed. An economic analysis was also conducted by comparing costs for different surface treatments such as painting and bridge washing. The benefits of bridge washing over painting was introduced as a future maintenance plan.

1.5 Scope of the study

The thesis is composed by six chapters including Chapter 1, which introduces the background problems of corrosion in infrastructures in Myanmar and aims of the research. Chapter 2 discusses about the measurement results on atmospheric corrosion at several locations through the nation and the category of corrosion severity of studied areas. Chapter 3 describes the accelerated test with consideration on different levels of salt concentration. The evaluation on the effectiveness of steel washing was also simulated in this chapter. In Chapter 4, the time-scaled correlation of measured corrosion data inside the chamber and the outdoor exposure is presented. Based on this, the derivation of acceleration coefficient in each test location was driven.

Chapter 5 carries out the reliability assessment of bridge under corrosion attack with its aging time. The level of safety was also discussed by the target reliability value specified by the AASHTO. Chapter 6 consists the field performance study of weathering steel bridges under the services condition. This chapter also recommends for the future actions to the safety measure of bridge. The maintenance plan and economic analysis of considered alternatives are described. In this study, the effectiveness of bridge washing over painting at the end of service life was highlighted to prolong the bridge life at relative low costs. The final part concludes the summary of the research and recommendations for the future study.

References

A. S. Nowak (2004). “System Reliability models for bridge structures.” Bulletin of the Polish Academy of Sciences Technical Sciences, Vol. 52, No. 4, January 2004.

A. S. Nowak, M. M. Szerszen (2001). “Reliability Profile for Steel Girder Bridges with regard to Corrosion and Fatigue.” Journal of Theoretical and Applied Mechanics, Vol. 2, No. 39, January 2001.

Brown P.W and Masters L.W, 1982. Atmospheric Corrosion, Wiley, New York.

Brown, C.W., Heidersbach, R.H. 1987. “Raman spectra of possible corrosion products of iron appl. Spectrosc”. The journal of SAGE 6, no. 62: 532-535.

BS EN 12500:2000 “Protection of metallic materials against corrosion - Corrosion likelihood in atmospheric environment - classification, determination and estimation of corrosivity of atmospheric environments”, British Standards Institution, London, 2000.

Crampton, D. D., Holloway, K. P., & Fraczek, J. (2013). Assessment of Weathering Steel Bridge Performance in Iowa and Development of Inspection and Maintenance Techniques (Final Report). In *Iowa Department of Transportation Office - Federal Highway Administration*.

Cremer, (1996). “The move to cyclic salt spray testing from continuous salt spray.” Anti-Corrosion Methods and Materials, Vol. 43, No. 3.

Czarnecki, A., (2006). “System reliability Models for Evaluation of Corroded Steel Girder Bridges.” PhD Dissertation in Civil Engineering. University of Michigan.

Ericsson R, 1978. Werks. Korros., 29:400.

Evans U. R. and Taylor C.A 1972. .J., Corros. Sci., 12:227.

Eom, J., (2014). “Reliability Analysis Model for Deflection Limit State of Deteriorated Steel Girder Bridges.” Journal of the Korea Institute for Structural Maintenance and Inspection Vol. 18, No. 2, March 2014.

Feliu S, Morcillo M an Feliu Jr. S, 1993. Corros. Sci., 34:403.

FHWA, (1989). “Uncoated Weathering Steel in Structures.” Technical Advisory 5140.22. https://www.fhwa.dot.gov/bridge/t514022.cfm [Accessed Jan. 16, 2015].

Goodwin F.E, 1990. Metallurgy and Perfomance, TMS, Warrendale, 183.

Guthrie, J., Battat, B., Grethlein, C., 2002. “Accelerated corrosion test.” The AMPTIAC Quarterly, Vol. 6, No. 3, pp 11.

Hiroshi Fujiwara, Yoshio Tahara, 1997. “Research on evaluation of long-term anticorrosion performance of steel bridge coating”. Proceedings of the Japan Society of Civil Engineers, Vol. 570, No. 570, pp 129-140.

http://corrosion-doctors.org/WhyStudy/Strategic-Impact.htm , Visited , 7th June 2019

ITD, (2008). “Bridge Design LRFD Manual.” Idaho Transportation Department

Lapuerta S, Bérerd N and et al., 2008. The influence of relative humidity on iron corrosion under proton irradiation *J. NUCL MATER*. 375 80-85.

Morcillo M, Chico B, Mariaca L and Otero E, 1999. Corros. Sci., 41:91.

Nanda Munasinghe, Shanika Jayathilake, Prediction of atmospheric corrosion – a review, ENGINEER-Vol.XLVII, No. 01,pp.[75-83], 2014.

Ohtsuk, T. 1996. “Raman spectra of passive films of iron in neutral borate solution. Mat. Trans”. The journal of electrochemical society 11, no. 146: 4061-4070.

Oriental Consultants, JICA, Investigation Record Books for Substructures of Bridges (Reference Data), The National Transport Development Plan, Rehabilitation and Modernization of Yangon-Mandalay Railway Project, September 2013.

Pierre R. Roberge, Handbook of corrosion engineering, McGraw-Hill, July 2017.

Public Works, Current Situation of Road Networks and Bridges, Ministry of Construction, Union of Myanmar, February 2013.

RIDOT, (2002). “Bridge Inspection/Washing Program - Bridge Drainage Program.” Rhode Island Department of Transportation, Operations Division.

Roberg., Pierre, R., Hand book of corrosion engineering, New York, 200, 58P, pp 66-69, pp 84-85.

Schweitzer, P.A. P.E, 2009. Fundamentals of Corrosions: Mechanisms, Causes, and Preventive Methods.

S.Syed, Atmospheric corrosion of materials, Journal of engineering research, 11(1), 1-24 (2006).

Yasser Sharifi and Jeom Kee Paik, 2009. “Environmental effects on ultimate strength reliability of corroded steel box girder bridges.” Tech Science Press, Vol. 2, No. 2, pp 81-101.

Y. Yu Kyi Win, T. Khaing, Z. Min Tun, & Y. Suzuki (n.d.) (2017). “Comparative Study on Atmospheric Corrosivity of Under Shelter Exposure in Yangon and Mandalay (Myanmar)”. ASRJETS, Vol 27, No. 1, pp 386-404.

Yu Yu Kyi Win (2017). *Assessment of Corrosion-induced Deterioration and Protection of Structural Steel Elements in Myanmar*. Thesis Submitted in Partial

Fulfilment of of the Degree of Doctor of Philosophy in Civil Engineering, Department of Civil Engineering, Yangon Technological University,Yangon, Myanmar.

Zaki Ahamad, Principles of corrosion engineering and corrosion control, Elservier, 2006. https://doi.org/10.1016/B978-0-7506-5924-6.X5000-4

Chapter 2

ATMOSPHERIC CORROSION TEST IN MYANMAR

2.1 Introduction

Myanmar is situated in the tropical climate region. However, a variation in climate is observed due to the long coast line from the South to the North. The classification with respects to meteorological aspects has been taken by coastal area, deltaic area, central dry area and northern highland area. These areas have the different climate characters based on annual rainfall and temperature, altitude and nature of geography. Based on the analysis of rainfall and temperature, the country climate is described by three seasons.

Starting from November to February, the city has winter or northeast monsoon season. Low temperatures prevail over the whole country during this season. During March to Mid of May, the temperature raise up to 37.8 °C and above occur in central and lower parts. Cyclonic storms and depressions sometimes form during May in the south Bay of Bengal. The rainy or southwest monsoon season is occurred in between mid of May and October. The total rainfall of the monsoon season is about 200 inches (5080 mm) in the coastal area and 25 inches (635 mm) in central of Myanmar. Due to its climate nature in Myanmar, the cities have high humidity through a year. Consequently there is high cost due to corrosion damage. Two types of atmosphere conditions are considered in the present study. One is an exposure test in outdoor atmosphere considering the effect of rain and wet dry effect due to direct exposure to the environment in un-shelter condition. The other is an exposure test under shelter atmosphere. The aim of this approach is to determine an appropriate atmospheric corrosion maintenance of steel under different exposure conditions.

The study on atmospheric corrosion in Myanmar has been started in 2017 in the collaboration with Kyoto University. The former Ph.D. student from YTU studied the field exposure test in Yangon, Yu Yu et.al (2017). According to her findings, the

corrosion aggressiveness in Yangon prones to C3 class defined by the ISO 9223 standard. Moreover, the researcher also measured an atmospheric corrosion in the shelter environment in Yangon and Mandalay. This measurement pointed out thtat the corrosion in Yangon is higher than Mandalay and different environmental conditions cerate different patterns of losses in between carbon and weathering steels.

The present study extends the previous atmospheric corrosion measurement under shelter condition by taking measurements at six exposure test sites through the country. A comparison of exposure test results in outdoor and shelter are discussed. The corrosivity categories are mapped by using measurement results from several Asia countries to see how the corrosion rates vary in Asia regions with understanding the effects of environmental parameters. The chapter also discusses a proper dose-response function for first year corrosion loss of carbon steel in Asia environment by considering on changes in temperature and chloride parameters of dose-response function described by ISO 9223 as proposed by Dara (2017). The applicability of proposed dose-response equation is confirmed by judging with measured data in Myanmar, Japan and Vietnam.

2.2 Field atmospheric corrosion test

The field exposure test approach is generally needed to determine the use of materials harmonized with the specific site environments. Atmospheric corrosion varies according to the exposure conditions such as the deposition of airborne salt on the metal surface will be different on the specimens exposed in the atmosphere which is directly contact with outdoor (un-shelter/outdoor) and in the atmosphere which is covered from the direct exposure with outdoor (shelter) due to the washing effect of precipitations on the metal surface in the direct contact exposure (un-shelter/outdoor) condition. This is important to account for making decisions respecting with corrosion protection under varying exposure conditions. Both shelter and un-shelter (outdoor) exposures tests were conducted in this study.

The purposes are to evaluate the first year corrosion losses of carbon and weathering steels under different exposures and generate the prediction equation for the others un-measureable locations. Moreover, analyzing the significant factor on long-term prediction equations for the carbon and weathering steels are carried out. Effective environmental parameter on long-term corrosion is also discussed by analyzing multiple regression models.

2.2.1 Exposure test sites

The eight exposure sites were chosen for the measurement under direct contact with outdoor atmosphere and three test sites were selected for the measurement under the shelter atmosphere. The locations of test sites are as shown in **Figure 2.1** and the information are provided in **Table 2.1**. Meteorological observation systems were installed at the exposure test sites to collect the environmental parameters; temperature, wind speed, humidity, rainfall and UV radiation in the outdoor environment.

Table 2.1 Characteristics of test sites

Site No.	*City Name*	*Distance from the sea-shore , (km)*	*Height above sea-level, m*	*Type of atmosphere*
T1	Sittwe	1.4	4	Coastal in the West
T2	Dawei	13	16	Coastal in the South
T3	Mawlamyine	21	21	Urban in the South
T4	Pathein	37	9	Urban in the delta
T5	Yangon	51	9	Urban in the South
T6	Maubin	63	3	Urban in the delta
T7	Hinthada	88	26	Urban in the delta
T8	Mandalay	342	74	Urban in the Central

The closet exposure site is located in 1.4 km from the coastline and the farthest exposure site is seen in 342 km away from the coastline.

2.2.2 Material

Two structural materials, carbon steel (SM) and weathering steel (SMA) were used for atmospheric corrosion tests in both outdoor and shelter atmospheres. The chemical composition of specimens are shown in **Table 2.2**. Specimen sizes of 50 × 50 × 2 mm and 150 × 150 × 3 mm were used for shelter and outdoor exposure tests, respectively. The specimens were exposed up to three years in both exposure conditions.

Table 2.2 Chemical composition of steels

Material	*Chemical Composition (% by weight)*									
	C	*Si*	*Mn*	*P*	*S*	*Cu*	*Cr*	*Ni*	*Nb*	*V*
SM	0.17	0.32	1.39	0.016	0.012	-	-	-	-	-
SMA	0.12	0.39	0.9	0.008	0.006	0.36	0.61	0.22	0.014	-

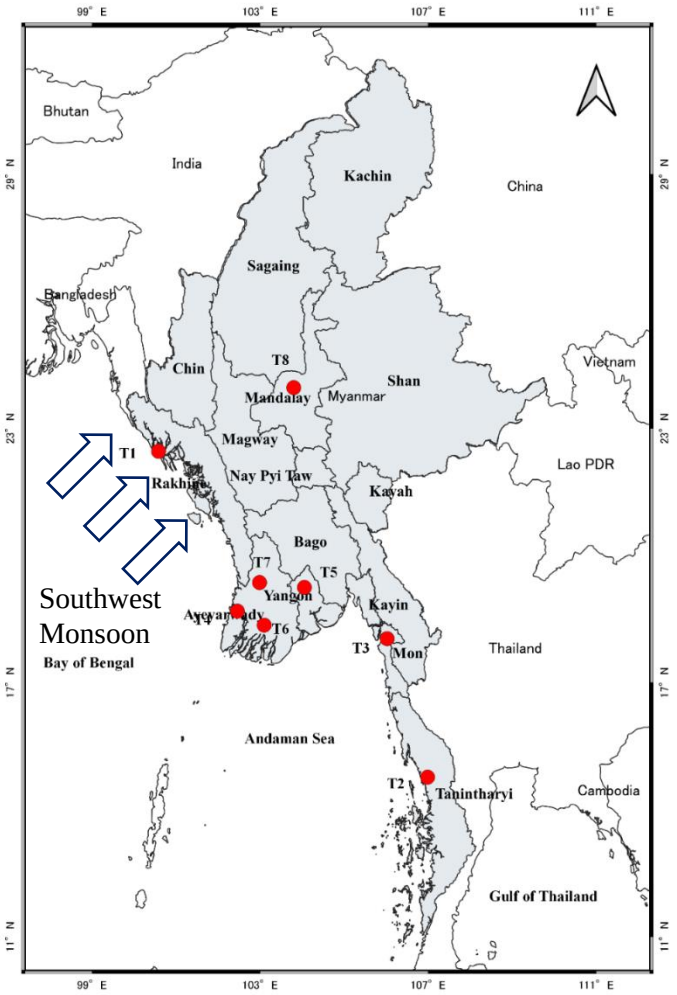

Figure 2.1 The position of test sites

2.2.3 Corrosion rate measurement

The corrosion rate is determined by mass reduction of specimen caused by corrosion attack. Accordingly, the measurement of mass reduction was accomplished by differencing the weight between original and cleaned specimens. The procedure of

specimen cleaning was finished by the standard ISO 8407 (1991). The chemical cleaning procedure according to the standard is shown in **Table 2.3**.

The corrosion products were removed after immersing the specimens into the solution for about 10 minutes. The standard temperature during cleaning process is kept between 20 and 25 °C. An ideal procedure of this standard is to remove only corrosion products without removing any of the base metal. To determine the mass loss of the base metal when removing corrosion products, replicate un-corroded control specimens were cleaned by the same procedure as used on the test specimen according to the standard.

Table 2.3 Chemical cleaning procedure for iron and steel as per ISO 8407

Material	Chemical	Time	Temperature	Remarks
Iron and Steel	-500ml hydrochloric acid -3.5 g hexamethylenetetramine -Distilled water to make 1000 ml	10 min	20°C to 25°C	Longer time may be required in certain circumstances

By weighting the control specimen before and after cleaning, the extent of metal loss resulting from cleaning can be utilized to correct the corrosion mass loss. The corrosion rate (CR) is calculated by the following equation:

$$CR\ (\frac{mm}{y}) = \frac{10\ W_y}{\rho A} \qquad \textbf{(2.1)}$$

W_y: Weight loss per year (g/y)

ρ: Density of steel (g/cm^3)

A: Exposed area (cm^2)

The corrosion rates have been calculated in every year and data were analyzed to study the behavior of atmospheric corrosion under considering different environmental conditions. The atmospheric corrosivity is also determined by using these calculated corrosion rate and measured environmental parameters.

2.3 Outdoor atmospheric corrosion

An outdoor exposure testing is used to assess the atmospheric corrosion of metals by direct measurement, if there has no pre-existing correlations between atmospheric corrosion rates and atmospheric parameters are available (Prier Roberg, 2008). The first year experimental results of outdoor atmospheric corrosion test in three major cities in Myanmar; Yangon, Mandalay and Mawlamyine are presented in this study. The measurement data from Yangon and Mawlamyine test sites has been done by a former Ph.D student from Yangon Technological University (Myanmar). The summary of outdoor atmospheric corrosion rates of carbon and weathering steels in Myanmar were discussed in this section.

2.3.1 Experimental setup

Exposure test racks were constructed according to the ISO 8565 standard (2017) and the setting of test racks were finished on the roof of the main building of Technological University at each exposure site. The installation of specimens were done by 45 degree inclination from the horizontal. **Figure 2.2** shows an installation of exposure rack with mounted specimens. Meteorological observation systems were also installed near the exposure test racks to collect the near-by environmental condition including temperature, wind speed, humidity, rainfall and UV radiation. The installation of weather station at the site is shown in **Figure 2.3**.

Chloride and SO_2 deposition rates were measured by using dry gauze and PbO_2 cylinder in accordance with JIS Z 2383 (1998). The dry gauze and PbO_2 was installed under an instrument shelter or rainproof location with open airflow, and the renewal was made in every month.

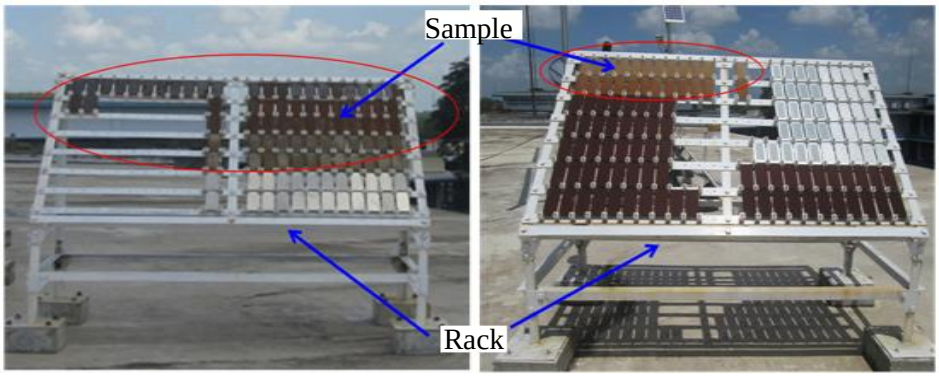

Figure 2.2 Test rack after placing the specimen

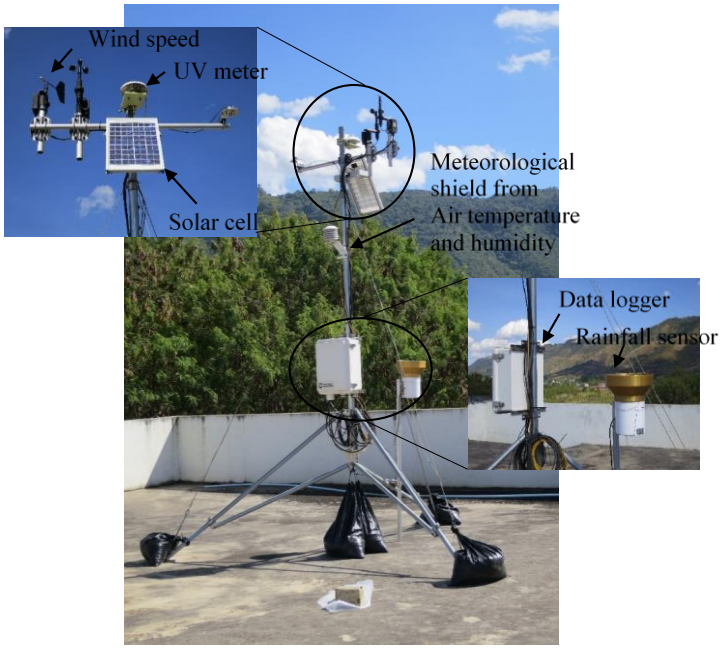

Fig. 2.3. Meteorological data observation system

The equipment installations for chloride and sulphur dioxide measurements at the test site are shown in **Figure 2.4**.

(a) Gauze Method (b) Cylinder Method

Figure 2.4 Chloride and Sulphur dioxide measurement

After every month of exposure, the chloride content and sulphur dioxide deposition were determined by applying the iron chromatograph method and Barium Sulphate Precipitation method, respectively.

2.3.2 Measured environmental parameters and atmospheric impurities

The monthly average air temperature (T) is presented in **Figure 2.5**. The monthly average temperature at the present sites are in a range within 25 and 35°C. A

high average temperature is observed in Mandalay with the maximum value is about 33.5°C, which is located at the middle of the country under dry steppe climate.

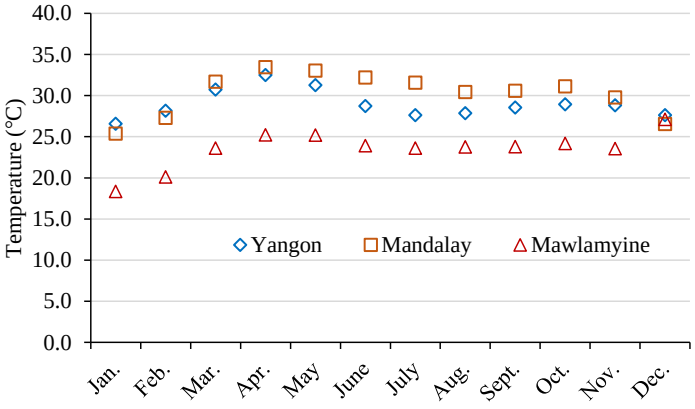

Figure 2.5 Monthly average temperature

Mawlamyine has the lowest temperature among three test sites. It is noticeable that almost uniform distribution of temperature is discovered at the present exposure sites with little fluctuation of value is about 10°C within a year.

The relative humidity (RH) of the test sites are described in **Figure 2.6**. According to the figure, it can be seen that the relative humidity in Mawlamyine is extremely high and even 100% of RH was occurred in June to October. Most of the time is highly humid in Mawlamyine where over 80% of relative humidity, which is the level of relative humidity to create an electrolyte water layer in the surface of specimens for corrosion process, was measured in every month.

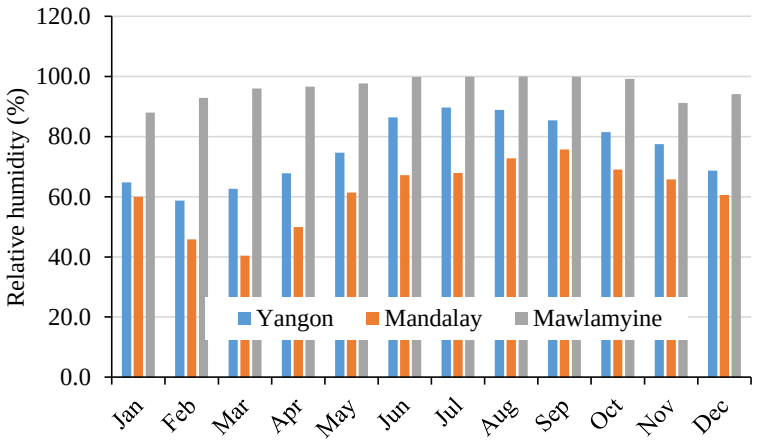

Figure 2.6 Monthly average relative humidity

S.SYED (2006) mentioned that the corrosion rate increases sharply at 75-80% relative humidity due to capillary condensation of moisture within the rust layer, moreover, 90% of relative humidity tertiary increase corrosion rate. Yangon also has a considerable relative humidity with the maximum RH of about 86% is observed between June and September. It is observed that the two cities, Yangon and Mawlamyine, under tropical humid climate have lengthy high humid seasons throughout a year.

Time of wetness (TOW) is calculated by the relative humidity and temperature to count the total numbers of hours that the probes are at a temperature above 0°C with a relative humidity greater than or equal to 80% (ISO 9223, 2012). The geographical location and seasonal changes of the stations are greatly influence on TOW measure because of the differences in temperature and relative humidity for each station. Time of condensation (TOC) which is a time period while the temperature is lower than the dew point. A film of dew, saturated with sea salt or acid sulfates, and acid chlorides of an industrial atmosphere provides an aggressive electrolyte for the promotion of corrosion. Highly condensation appears in humid tropics where nightly condensation appears on surfaces and picks up carbon dioxide and becomes aggressive as a dilute acid. The monthly average TOW and TOC are described in **Figure 2.7**.

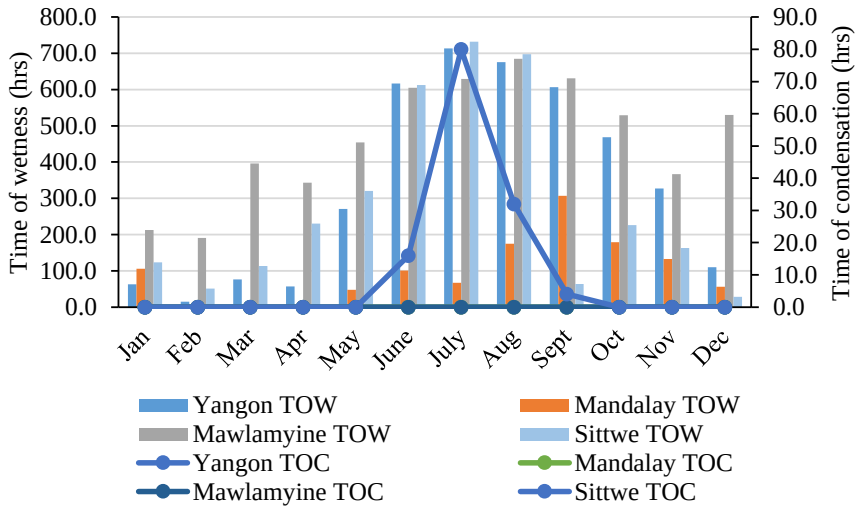

Figure 2.7 Monthly average time of wetness and time of condensation

Mawlamyine has the highest TOW value and the maximum time periods of between 600 and 700 hrs was discovered in June, July and August. Annual TOW are 5532 hrs and 4002 hrs in Mawlamyine and Yangon, respectively. Mandalay has the

lowest TOW because of high temperature and its annual TOW is about 1172 hrs. The measured TOC in Yangon, Mandalay and Mawlamyine show 0 hrs of TOC values. The measurement was also taken in Sittwe, 1.4km distance from the sea, to see how TOC relates with temperature and humidity. Some distinct amount of TOC was observed in that site with the peak value is about 80 hrs in July. According to this, TOC does not directly relate to humidity since Yangon and Sittwe have same humidity. Therefore, TOC is not a significant factor for corrosion losses at the present test sites.

The amount of rainfall at exposure sites are described in **Figure 2.8**. A remarkable rainfall is measured in Mawlamyine with a monthly total rainfall is about 826mm in August when is the heaviest rainfall season in Myanmar. The amount of rainfall in Yangon is moderate and the peak value is about 524mm in July. Mandalay has the lowest rainfall among the test sites with the maximum rainfall is about 263.5mm.

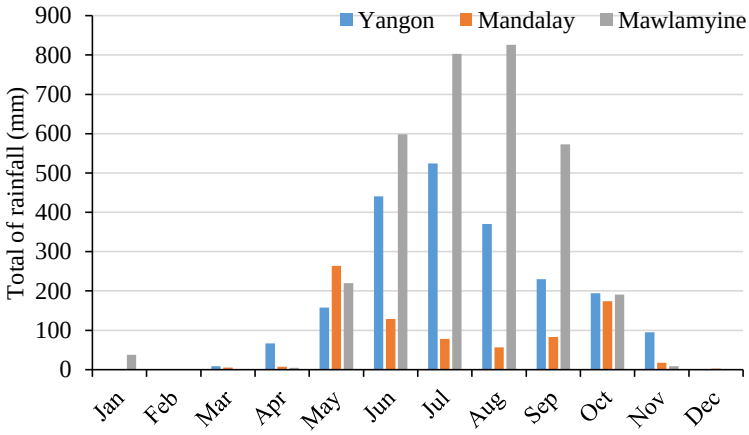

Figure 2.8 Monthly rainfall

Monthly average flying salt was also measured at the test sites and the results are shown in **Figure 2.9**. Yangon has the highest flaying salt concentration and the maximum amount of flying salt is about 0.062mdd observed in May and July. According to the Myanmar climate report (2017), the monsoon wind passes through the country and even typhoon often happens during this period. Therefore, not only the highest wind speed but also the highest chloride contents were measured in Yangon during this period. Low level of airborne salt contents which is well under 0.05mdd were measured in Mawlamyine test site. Mandalay has the lowest flying slat content and it is also the farthest test site from the seashore.

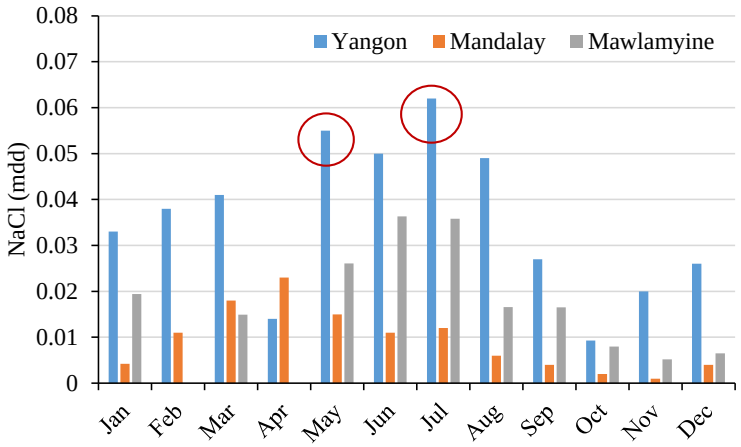

Figure 2.9 The monthly average values of flying salt

Sulphur, transmitted from industrial and traffic activities, is also considered as an important parameter for atmospheric corrosion in Myanmar. The measurement of sulfur dioxide was also taken in Yangon and Mandalay. These two cities have considerable amount of traffic as Yangon is a major economical city and Mandalay is the country central city where all the domestic traffics are passing through. **Figure 2.10** shows the results of measurement.

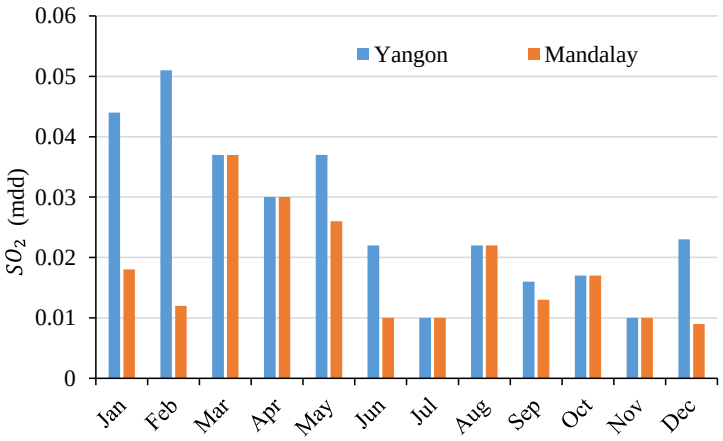

Figure 2.10 The monthly average values of SO_2 deposition rate

According to the measurement results, Sulphur dioxide in Yangon is the highest among the test sites with the maximum value of about 0.05 mdd. Mandalay also has some extent of sulfur dioxide with the maximum value is about 0.036 mdd, however, the content is lower than Yangon.

2.3.3 Corrosion rate (CR)

The corrosion rates by **Equation 2.1** is shown in **Table 2.4**. As shown in table, Mawlamyine has the highest corrosion rate with the maximum rate is about 17.2 µm/year in SM steel and 16.8 µm/year in SMA steel, respectively. The corrosion rates in study locations are increasing in a order with **Mandalay < Yangon < Mawlamyine**. In a consideration on the geography of current test sites, it can be seen that corrosion rates vary with test location distance from the coastal although it is not dominant by the attitude in present test sites due to all are located almost in the flat region.

Table 2.4 Corrosion rates

Site	Corrosion Rate, µm/year	
	SM	SMA
Yangon	15.5	13.7
Mandalay	8.92	6.76
Mawlamyine	17.2	16.8

A comparison of corrosion rates on carbon and weathering steels can be seen in **Figure 2.11**.

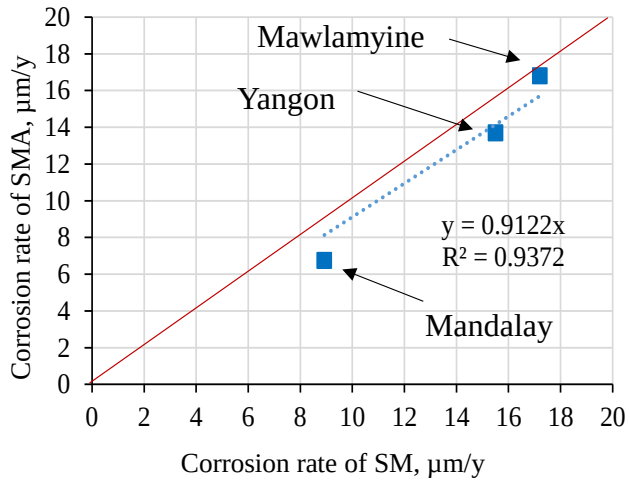

Figure 2.11 Comparison of WS and CS corrosion rates

The figure shows that weathering steel corrosion rate is a little lower than carbon steel corrosion rate, which is describing that more or less protectiveness of weathering steels are forming during this one year exposure.

2.3.4 Atmosphere Corrosion Classification by Environmental Parameters

The corrosivity of atmosphere is determined by calculated time of wetness from measured site, temperature, relative humidity and atmospheric pollutant levels (sulphur dioxide and airborne salt). The classification has been taken according to the ISO 9223 standard (1998). The classification of environmental parameters and atmosphere corrosivity are presented in **Table 2.5**.

The highest atmosphere corrosivity class of C3 is observed at the present test sites where high humidity levels are measured. ISO 9223 presented the numerical values of the first year corrosion rates for standard metals (carbon steel, zinc, copper, aluminum) for each corrosivity category.

Table 2.5 Atmosphere corrosivity classification by ISO 9223

Site	SO_2		CL^-		TOW		Corrosion Class, C
	Deposition rate (mmd)	Class	Deposition rate (mmd)	Class	Hour/y	Class	
Yangon	2.41	P_0	3.7	S_1	5183	τ_4	3
Mandalay	2.40	P_0	1.2	S_0	1175	τ_3	2-3
Mawlamyine	-	-	1.89	S_0	5253	τ_4	3

The standard specified the corrosion rate of carbon steel for C2 is within 1.3 and 25 μm/year and for C3 is within 25 and 50 μm/year.

2.4. Shelter atmospheric corrosion

In the shelter exposure, the surface is shielded from direct precipitation and solar radiation and it is also prevented from coarse aerosol particles, such as windblown sea salt or soil dust, from reaching the corroded surface, at that time; its allows interaction with smaller aerosol particles and gases. These modifications of conditions influence the corrosion process depends on the actual exposure conditions and varies from one case from another [Leygraf C., 2016]. The button specimens were installed at eight exposure test sites (T1 to T8) located at the middle and lower part of the country as described in Figure 1. The experiment period is about three years starting from July, 2016 to January; 2019 in some exposure sites and one year in some exposure sites.

The measurement was also carried out in Okinawa, Japan to see the variation in corrosion rates at the exposure at different geographical conditions. The test site is situated in Nago city, Okinawa and the location of exposure site is 0 km from the East China Sea. The city owns the sub-tropical climate conditions with very mild winters and long, muggy and rainy summers. The specimens' installation period is about one year and the installation condition is in shelter exposure in which rainfall effect is neglected.

2.4.1 Experimental setup

Three specimens of both carbon steel (SM) and weathering steel (SMA) were set up for each time measurement. A standalone data logger (Easy USB-2) was used to collect average annual temperature and relative humidity in shelter atmosphere. The data logger was installed at the location near the specimens. The installation of test specimen and data logger at the sites are shown in **Figures 2.12 and 2.13**. Temperature and relative humidity data logger was also installed at the same time as specimen exposure.

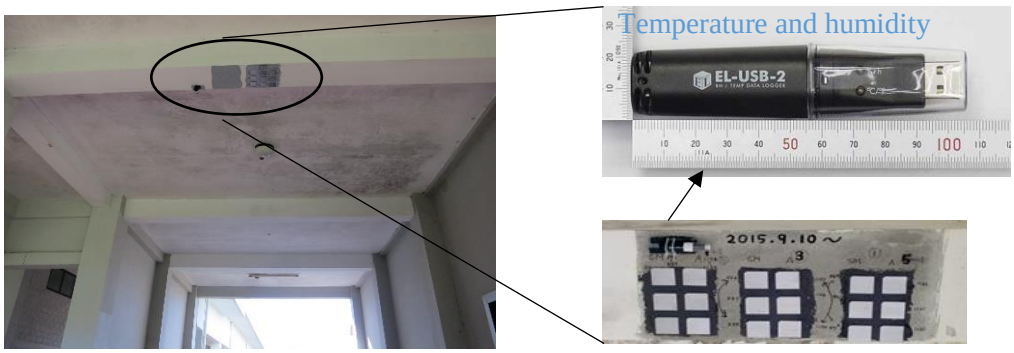

Figure 2.12 Specimen installations in Myanmar

Figure 2.13 Specimen installations in Nago City, Okinawa, Japan

Specimens in the deltaic region in Myanmar and Okinawa in Japan were dismounted in every season to see the seasonal effect on corrosion rate variations.

Other specimens were dismounted in every year and corrosion thickness and weight losses were measured. The temperature and relative humidity were recorded hourly by the logger.

2.4.2 Measured temperature and relative humidity data

An annual average temperature and relative humidity of the test sites are presented in **Figure 2.14**. The figure shows that the maximum temperature was observed in Mandalay with maximum annual average temperature is about 30.3°C. Temperature variation in other test sites are in within 26 and 28°C. It is observed that temperature at the test sites under tropical humid climate have small differences between each other's.

Mawlmyine has a very high relative humidity with the maximum value is about 98% because the geography of this city is surrounded by the mountains and has lengthy rainy seasons. In contract, the lowest humidity found in Mandalay which value is less than 60%. Almost similar relative humidity was measured at other exposure sites.

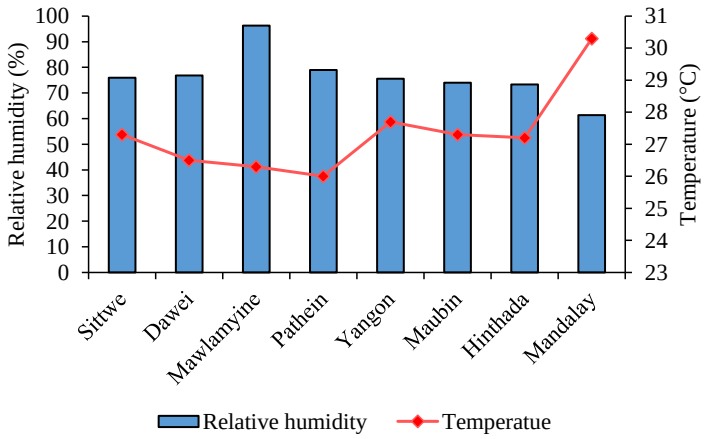

Figure 2.14 Annual average temperature and relative humidity

According to the figure, it is noticing that the relative humidity is low at the test sites where there have high temperature. Monthly average temperature and relative humidity of exposure sites are given in **APPENDIX A**.

2.4.3 Corrosion rate (CR)

The measured first year corrosion rates of SM and SMA steels are shown in **Figure 2.15**. Atmosphere corrosivity C2 is classified at the present test sites in shelter conditions.

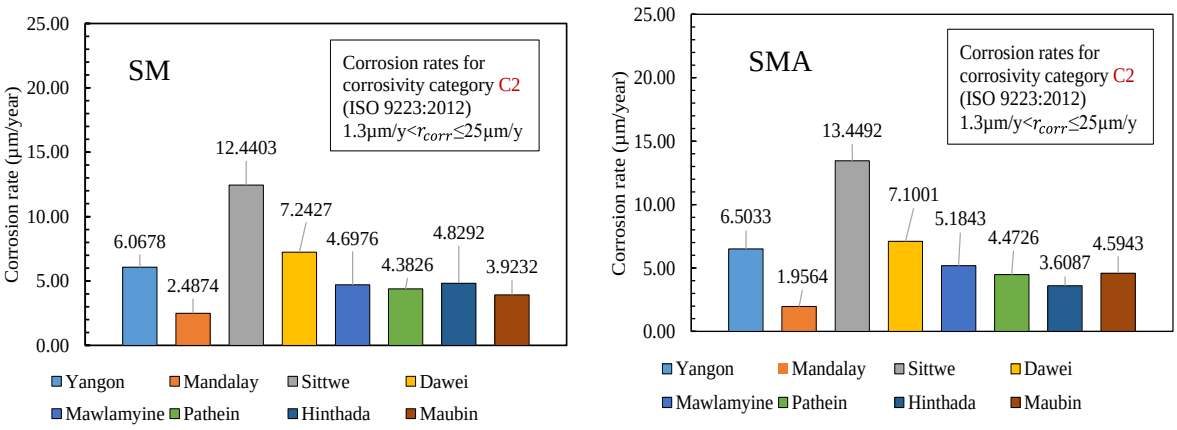

(a) Carbon steel (SM)

(b) Weathering steel (SMA)

Figure 2.15 Corrosion rates

The maximum first year corrosion rate of carbon steel under the shelter environment is about 12.44μm/yr and observed in Sittwe. Dawei has the second largest corrosion rate with the value is about 7.24 μm/yr. These two test sites are the closet test sites to the coast line. Yangon also has a considerable rate compared to others test sites because of its air impurities such as chloride and shulphur dioxide as described in **Section 2.1**. The lowest corrosion rate was measured in Mandalay which has first year corrosion rate is about 2.48 μm/yr for carbon steel. Similar performances of corrosion rate was discovered for weathering steel at the present test sites. The corrosion rates increase with the order **Mandalay < Hinthada < Pathein < Maubin < Mawlamyine < Yangon < Dawei < Sittwe**.

Comparison to the corrosion rate of carbon and weathering steel under shelter exposure test shows that the corrosion rate of weathering steel is higher than carbon steel at all the exposure sites. This is because of the specimen surfaces are shielded from the direct precipitation and solar radiation. The shelter also prevents coarse aerosol particles, such as windblown sea salt or soil dust, from reaching the corroded surface, at that time; it allows interaction with smaller aerosol particles and gases. Kreislova (2014) studied a comparison of long term exposure in outdoor and shelter conditions in

high air pollution atmospheres (industrial and marine). The researcher found that corrosion rate of weathering steel is higher than carbon steel in shelter conditions after longer exposures due to the commutation of corrosion simulator on steel surfaces.

Moreover, the non-homogeneous rust layer formed which obtained higher concentration of corrosion simulators (sulphates, chlorides) in shelter conditions. The corrosion defects in weathering steel bridges initiated by both cases (effect of sheltering or design). The atmosphere for present study areas are urban and coastal atmospheres. According to the corrosion rate measured in this study, it can be concluded that corrosion rate of weathering steel is higher than carbon steel in shelter conditions in all sorts of atmosphere types (such as urban, marine, industrial and coastal). However, the intensity of difference depends on the type of atmosphere and its severity. The present exposure sites have lower atmospheric impurity, therefore, the differences are not so high. Almost similar performances of corrosion resistance are observed in carbon and weathering steels in present study area.

The corrosion rate in Okinawa is almost 10 times higher than measured corrosion rates in Yangon (Myanmar) as shown in **Figure 2.16**.

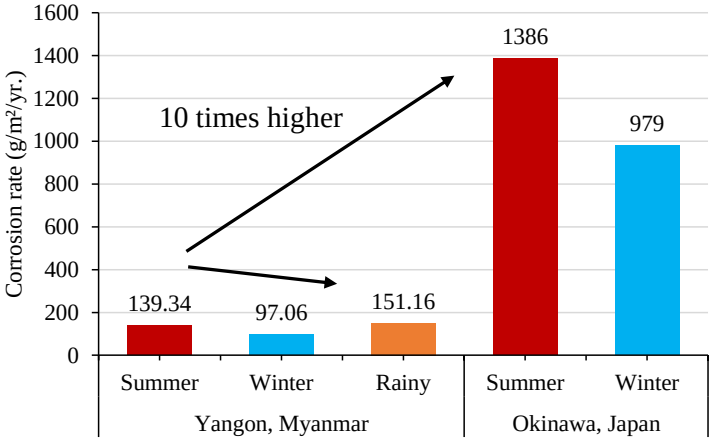

Figure 2.16 Corrosion in Yangon, Myanmar and Okinawa, Japan

The corrosion process in Myanmar increased higher in the rainy season than others since humidity is high during that season. Summer season in Japan produces higher corrosion rates than winter. According to the climate, lengthy raining days are occurred in Okinawa during the summer.

Rain can increase corrosion rate of specimens under the shelter condition due to increase in humidity by the evaporation effects.

According to the guideline of weathering steel use in Japan defined an applicable zone for weathering steel. The region where corrosion loss is less than 30 μm/year and airborne salt amount is less than 0.05 mdd is described as an appropriated zone to use weathering steel. Therefore, the use of weathering steel in Myanmar is acceptable since the corrosion rates of current exposure sites in Myanmar are less than a prescribed value.

2.4.4 Relationship between corrosion rate and coastal distance

According to the measured corrosion rates and coastal distance of test sites, negative logarithmic relation is defined in correlation between corrosion rates and distance from the coastal of exposure sites as shown in **Figure 2.17**. The strong relationships with high correlation coefficients are observed in both carbon and weathering steels. This is due the fact of weather conditions and chloride contribution to the inland exposure sites. Therefore, it can be concluded that the corrosion rates vary with varying off shore distances of exposure sites.

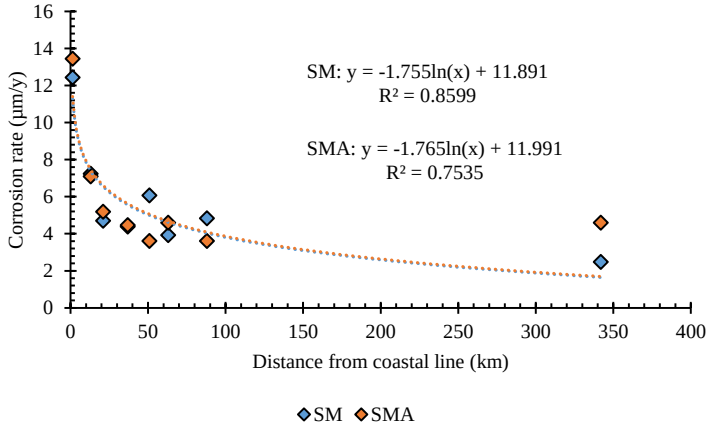

Figure 2.17 Correlation between corrosion rates and coastal distance

2.4.5 Dose-response function of atmospheric corrosion in shelter conditions

A dose-response function of atmospheric corrosion in shelter condition is determined by measured environmental and geographical parameters. Multiple regression was carried out to determine to what degree the continental data have strong effect on first year corrosion losses prediction compared with environmental variables. The data collected during exposure period and logarithmic transformation of coastal distance used in regression treatments are shown in **Table 2.6**. Monthly average temperature and relative humidity for the test sites are attached in **APPENDIX A**.

Two types of regression methods are considered to evaluate the effect of continental variables. The first equation was built by considering both environmental variables (temperature and relative humidity) and continental variables (elevation and distance from sea shore). But, only environmental parameters were applied in modelling of the second regression equation.

Table. 2.6 Experimental data for regression analysis

Test sites	Corrosion rate (µm/year), SM $\boldsymbol{K_{corr\_SM}}$	Corrosion rate (µm/year), SMA, $\boldsymbol{K_{corr\_SMA}}$	Log-transform coastal distance , D	Annual average temperature (°C), T	Annual average humidity (%), RH
T1	12.440	13.449	0.146	27.4	76
T2	7.243	7.100	1.114	27.5	76.5
T3	4.698	5.184	1.322	26.3	76
T4	4.383	4.723	1.568	26	79
T5	6.068	3.609	1.708	29	76
T6	3.923	4.594	1.799	27.3	74
T7	4.829	3.609	1.944	27.2	73
T8	2.487	4.594	2.534	30.5	61

With respect to the proposed consideration, the linear regression equations expressing the relationship between carbon and weathering steels corrosion rates and corresponding environmental parameters are proposed as:

$$K_{corr} = a_1 T + a_2 RH + a_3 D* + a_4 E + a_5 \quad \textbf{(2.2)}$$

where:

K_{corr} = corrosion rate after one year exposure, µm/year,

a_1, a_2, a_3, a_4, a_5 = constants,

T = annual average temperature, °C,

RH = annual average relative humidity, %,

$D*$ = logarithmic transformation of distance from sea shore to the test site, km,

E = evaluation of test site above the sea level, m.

The regression equations for corrosion of carbon steel after one year exposure were found as follow:

$$K_{corr\_SM} = 0.9392T + 0.0177RH - 4.836D * -0.0134E - 14.13 \quad \text{R=0.98} \quad \textbf{(2.3)}$$

$$K_{corr\_SM} = 1.4209T + 0.5714RH - 75.8338 \quad \text{R=0.56} \quad \textbf{(2.4)}$$

Table 2.7 gives the comparison results of actual data and calculated results using formulated equations. It can be seen that the error percentages using equation 3 are ≤ 17% errors with the regression coefficient R^2 is 0.9829. In contract, higher error percentage up to almost 47% with regression coefficient R^2 is 0.3202 was observed using the prediction model without continental parameters. The effects of consideration on coastal distance and elevation of test sites show high influent on the corrosion losses. Temperature and relative humidity are positively affect the corrosion deterioration. It means that higher temperature and relative humidity contributes more severe corrosion deterioration for the first year corrosion of carbon steel. Otherwise, negative effect of coastal distance and elevation of test locations were observed for the current test locations. In this case, climate conditions for current test sites are a tropical dry and monsoon. Temperate climate in the high mountain region is not included in his of corrosion simulation. However, the current formula can be useful at the locations for similar climate conditions and maximum elevation of test sites from sea level is not more than 100 m.

Table 2.7 A comparison of corrosion rates by experiment and calculation (SM)

Test sites	Obs. Corr. rate	Cal. Corr. Rate[3]	Errors , %	Cal. Corr. Rate[4]	Errors, %
T1	12.440	12.200	-2	6.529	-47
T2	7.2427	7.478	2	6.957	-4
T3	4.697	5.269	11	4.966	5
T4	4.383	4	-10	6.254	30
T5	6.068	6.103	1	8.231	26
T6	3.923	4.089	4	5.244	25
T7	3.517	2.991	-17	4.531	-19
T8	2.581	2.430	-6	2.363	-9

[3] Using Equation 2.3 (considering both continental and environmental parameters)

[4] Using Equation 2.4 (only environmental parameters are included)

Similar method is used for the calculation of weathering steel regression analysis under same exposure period. The regression equations for first year weathering steel corrosion are as shown in **Equations 2.5 and 2.6**. According to these equations, it can be seen that the effects of relative humidity is somewhat different from the SM steel. The negative correlation showed with the weathering steel corrosion rate. Higher relative humidity at the very first specimen exposure condition promotes the formation of protective oxide layer on the weathering steel surfaces in the shelter environments.

$$K_{corr\_SMA} = 0.778T - 0.129RH - 5.106D * -0.047E + 2.615 \qquad \text{R=0.98} \quad \textbf{(2.5)}$$

$$K_{corr\_SMA} = 1.515T + 0.643RH - 83.464 \qquad \text{R=0.58} \quad \textbf{(2.6)}$$

The results of the calculations for each test site are shown in **Table 2.8**. The same situations are occurred as carbon steel corrosion. The errors are ≤14% compared with observed average corrosion rates when considering both continental and environmental parameters **Equation 2.5**. Calculation based on **Equation 2.6** showed very high error percentage (48%) when the regression was done by using only temperature and relative humidity of the test sites. According to behaviors of these calculated prediction equation, it can be concluded that the continental effects are also considerable parameters for on atmospheric corrosion of materials.

Table 2.8 A comparison of corrosion rates by experiment and calculation (SMA)

Test sites	Obs. Corr. Rate	Cal. Corr. Rate[5]	Errors , %	Cal. Corr. Rate[6]	Errors, %
T1	13.449	13.151	-2	6.875	-48
T2	7.100	7.654	7	7.358	3.5
T3	5.184	5.479	5	5.219	1
T4	4.473	4.173	-7	6.692	33
T5	6.503	6.374	-2	8.667	25
T6	4.594	4.939	7	5.449	16
T7	3.609	3.153	-14	5.321	32
T8	1.956	1.971	1	1.915	-2

[5]Using Equation 2.5 (considering both continental and environmental parameters)

[6]Using Equation 2.6 (only environmental parameters are included)

It is noted that the coastal distance (in the reciprocal form of atmospheric chloride) more strongly influence the corrosion rate of both carbon and weathering steels in current test locations. This is due to the similar weather conditions with so much differences are not observed in their temperature and relative humidity. For this case, atmospheric chloride extent is the vital factor for first year corrosion prediction. Similar performances were observed in both carbon and weathering steels in their very first year of exposure.

2.5 Analysis of long-term atmospheric corrosion

Linear bi-logarithmic law **Equations 2.7 and 2.8** are utilized as the most common approach for prediction of long-term atmospheric corrosion. According to this law, atmospheric corrosion damage is considered as a function of time on the mathematical basis since the atmospheric corrosion rate usually is not linear with time and the buildup of corrosion rate over time. This law has shown to be applicable to different types of atmospheres (rural, marine, industrial etc.) and for a variety of alloys, such as carbon steels, weathering steels, galvanized steels, and aluminized steels. Combination of so many alloy and environment are not allowed for this law (S.Syed, 2006). The linear bi-logarithmic law can be expressed mathematically expressed as:

$$C = kt^n \tag{2.7}$$

or

$$log_{10}C = log_{10}k + nlog_{10}t \tag{2.8}$$

where: C is the corrosion loss and t is the exposure time; k is a function of environmental and atmospheric parameters (TOW, CL^-, SO_2, T, etc..)

According to linear bi-logarithmic law, the atmospheric behavior of a specific material at a specific location can be defined by the two parameters k and n. The initial corrosion rate, observed during the first year of exposure, is described as k, while n is a measure of the long-term decrease in corrosion rate or passivation of materials which is directly dependent on the metal, the physical-chemical atmospheric conditions and the exposure conditions.

Higher n value which is greater than 0.5 suggests that the rust layer is loosely adherent, results in and increase in the corrosion reaction. A value of n lower than 0.5 results from a decrease in the diffusion coefficient with time through re-crystallization, compaction of rust layer, etc. The equation can be generalized to any location by defining the k and n values as a function of atmospheric variables. Logarithmic conversion of data for long term atmospheric corrosion of the measured test sites and exposure time were used to find n values for each test locations.

2.5.1 Prediction equations for outdoor atmosphere

Outdoor exposure corrosion losses data for 3 years exposure at Yangon and Mandalay test sites are shown in **Figure 2.18**. Corrosion losses in Yangon in both SM and SMA steels are higher than that in Mandalay. SM steel corrosion losses in both test sites are higher than SMA steels. Therefore, weathering steel protective layer formation is in progress until three years of exposure. It can also be seen that corrosion losses are still increasing at three years of exposure period.

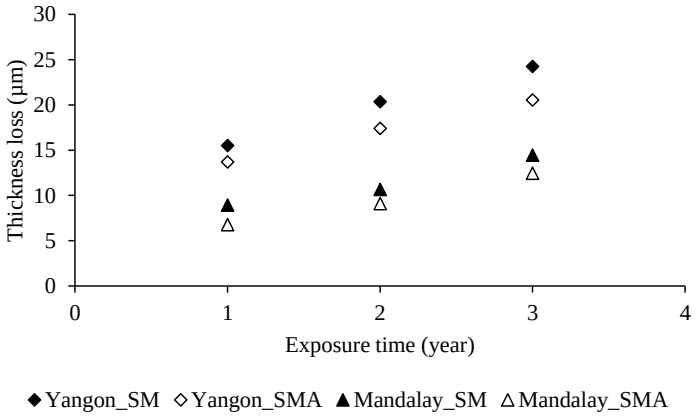

Figure 2.18 Long-term corrosion in outdoor atmosphere

Prediction of long-term corrosion under outdoor atmosphere have been formulated by using measured corrosion data and exposure period. The prediction equations are modelled by Linear Bi-logarithmic Law (Equations 7 and 8). The calculated prediction equations are shown in **Table 2.9**.

The n values of lower than 0.5 are observed in both SM and SMA prediction equations under outdoor exposure test.

Table 2.9 Variables of prediction equations' trend curves (n and k)

Test Site	Carbon steel (SM)		Weathering steel (SMA)	
	n	*k*	*n*	*k*
Yangon	0.405	15.5	0.366	13.7
Mandalay	0.419	8.92	0.366	6.76

According to this, the stabilization is initiating at three years exposure time. Moreover, weathering steel seems more protective in corrosion than carbon steel in outdoor atmosphere.

2.5.2 Prediction equations for shelter atmosphere

Measurement of 3.5 years corrosion losses have been taken in eight test sites. The highest losses were observed in Sittwe, the closet city to the sea with the highest thickness losses is over 0.025 mm in both SM and SMA steels. Similar performances were observed for both SM and SMA steels. All specimens are in their incubation period and stabilized corrosion layers have not developed yet in all the test sites. The measurement results are as shown in **Figure 2.19.**

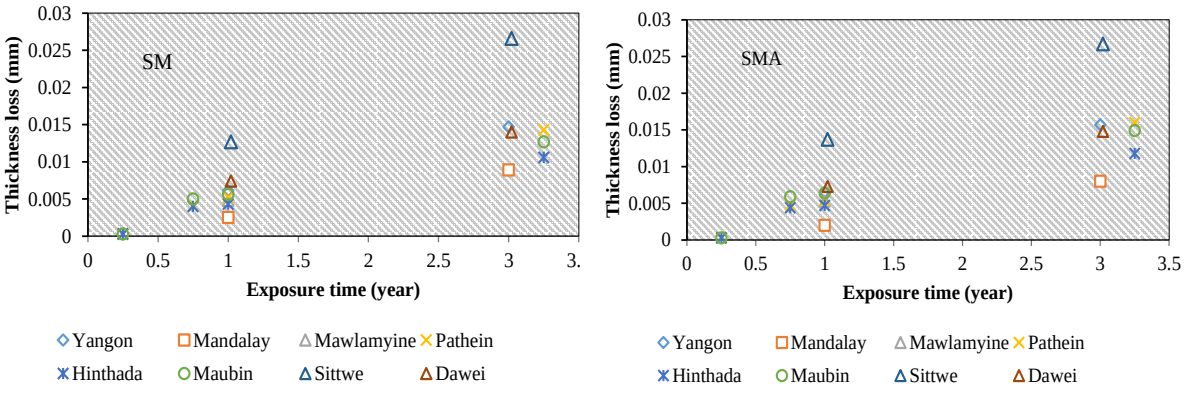

(a) Carbon steel (SM) (b) Weathering steel (SMA)

Figure 2.19 Long-term corrosion losses of SM and SMA steels (shelter)

The results of power coefficients by simple linear regression of corrosion rates against exposure period of SM and SMA steels at the each test site are shown in **Table 2.10**. High power coefficients greater than 0.5 are observed in both SM and SMA steels.

These higher n values revel that the corrosion process of all specimens are in progress during these exposure period. More exposure time is necessary to study the

formation of stabilized corrosion layers on weathering steel specimens under shelter atmosphere.

Table 2.10 Regression analysis result on power coefficients (n and k)

Test site	SM		SMA	
	n	*k*	*n*	*k*
Sittwe	0.931	12.7	0.937	13.7
Dawei	0.746	7.4	0.758	7.3
Pathein	0.910	5.2	0.945	5.4
Yangon	0.746	6.1	0.766	6.5
Maubin	0.896	5.6	0.949	6.4
Hinthada	0.826	4.3	0.861	4.7
Mandalay	0.568	2.5	0.528	2.0

For better understanding of long term atmospheric corrosion kinetics and to determine the usability of atmospheric and geographical parameters for multi-year corrosion prediction, multiple linear regression analyses were carried out by using calculated slope values and respective environmental parameters (temperature, relative humidity, distance from the sea shore and elevation). 95% confidence level is considered in the analysis. The summary of regression analysis results for SM and SMA steel are shown in **Tables 2.11 and 2.12**.

By reviewing the tables, it is clear that environmental and geographical parameters of the test sites are strongly influent on the variance of slope variable in long term corrosion prediction model. Most of the parameters considered in regression analysis are significant. The best regression model is specified as the one giving the smallest standard error and highest F value. The regression that produced the highest F value for both SM and SMA steel is T (temperature). This regression showed significant R^2 value and also the highest F values. The negative correlation was observed between temperature and the intercept values. It means that the temperature deaccelerate the long-term corrosion in both SM and SMA steels. However, relative humidity effect is positive in both types of steels, i.e. higher relative humidity causes the rust layer to be less protective. Both geographical parameters (costal distance and elevation) show the negative effect on the time exponent with very high F value observe in elevation. This

regression against the time exponent and environmental parameters showed that both SM and SMA steel exponents were increased by relative humidity and decreased by temperature.

The prediction of long term atmospheric corrosion loss is carried by the formulated equations using measured corrosion rates and atmosphere parameters of each test sites. The estimated 100 years corrosion thickness loss of SM and SMA steels are shown in **Figure 2.20 and Figure 2.21** regarding with distance from coastal.

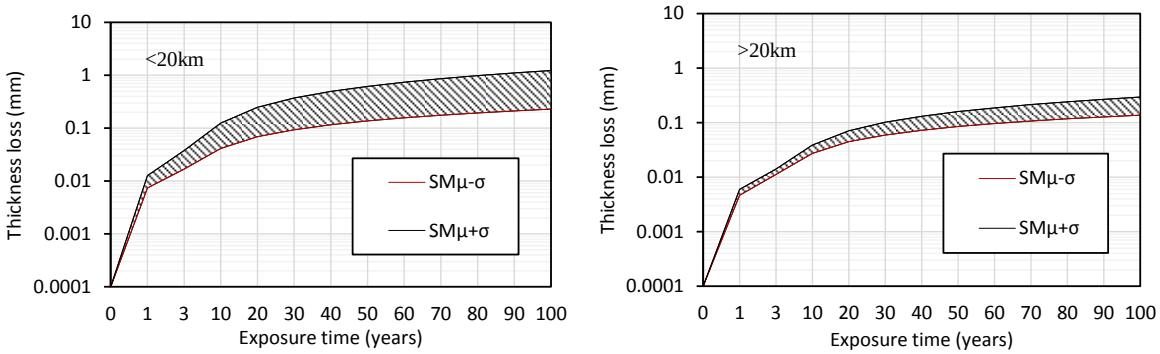

(a) Coastal distance < 20 km (b) Coastal distance > 20 km

Figure 2.20 Long-term prediction of SM steel (shelter exposure)

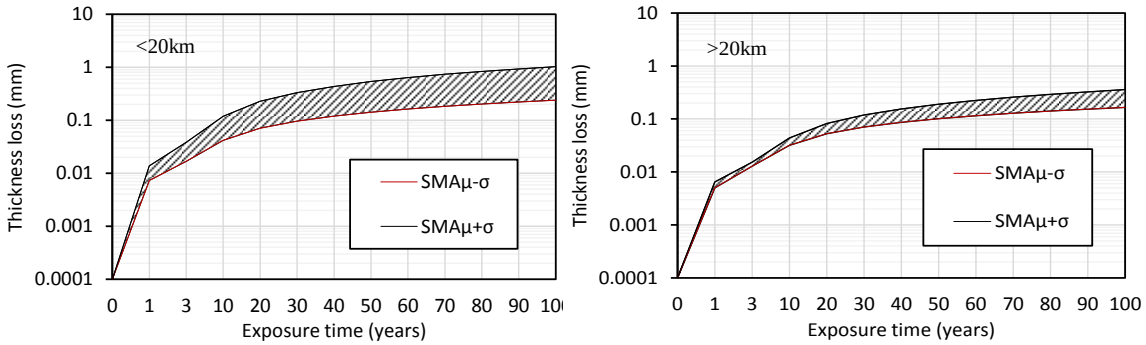

(a) Coastal distance < 20 km (b) Coastal distance > 20 km

Figure 2.21 Long-term atmospheric corrosion of SMA steel (shelter exposure)

All prediction equations in figures are driven by the corrosion losses of unpainted carbon and weathering steels. Coastal distance 20 km is defined as a referenced distance because the concentration of flying salt content in Mawlamyine test site (21 km away from the seashore) is well below the limit chloride deposition value, 0.05 mdd. Although painted carbon steels are mostly used in real structures, thickness loss by corrosion can be judged by this predicted SM steel corrosion loss. The prediction curve for weathering steel can be useful for determining the suitability of unpainted weathering steel consideration on the coastal distance.

The present predicted losses are based on three years results of thickness loss measurement. Corrosion stabilization phase of weathering steels cannot contain in this study. More exposure time and data are needed to improve this prediction trend curve, especially for weathering steel. A graphical representation of corrosion severity of test sites through the country is provided in **APPENDIX B**.

2.5.3 Comparative study of outdoor and shelter corrosion

Corrosion rates in outdoor exposure are much higher than that in shelter exposure. It is explaining that corrosion losses change with type of exposure conditions.

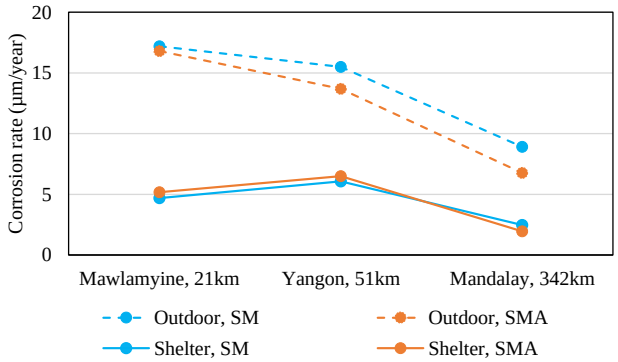

Figure 2.22 Outdoor and shelter corrosion rates

According to **Figure 2.22**, it can be seen that corrosion rate of carbon steel is higher than weathering steel in outdoor exposure test, however, the results show reverse in shelter exposure results. It can be concluded that wet-dry cycle induced by rain effect and direct sunlight in outdoor exposure environment provides a faster production of weathering steel protective rust layer than shelter exposure environment. The observation of protective layer formation on the weathering steel needs more exposure time and it is still ongoing at the test sites.

Table 2.11 Summary of regression analysis on slope vale with atmospheric and geographical data (SM steel)

Regression variables	R^2	SE	F	$T^{(1)}$		$RH^{(2)}$		$D^{(3)}$		$E^{(4)}$		$Int^{(5)}$
				Coef.	t	Coef.	t	Coef.	t	Coef.	t	
T, RH, D, E	**0.993**	0.058	6.939	-0.077	**-2.347**	-0.019	-0.996	6.11E-5	0.06	-0.0056	**-1.749**	4.511
T, RH, D	0.83	0.075	4.822	-0.074	-1.753	-0.017	-0.653	-0.0009	-0.894	-	-	4.198
T, RH	0.785	0.073	7.291	-0.062	-1.589	-0.004	-	-	-	-	-	2.206
T, D	0.805	0.069	8.298	-0.057	-1.845	-	-0.0003	-0.0003	-0.813	-	-	2.428
RH, D	0.656	0.092	3.811	-	-	-0.101	-0.0003	-0.0003	-0.284	-	-	0.046
T, E	**0.861**	0.058	**12.438**	-0.047	**-1.922**	-	-	-	-	-0.0023	**-1.592**	2.174
RH, E	0.734	0.081	5.521	-	-	-0.001	-	-	-	-0.0041	-1.132	0.784
D, E	0.737	0.006	5.624	-	-	-	0.0002	0.0002	0.25	-0.0054	-1.218	0.893
T*	**0.773**	0.066	**17.093**	-0.077	**-4.134**	-	-	-	-	-	-	2.952
RH	**0.649**	0.083	**9.241**	-	-	0.018	**3.04**	-	-	-	-	-0.497
D	0.640	0.084	8.906	-	-	-	-0.0008	-2.984	-2.984	-	-	0.878
E	**0.734**	0.073	**13.765**	-	-	-	-	-	-	-0.892	**-3.71**	0.892

(1) T is the average measured temperature in °C.
(2) RH is the relative humidity in %.
(3) D is the distance from the sea to the test site in km.
(4) E is the test site location height above the sea level.
(5) Int is the intercept values of regression.
R2 is the square of the multiple correlation coefficients.
SE is the standard error of the regression.
F is the ratio of regression variance to residual variance and t is the ratio of coefficient value to its standard deviation.

Table 2.12 Summary of regression analysis on slope vale with atmospheric and geographical data (SMA steel)

Regression variables	R^2	SE	F	$T^{(1)}$		$RH^{(2)}$		$D^{(3)}$		$E^{(4)}$		$Int^{(5)}$
				Coef.	t	Coef.	t	Coef.	t	Coef.	t	
T, RH, D, E	**0.971**	0.0447	**16.931**	-0.0895	**-3.531**	-0.0213	-1.369	0.0003	0.354	-0.0073	**-2.918**	5.006
T, RH, D	0.849	0.0837	5.63	-0.0865	-1.823	-0.0174	-0.599	-0.0011	-0.868	-	-	4.599
T, RH	0.811	0.0812	8.599	-0.0732	-1.684	0.0058	0.537	-	-	-	-	2.431
T, D	**0.831**	0.0768	**9.842**	-0.0692	**-2.006**	-	-	-0.0003	-0.89	-	-	2.782
RH, D	0.682	0.1053	4.289	-	-	0.0148	0.512	-0.0003	-0.237	-	-	-0.241
T, E	**0.896**	0.0603	**17.179**	-0.056	**-2.192**	-	-	-	-	-0.0028	-1.939	2.438
RH, E	0.771	0.0894	6.723	-	-	0.0012	0.071	-	-	-0.0051	-1.275	0.834
D, E	0.779	0.0879	7.027	-	-	-	-	0.0004	0.381	-0.0071	-1.455	0.931
T*	**0.787**	0.0752	**19.715**	-0.0932	**-4.44**	-	-	-	-	-	-	3.417
RH	**0.678**	0.0949	**10.504**	-	-	0.0215	**3.241**	-	-	-	-	-0.76
D	0.661	0.0972	9.757	-	-	-	-	-0.001-	-3.124	-	-	0.911
E	**0.770**	0.0801	**16.79**	-	-	-	-		-	-0.0053	**-4.096**	0.929

(1) T is the average measured temperature in °C.
(2) RH is the relative humidity in %.
(3) D is the distance from the sea to the test site in km.
(4) E is the test site location height above the sea level.
(5) Int is the intercept values of regression.
R2 is the square of the multiple correlation coefficients.
SE is the standard error of the regression.
F is the ratio of regression variance to residual variance and t is the ratio of coefficient value to its standard deviation.

2.6. Atmospheric Corrosion in Asia

An atmosphere in Asia has not only high temperature but also high humidity and which can stimulate a high risk of material deteriorations so called atmospheric corrosion. E-Asia project named "*Corrosion Mapping of Structural Materials in Asia Area with Understanding Effects of Environmental Factors*" has been started in Japan, Vietnam and Thailand during 2013-2015. Dara (2017), a former doctoral student from Yokohama University (Japan), measured atmospheric corrosion in Cambodia and mapped the atmospheric corrosion in Asia region with the data combination with E-Asia data. According to the author, behaviors of atmospheric corrosion in Asia region are different. The corrosion rates in Asia atmospheres are highly affected by temperature and chloride deposition rate; while those in the Europe atmospheres (Czech Republic), the corrosion rates are predominated by SO_2 deposition rates. MICAT research program (M. Morcillo, 1995) conducted atmospheric corrosion surveys in the South-America, and the results show that temperatures, relative humidity and time of wetness are insensitive to corrosion rates; while the SO_2 and Cl^- deposition rates notably affected to the atmospheric corrosion. Corrosion rates are different against the location of test sites.

In this study, mapping of corrosion definition of the influenced factors of atmospheric corrosion in Asia environment by using adopted environmental and corrosion data in Japan and Vietnam and measured experimental data in Myanmar (Section 2.3.3). These investigation includes data of 25 test sites in Japan and 22 test sites in Vietnam. The referenced atmospheric corrosion and environmental data of Japan and Vietnam are given in APPENDIX C. Moreover, the experimental results by Sato (2010), corrosion rates in Kular Lumpu, Malaysia and Singapore are also presented on the corrosivity map.

2.6.1 Corrosivity category mapping

The corrosivity of atmosphere in Asia regions are defined according to the ISO standard. **Table 2.13** and **Figure 2.23** show the measured corrosivity class and corrosivity map. A corrosivity range from C2 and C3 is mostly classified in Asia's atmosphere. The highest corrosivity, C4, is observed in Phuket, Thailand and Okinawa, Japan because these two test sites are located in coastal zones where airborne salt concentrations are high.

The corrosivity in Vietnam increases from the south to the north where the areas are covered by mountainous regions and high RH is noted which leads to higher corrosion rate than the southern part of the country. Low corrosivity, C2, is observed in the inland of Thailand and Cambodia except some coastal test sites have medium corrosion, C3. Singapore and Kuala Lumpur, Malaysia also have low corrosivity atmosphere. The southern part of Myanmar is covered by the flat regions with tropical monsoonal climate which belong to the Bay of Bengal and the Andaman Sea. The central part of the country has dry steppe climate with tremendous high temperature. The northern part of the country are all mountainous regions and own temperate dry climate. The current measurement results show that the corrosion in the south part is higher than the central part. It seems that the corrosion rates are different with climatic and geographical conditions. The experiment at the northern part of the country is still doing and the map will be completed with updated information in the future.

Table 2.13 Corrosivity classifications

Country	**Japan**		**Vietnam**	
No	Test sites	Category	Test sites	Category
1	Asahikawa	C2	Son La	C2
2	Akkeshi	C2	Yen Bai	C3
3	Sapporo	C2	Cua Ong	C3
4	Niigata	C2	Hanoi	C3
5	Fukui	C2	ConVanh	C3
6	Sendai	C2	Dong Hoi	C3
7	Tsukuba	C2	Dung Quat	C3
8	Choshi	C3	Pleiku	C2
9	Yamanakako	C2	Phan Rang	C2
10	Shimizu	C2	Bien Hoa	C2
11	Fukuyama	C3	Can Tho	C2
12	Fukuoka	C3	Rach Gia	C2
13	Kagoshima	C3	Ca Mau	C2
14	Nishihara	C3	Tam Dao	C3
15	Uruma	C3		
16	Miyakojima	C4		

Table 2.13 Corrosivity classifications (continued)

Country	**Singapore**		**Malaysia**	
No	Test sites	Category	Test sites	Category
1	Singapore	C2	Kuala Lumpur	C2
Country	**Thailand**		**Cambodia**	
No	Test sites	Category	Test sites	Category
1	Chiangmai	C2	Phnom Penth	C2
2	Khon-Kaen	C2	Kampong Cham	C2
3	Pathumthani	C2	Sihanoukville	C3
4	Bangkok	C2		
5	Cholburi	C2		
6	Rayon	C2		
7	Phuket	C4		
Country	**Myanmar**			
No	Test sites	Category		
1	Yangon	C3		
2	Mandalay	C2		
3	Mawlamyine	C3		

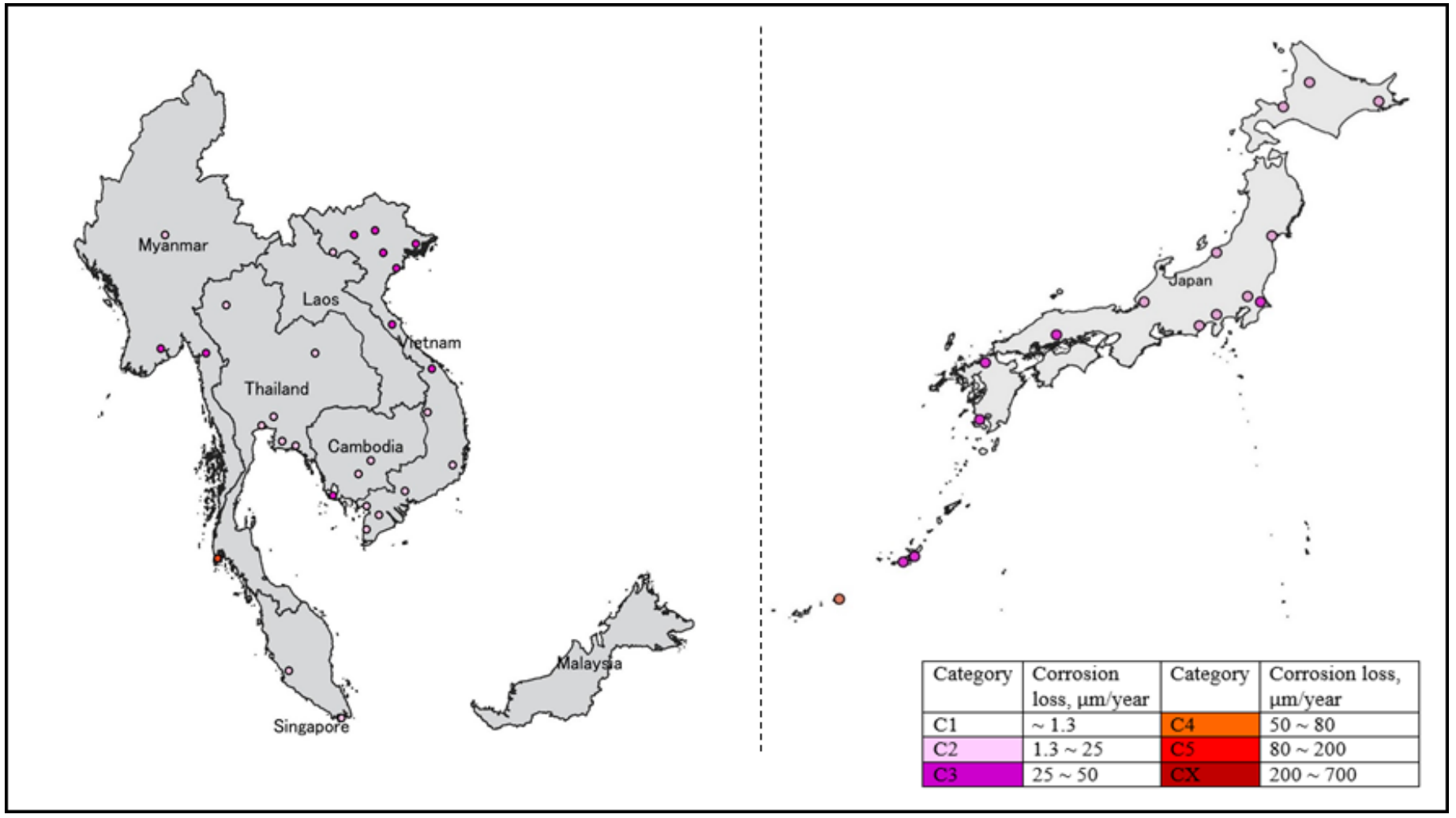

Figure 2.23 Atmospheric corrosivity classification in Asia region by ISO 9223

2.6.2 Factors influencing atmospheric corrosion in Asia environment

The relation between corrosion rate of carbon steel and temperature is shown in **Figure 2.24**. In this figure, it can be realized that the corrosion rate at the temperature less than 23 °C increase with increasing air temperature. However, the corrosion rate at the temperature higher than 23 °C shows decreasing with increased air temperature. The reason of this mechanism is that higher air temperature create the specimen surfaces dry faster and reduce the time of surface wetting to accelerate the corrosion process. It is also observed that temperature in Myanmar and Vietnam are higher than Japan which leads to downgrade the corrosion rate with increasing temperature in this two countries.

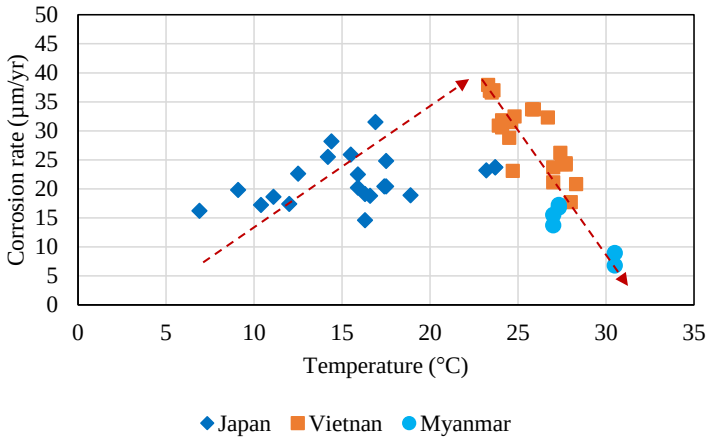

Figure 2.24 Relationship between corrosion rate and temperature

Figure 2.25 shows a correlation between corrosion rate and relative humidity. As can be seen in the figure, corrosion rates in Japan, Vietnam and Myanmar are increased with increasing humidity. It can also be noted that corrosion rate in Myanmar is lower than other countries where they have higher airborne salt and the sulphur dioxide in the atmosphere.

The relationship between corrosion rates and TOW is given in **Figure 2.26**. TOW in Myanmar and Vietnam are higher than in Japan. A positive linear relationship is observed between corrosion rate and TOW which is same is correlation with humidity.

The expression of correlation between corrosion rate and airborne salt is shown in **Figure 2.27**. The correlation is not so clear in airborne salt content less than 10mmd, however, a trend looks positive linear correlation after the airborne salt content of 5

mmd. It might be discussed that airborne salt content higher than 5 mmd promotes atmospheric corrosion process in Asia environment.

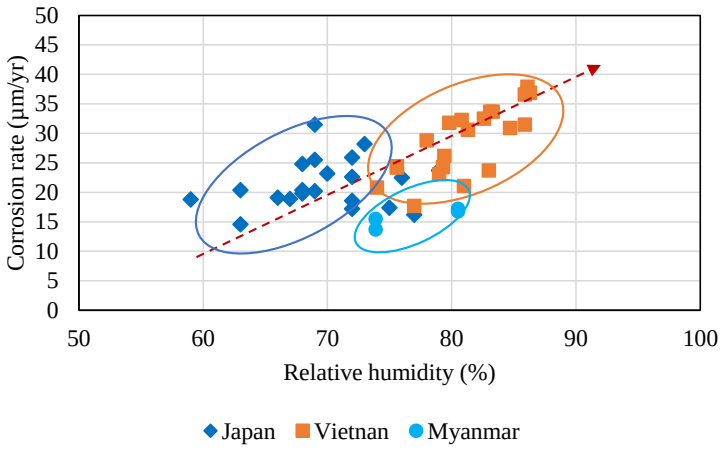

Fig. 2.25 Relationship between corrosion rate and relative humidity

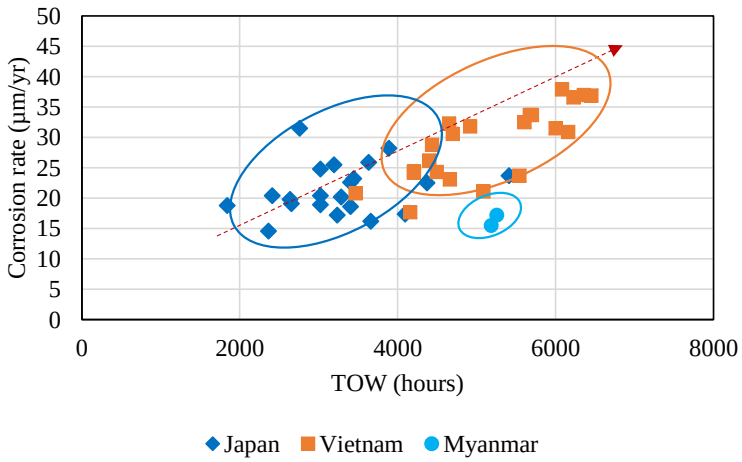

Fig. 2.26 Relationship between corrosion rate and time of wetness

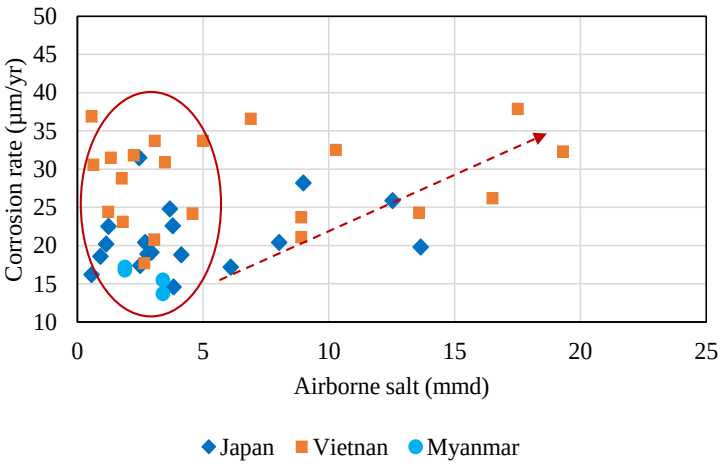

Fig. 2.27 Relationship between corrosion rate and airborne salt

Figure 2.28 shows the relation between corrosion rate and sulphur dioxide. The figure shows that the data are very scattered and clear relation is not able to decide. It can be roughly discussed that sulphur dioxide does not dominate on the corrosion rates in Japan and Myanmar.

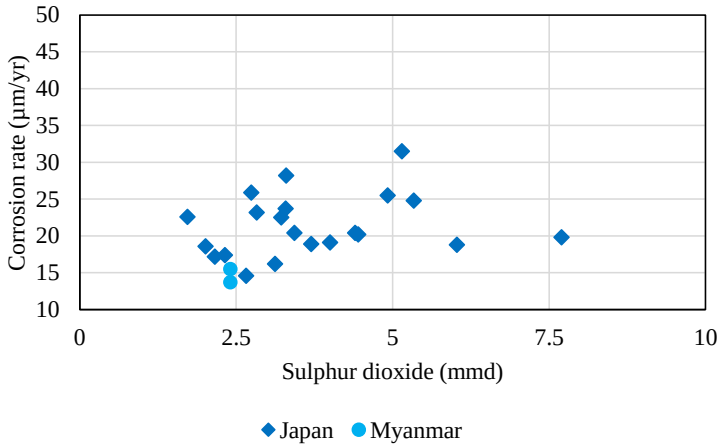

Fig. 2.28 Relationship between corrosion rate and sulphur dioxide

Temperature and humidity influence predominantly on corrosion rates in Asia environment. Moreover, higher concentration of airborne salt can also accelerate the corrosion process. The sulfur dioxide content in the present study are not significant to find out the relation with corrosion rates.

2.6.3 Comparison of Measured Corrosion Losses and Approximated Corrosion Losses by ISO 9223

The ISO 9223 standard (ISO 9223, 2012) describes a Dose-response function to calculate the first year corrosion of four standard metals; carbon steel, zinc, copper and aluminium. The standard presents the corrosion attack after the first year of exposure in open air as a function of SO_2 dry deposition, chloride dry deposition, temperature and relative humidity. The functions of that standard are based on results of worldwide corrosion exposures and cover climatic earth conditions and pollution situation. A Dose-response function provided by the ISO 9223 standard (ISO 9223, 2012) is shown in **Equation 2.9**. According to the finding of atmospheric corrosion in Asia by Dara (2017), Dose-response functions suggested by ISO 9223 are not applicable to predict the atmospheric corrosion rate in Asia atmospheres. The author also drove a modified Dose-response function to fit the actual atmospheric corrosion

test by using data from E-Asia research project, which is an atmospheric corrosion research through Japan, Vietnam and Thailand. The modified Dose-response function by Dara is as shown in **Equation 2.10**. The equation considered changes in temperature range and reducing in the effect of sulphur dioxide to fit with Asia atmosphere.

$$r_{corr} = 1.77 \cdot P_d^{0.52} \cdot \exp(0.02 \cdot RH + f_{st}) + 0.102 \cdot S_d^{0.62} \cdot \exp(0.033 \cdot RH + 0.04 \cdot T) \quad \textbf{(2.9)}$$

$$f_{st} = 0.1 \cdot (T - 10)\ where\ T \leq 10\ °C; otherwise - 0.054\ (T - 10)$$

$$r_{corr} = 1.77 \cdot P_d^{0.52} \cdot \exp(0.02 \cdot RH + f_{st}) + 0.4 \cdot S_d^{0.3} \cdot \exp(0.033 \cdot RH + 0.04 \cdot T) \quad \textbf{(2.10)}$$

$$f_{st} = 0.1 \cdot (T - 20)\ where\ T \leq 20\ °C; otherwise - 0.15\ (T - 20)$$

where:

r_{corr} = a first-year corrosion rate of steel, µm/y

T = the annual average temperature, °C

RH = the annual average relative humidity, %

P_d = the annual average SO_2 deposition rate, mg/m^2.day

S_d = the annual average Cl^- deposition rate, mg/m^2.day

The current study evaluates these two equations by considering on adopted data in Japan and current measured data in Myanmar. The comparison of actual corrosion loss versus calculated corrosion loss based on these two equations are shown in **Figure 2.29**.

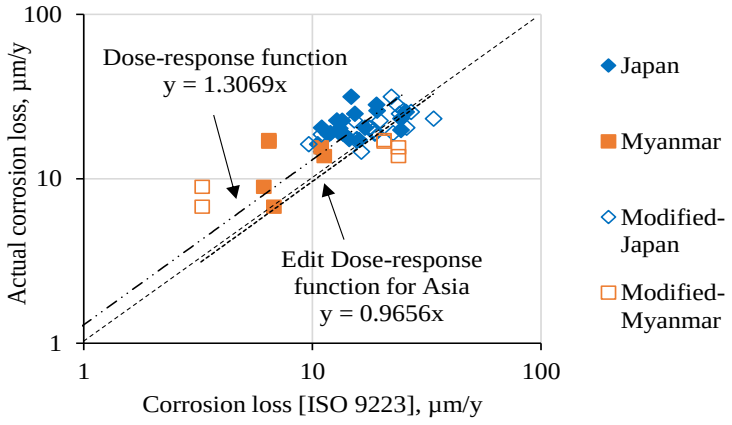

Figure 2.29 Relationship between actual and ISO 9223 corrosion losses

A high error percentage of about ±30% is observed in the results estimated by the equations prescribed by the ISO 9223 standard and the measured values at most sites are higher than the estimated values. However, the modified equation gives only ±3% of error. Therefore, it can be judged that **Equation 2.10** provides more precise corrosion rates to the measured data in Japan and Myanmar than **Equation 2.9**. By this study, it can be confirmed that the modified Dose-response function is suitable to predict the corrosion rate in Asia atmospheres including Myanmar.

2.7. Discussion and conclusions

This chapter discusses about the atmospheric corrosion measurements of carbon steel (SM) and weathering steel (SMA) at three exposure test sites under outdoor exposure environment and eight exposure test sites under shelter environment in Myanmar. The test sites are located in the southern and central part of the country. First-year corrosion losses at three test sites and four years measurement data at eight test sites are presented. High temperature and relative humidity atmosphere is observed in Myanmar. Level of atmospheric impurities are low at the current test sites. Outdoor corrosion test revels that more or less protectiveness of weathering steels are forming during one year exposure period. Atmosphere corrosivity between C2 and C3 according to the ISO 9223 standard is classified in the southern and middle part of Myanmar. The atmospheric corrosivity class defined by actual measurement on specimen is lower than the corrosivity class determined by environmental parameters according to the ISO 9223 standard. The prediction of corrosion for SM and SMA steels are modeled by using measured 3 years data under the shelter exposure condition.

Corrosion rates of both SM and SMA steels relate with the distances from the sea shore logarithmically. According to the measured data and guideline for weathering steel use, it is defined that the use of weathering steel in Myanmar is recommended. Determination of Dose-response functions of corrosion under shelter exposure expresses that geographical parameters are considerable for the first-year corrosion loss calculation. The comparative study of outdoor and shelter exposure test results show that weathering steel can develop protective rust layer faster in outdoor exposure than in shelter exposure due to the wet-dry cycles induced by direct rain and sunlight effects.

The corrosivity classifications in several Asia countries are mapped. To define the influenced parameters of atmospheric corrosion in Asia Region, correlations of atmospheric corrosion rates and environmental parameters in Japan, Vietnam and Myanmar were carried out. A complex nature of the effect of temperature on atmospheric corrosion is observed. Corrosion rates increase with increasing air temperature when T < 23 °C and decrease when T > 23 °C. Relative humidity mainly predominate on the corrosion rate. Combined effect with relative humidity and air impurities can be seen in Japan and Vietnam since corrosion rates in these two countries are higher than Myanmar when similar RH value is observed. TOW also shows positive linear effect on corrosion rates. Airborne salt content lower than 10mmd shows low influence on corrosion rate, however, there has relation between corrosion rate and airborne salt at the airborne salt content is higher than 10mmd. Sulfur dioxide has no significant effect on corrosion rate because the data adopted in present study are the measurement results in urban environment and own low SO_2 deposition rate.

A suitable Dose-response function has been approved to calculate the first-year corrosion of carbon steel in Asia atmosphere. It is noticeable that a Dose-response function prescribed by ISO 9223 cannot use in Asia atmosphere due to differences nature of atmospheric conditions. A modified Dose-response function with higher temperature ranges and lower Sulfur dioxide effects is determined as an appropriate Dose-response in Asia region.

References

Annual Atmospheric Corrosion of Carbon Steel Worldwide (2017). An Integration of ISOCORRAG, ICP/UNECE and MICAT Databases. *Materials*, *10*(6), 601. https://doi.org/10.3390/ma10060601

Aung L. L., Zin E. E., Theingi P., Elvera N., Aung P. P., Han T. T., Skaland R. G. (2017). Myanmar Climate Report. *Norwgian Meterological Institute*, (9), 105.

Brown P.W and Masters L.W, 1982. Atmospheric Corrosion, Wiley, New York.

Brown, C.W., Heidersbach, R.H. 1987. "Raman spectra of possible corrosion products of iron appl. Spectrosc". The journal of SAGE 6, no. 62: 532-535.

Belén Chico, Daniel de la Fuente, Iván Díaz, Joaquín Simancas and Manuel Morcillo, Annual Atmospheric Corrosion of Carbon steel Worldwide. An Integration of ISO CORRAG, ICP/UNECE, and MICATDatabases, Madrid, Spain (2017).

Corrosion-doctors.org. 2021. *Factors Affecting Atmospheric Corrosion*. [online] Available at: <https://corrosion-doctors.org/Corrosion-Atmospheric/Factors-atmospheric.htm> [Accessed 26 April 2021].

Corvo, F., Perez, T., Dzib, L. R., Martin, Y., Castañeda, A., Gonzalez, E., & Perez, J. (2008). Outdoor-indoor corrosion of metals in tropical coastal atmospheres. *Corrosion Science*, *50*(1), 220–230. https://doi.org/10.1016/j.corsci.2007.06.011

Corrosion of metals and alloys-removal of corrosion products from corrosion test specimens, ISO 8407, 2009.

Corrosion of metals and alloys-corrosivity of atmospheres-determination of corrosion rate of standard specimens for the evaluation of corrosivity, ISO 9226, 1992.

Corrosion of metals and alloys-corrosivity of atmospheres-classification, determination and estimation, ISO 9223, 2012.

Dara, T. (2017), Evaluation of Atmospheric Corrosion in Steels for Corrosion Mapping in Asia, *Doctor Thesis*, (September).

Ericsson R, 1978. Werks. Korros., 29:400.

Evans U. R. and Taylor C.A 1972. .J., Corros. Sci., 12:227.

Feliu S, Morcillo M an Feliu Jr. S, 1993. Corros. Sci., 34:403.

Fontana, M. G. (Mars G. (1986). *Corrosion engineering*. McGraw-Hill.

Goodwin F.E, 1990. Metallurgy and Perfomance, TMS, Warrendale, 183.

Roberg., Pierre, R., Hand book of corrosion engineering, New York, 200, 58P, pp 66-69, pp 84-85.

http://corrosion-doctors.org/WhyStudy/Strategic-Impact.htm , Visited , 7th June 2012

ISO 8565, 2011: metals and alloys-Atmospheric corrosion testing-*General requirements*

ISO 8407, 1991: Corrosion of metals and alloys - *removal of corrosion products from corrosion test specimens*

ISO 9223, 2012: Corrosion of metals and alloys - *corrosivity of atmospheres - classification.*

Japan Industrial Standard, *JIS Z 2382*, 1998: Determination of pollution for evaluation of corrosivity of atmosphere.

Japan Weathering Test Centre (2006). *Research on Long-Term Durability and Standardization of Life Prediction of Elemental Equipment Related to New Power Generation*, Research Project for Standardization of Development Result, Consignment of New Energy and Industrial Technology Development Organization Result Report, 100007184 (in Japanese).

Japan Industrial Standard, JIS Z 2382, Determination of pollution for evaluation of corrosivity of atmosphere.

Klinesmith, D.E., McCuen, R.H. & Albrecht, O. 2007. Effect of Environmental Conditions on Corrosion Rates. ASCE.

Kreislova, K., Knotkova, D., Krivy, V. & Podjuklova, J. 2014. The Effect of Differentiated Exposure Conditions on Corrosion Behavior of Weathering Steel on Bridges. Research Gate.

Leygraf, C., Wallinder, I.O., Tidblad, J. & Graedel, T. 2016. Atmospheric Corrosion. Second Edition.

L. T. H. Lien, P. T. San, & H. L. Hong (2007). Results of studying atmospheric corrosion in Vietnam 1995-2005. *Science and Technology of Advanced Materials, 8*(7–8), 552–558. https://doi.org/10.1016/j.stam.2007.08.011

L. T. H. Lien and P. T. San, "The effect of Environmental Factors on Carbon Steel Atmopsheric Corrosion; The Prediction of Corrosion," in *Outdoor Atmospheric Corrosion*, ed. H. Townsend (West Conshohocken, PA: ASTM International, 2002), 103-108. https://doi.org/10.1520/STP10886S

L. T. H. Lien, P. T. San, H. L. Hong, "Atmospheric corrosion of carbon steel in Vietnam, The relationship between corrosion rate and environmental parameters, The classification of atmospheric corrosivity of carbon steel", Zairyou-to-Kankyo 2009, A-305 (2009)

Morcillo M, Chico B, Mariaca L and Otero E, 1999. Corros. Sci., 41:91.

M. Morcillo, "Atmospheric Corrosion in Ibero-America: The MICAT Project," in *Atmospheric Corrosion*, ed. W. Kirk and H. Lawson (West Conshohocken, PA: ASTM International, 1995), 257-275. https://doi.org/10.1520/STP14924S

Mikhailov, A. A., Strekalov, P. V., & Panchenko, Y. M. (2007). Atmospheric corrosion in tropical and subtropical climate zones: 3. Modeling corrosion and dose-response function for structural metals. *Protection of Metals*, *43*(7), 619–627. https://doi.org/10.1134/S0033173207070028

Nanda Munasinghe, Shanika Jayathilake, Prediction of atmospheric corrosion – a review, ENGINEER-Vol.XLVII, No. 01,pp.[75-83],2014.

Ohtsuk, T. 1996. "Raman spectra of passive films of iron in neutral borate solution. Mat. Trans". The journal of electrochemical society 11, no. 146: 4061-4070.

Ríos-Rojas, J. F., Aperador-Rodríguez, D., Hernández-García, E. A., & Arroyave, C. E. (2017). "Annual atmospheric corrosion rate and dose-response function for carbon steel in Bogotá". *Atmosfera*, *30*(1), 53–61.

Roberge, P. R. (2008). 59. Corrosion Engineering Principles and Practice, McGraw-Hill, New York, US. In *McGraw-Hill, New York, US*.

SATO, 2010. "Study on the corrosion of weathering steel in southeastern Asia", the conference proceeding of 68th Japan Society of Civil Engineers 2010 Annual Meeting, Japan.

Surnam, B.Y.R. & Oleti, C.V. 2012. Atmospheric Corrosion in Mauritius. Corrosion Engineering, Science and Technology, Vol. 47(6) 446-455.

S.Syed, Atmospheric corrosion of materials, Journal of engineering research, 11(1), 1-24 (2006)

S. Dean and D. Reiser, "Analysis of Long-Term Atmospheric Corrosion Results from ISO CORRAG Program," in *Outdoor Atmospheric Corrosion*, ed. H. Townsend (West Conshohocken, PA: ASTM International, 2002), 3-18.

Y. Yu Kyi Win, T. Khaing, Z. Min Tun, & Y. Suzuki (n.d.) (2017). "Comparative Study on Atmospheric Corrosivity of Under Shelter Exposure in Yangon and Mandalay (Myanmar)". ASRJETS, Vol 27, No. 1, pp 386-404.

Zaki Ahamad, Principles of corrosion engineering and corrosion control

Chapter 3

ACCELERATED LABORATORY CORROSION TESTS

3.1 Introduction

Many researches about the evaluation and prediction of long-term durability anti-corrosive performances of structural steels have been mostly done by the field exposure measurements. However, it may take a long time before any of the deterioration to make examination of performances. Moreover, the field exposure test can sometimes be adhered by the abnormal environmental conditions such as tropical typhoon and other seasonal factors. To avoid this kinds of unfavorable measurement results, accelerated exposure tests were invented in the early 1990s. The accelerated corrosion test is commonly referred as a cabinet test method during which a specimen is exposed to a stress or combination of stresses for a given period of time. After the specific exposure period, the specimens are examined for rust, blisters, pitting, etc. Two main types of tests can be distinguished: static atmospheric testing and cyclic corrosion testing (C. L. Meade, 2000). The statistic environment testing applied a constant single environment throughout the complete during of the test. A well-known example is the salt fog test (ASTM B 117, 2019). The reliable test method for actual outdoor environment is cyclic corrosion test. Numerous accelerated corrosion tests such as SS, S6, DS, JASO, NS and ASTM-cycles etc. are available, nowadays.

Fujiwara (1995) conducted seven sets of test environment (including SS, S6 and others) in the chamber and then compared with the outdoor exposure results at five test sites in Japan for three years. According to the author's finding, S6 cycle test condition could provide the most similar results with the outdoor exposure tests. The S6 cycles accelerated corrosion test specified by Japanese Industrial Standards (JIS K 5621, 2008) with different salt solution intensities were carried out on two kinds of structural steels such as carbon steel (SM) and weathering steel (SMA) in this study.

The use of steel material in bridge requires an adequate protective system to enhance the propagation of corrosion attack. There are several factors to develop the corrosion on steel girders. Exposure to polluted environments, leaking of deicing compounds from the deck, the accumulation of dirt, debris, or sand, and water spray produced by moving vehicles are common sources to initiate the process of corrosion on steel elements (Kayer, 1988; RIDOT, 2002; Crampton et al., 2013). The research by Bowman and Moran (2015), bridge preventive maintenance activities were analyzed as alternative to preserve and maintenance activities. Several bridge maintenance activities are analyzed as alternatives to preserve and extend the bridge service life at a low cost. The study found that bridge superstructure washing with proper frequency can capable of extending the service life of steel girders. Therefore, this activity is performed as alternative activity for bridge maintenance to enhance corrosion in bridge girder.

The objective of this chapter is to study the propagation of corrosion under the simulated atmosphere inside the accelerated chamber. The S6-cycles accelerated test with two different salt solutions (0.5% NaCL concentration and 0.05% NaCl concentration) were performed for about 75 days for each test. The formation of protective layer on the weathering steel surfaces were also identified by changing the program with different solution. Specimen washing with regular frequencies were taken to evaluate the performance of steel washing for the reduction of the corrosion rate. Proper time interval was also addressed for the actual structures in the different corrosive environments.

3.2 Experimental procedures

3.2.1 Combined cyclic test instrument and test conditions

A large-sized combined cyclic corrosion instrument (CPY- 120D) produced by Suga Test Instrument Co., Ltd, which can operate automatically the condition of atomizing of salt water, temperature, humidity in arbitrary order and combinations, was used in this study. This machine can be applicable to performs different cyclic test program such as JIS, ASTM, and ISO. **Figure 3.1 and 3.2** show the overview and the inside view of the machine with specimen installation. The outer dimensions of instrument are 2300 mm in width, 1080 mm in depth and 2150 mm in height. The

available maximum numbers of specimens inside the chamber is up to 88 pieces (150 × 70 × 1 mm). The condition inside the chamber is able to adjustable depends on the desired test conditions.

Two types of S6 cycle tests with varying chloride solution intensity were conducted. The atomizing of chloride solution changed in current tests are conventional 5% salt water for both carbon and weathering steels. In addition, diluted salt water with 0.05% NaCL solution was conducted for weathering steel to find the corrosion products stabilization of weathering steel specimens. The detailed test condition of S6-cycle test according to JIS K 5621 is shown in **Table 3.1**.

Figure 3.1 Combined cycle corrosion test instrument

Figure 3.2 Inside view of chamber with specimen installation

Table. 3.1 S6-cycles combined corrosion test condition

Test condition	Temperature (°C)	Relative humidity (%)	Time (mins)
salt spray	30	98	30
wetting	30	98	90
drying	50	20	120
drying	30	20	120

Total time necessary to accomplish one cycle is six hours which includes 30 mins of salt water atomizing, 90 mins of wetting, 120 mins of drying by hot wind and 120 mins of drying by warm wind. Maximum of 400 cycles were done for the ordinary S6-cycle test and 600 cycles were completed for diluted S6-cycle test.

3.2.2 Specimens preparation

Two kinds of structural steels carbon steel (JIS G 3106) and weathering steel (JIS G 3114) specimens with the sizes of 150 × 70 × 9 mm were prepared to expose under the chamber environment. The chemical composition of specimens are shown in **Table 3.2**.

Table. 3.2 Chemical composition of steels, in wt%

Steel	**C**	**Si**	**Mn**	**P**	**S**	**Cu**	**Cr**	**Ni**
SM 490A	<0.23	0	>25*C	<0.035	<0.035	0	0	0
SM 490AW	<0.18	0.15-0.65	<1.25	<0.035	<0.035	0.3-0.5	0.45-0.75	0.05-0.3

A well-defined surface preparation of specimens prior to the exposure has been done by blasting using steel girt, and then checked to ensure free from oil, grease, dirt, dust, mill scale, rust, oxide according to the methods shown in ASTM G1 Standard (ASTM G1-03, 2017). The preliminary data of specimens such as sizes, weight and thickness were also measured before setting inside the chamber. The electric caliper

with accuracy of 0.01 mm precision and weight balance as shown in **Figure 3.3** were used for specimen size and thickness measurement.

After all this preparation, the specimens were installed inside the chamber with 15° inclination from the vertical positon. In every 100 cycles (25 days of exposure), the specimens were dismounted and measured for the weight and thickness losses. Three specimens were picked up for each time measurement. The installation of the specimens inside the chamber is as shown in **Figure 3.3**.

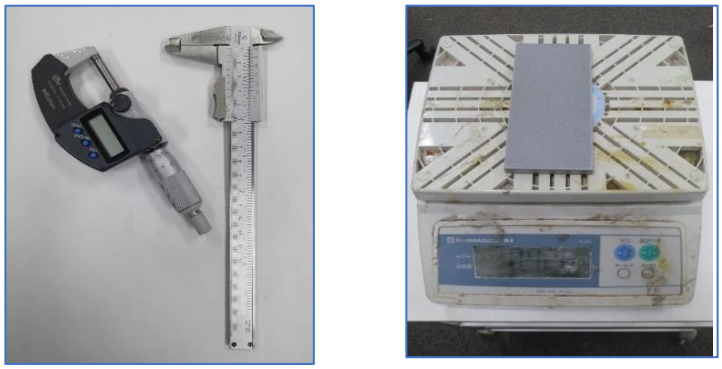

(a) Caliper (b) Weight balance

Figure 3.3 Sizes and thickness measurement

Total of 18 specimens of carbon and weathering steels were installed for 300 cycle exposure period. Every dismounting is followed by corrosion thickness and weight loss measurement.

3.2.3 Corrosion thickness and weight loss measurements

Corrosion thickness measurements on the surface of the specimens were measured by using Advanced Coating Thickness Gauge (Model LZ-370) in **Figure 3.4**. This device can measured the thickness of non-ferrous (non-magnetic) coating on both ferrous (magnetic) and non-ferrous substrates. Both the electromagnetic and eddy current probes are provided for this type of thickness gauge. Measurement range of electromagnetic type is from 0 to 2500 μm and eddy current type is from 0 to 1200 μm. Maximum of 39000 data sets can be saved in the internal memory. 14 measurement points were made on grid and averaged to get the corrosion thickness of the whole surface.

Figure 3.4 Coating thickness gauge (Model LZ-370)

The removing of rust on the test specimens were done by the procedure specified in ISO 8407 (ISO 8407, 1985). This standard includes three general categories such as chemical, electrolytic and mechanical. Chemical cleaning process was used for cleaning of both SM and SMA steels. The procedure of chemical cleaning by ISO 8407 is as shown in **Table 3.3**. Procedure C3.5 was applied in the current study.

Table. 3.3 Chemical procedures for cleaning for corrosion products by ISO 8407

Designation	Material	Chemical	Time	Temperature	Remarks
C.3.1	Iron and Steel	100 ml hydrochloric acid (HCl,ρ= 1.19 g/ml) , 20g antimony trioxide (Sb_2O_3), 50g stannous chloride ($SnCl_2$)	1 to 25min	20 to 25°C	Solution should be vigorously stirred or specimen should be brushed. Longer times may be required in certain instances.

Table. 3.3 Chemical procedures for cleaning for corrosion products by ISO 8407 (continued)

Designation	Material	Chemical	Time	Temperature	Remarks
C.3.2		50g sodium hydroxide (NaOH), 200g granulated zinc or zinc chips, Distilled water to make 1000 ml	30 to 40min	80 to 90°C	Calculation should be exercised in the used of any zinc dust since spontaneous ignition upon exposure to air can occur.
C.3.3		200g sodium hydroxide, 20g granulated zinc or zinc chips, Distilled water to make 1000ml	30 to 40min	80 to 90°C	Calculation should be exercised in the used of any zinc dust since spontaneous ignition upon exposure to air can occur
C.3.4		200g diammonium citrate [$(NH_4)_2HC_6H_5O_7$]	20 min	75 to 90°C	-
C.3.5		500ml hydrochloric acid (HCl,ρ= 1.19 g/ml), 3.5g hexamethylene tetramine, Distilled water to make 1000ml	10 min	20 to 25°C	Longer times may be required in certain instances.

An ideal procedure of this standard is to remove only the corrosion products without removing any of base metal. To determine the mass loss of the base metal when removing corrosion products, replicate un-corroded control specimens were cleaned by

the same procedure as used on the test specimen according to the standard. By weighting the control specimen before and after cleaning, the extent of metal loss resulting from cleaning can be utilized to correct the corrosion mass loss.

The procedure of the rust cleaning is as shown in **Figure 3.5**. During the process of removing the corrosion products, the hydrochloric acid was stirred vigorously for about 10 minutes at room temperature. Soaking of specimens in the prepared solution and loss measurement are shown in **Figure 3.6**.

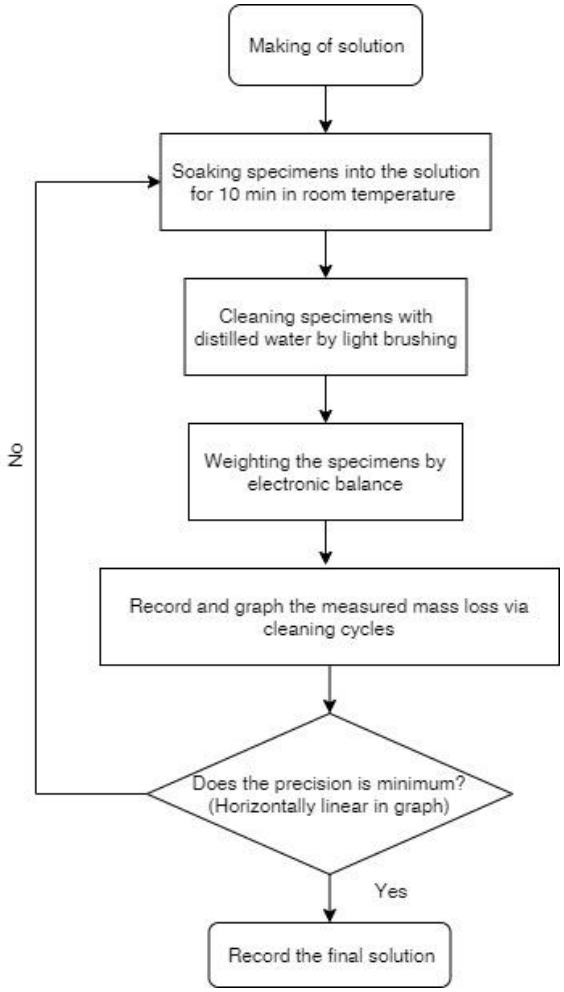

Figure 3.5. Rust cleaning procedures

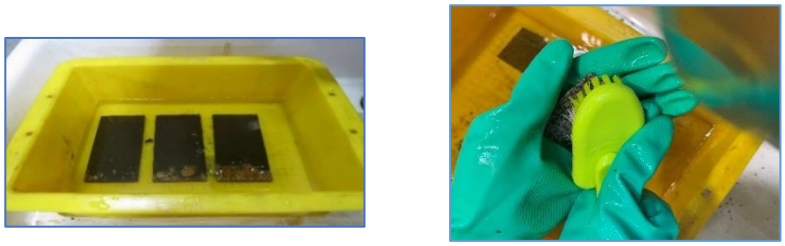

(a) Soaking specimens in solution (b) Light brushing

Figure 3.6. Rust removing process

After the corrosion products had been completely removed, the specimens were rinsed in distilled water following with light brushing. Drying with paper towel and air blowing are also part of the cleaning procedure. The procedure is repeated for the precision of weight loss data. For every specimen, three times of cleaning are taken in minimum. The cleaning procedure is accomplished after whole area of specimens are free from the rust. The surface configuration of cleaned specimen compared with corroded specimens are as shown in **Figure 3.7**.

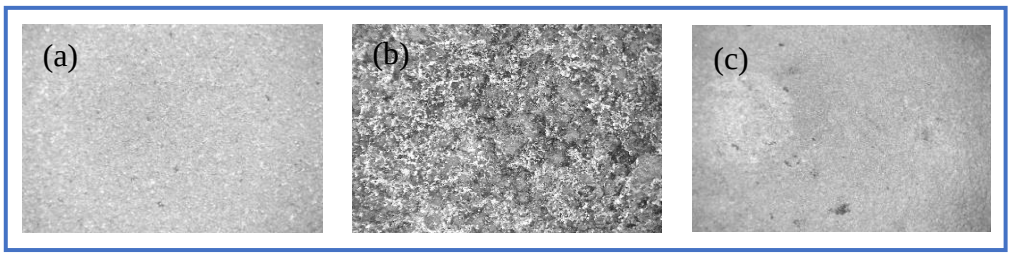

Figure 3.7 Surface configuration ((a) New (b) Corroded (c) Cleaned specimens)

The weight loss was evaluated by subtracting the weight after cleaning from the original specimen weight. The thickness losses of the specimens can be calculated based on the measured weight losses as shown in Equation 3.1.

$$Thick.loss\ (mm) = \frac{Weight\ loss\ (g)}{Surface\ area\ (mm^2) * Specific\ density\ (g/mm^{3)}} \quad \textbf{(3.1)}$$

The stabilization of corrosion layer on the weathering steel surfaces was analyzed by comparing the thickness loss outputs for each time measurement by assuming when the difference is less than 10% of losses.

3.3 Steel washing evaluation

A common method of bridge superstructure washing in the real structure includes the collection and cleaning of solid materials from the superstructure, and followed by the spray of pressured clean water to remove the contaminant compounds from the girder surface. Chloride compounds are the most common and aggressive substances attacking to the girder. Also the accumulation of dirt debris, and dust in the source for corrosion initiation should be cleaned from the steel girder surfaces (Berman

et al., 2013). Appleman et al. (1995), Hara et al. (2005), and Crampton et al. (2013) found that the superstructure water washing is useful to reduce the corrosion initiation due to deicing salt products and other compounds. Although there is an agreement on the benefits of bridge water washing, it is necessary to study the appropriate frequency of washing to obtain the best benefits in different atmospheres.

In present study, steel washing procedure was performed regularly with differences frequencies to evaluate the effect of bridge washing on the reduction of corrosion rates. After getting an adequate frequency washing interval, the equivalent washing period which is necessary for the real structure can be calculated. The purpose of the program is to remove chlorides on the specimen surfaces before they are trapped by the additional dirt debris and soot. Evaluation of water washing effectiveness on chloride removing from weathering steel platina was completed by considering on formation of protective layer on weathering steel. S6-cycle accelerated test with 0.05% NaCl solution and 5% NaCl solution were simulated for about 2 months (200 cycles) testing time. Flat plate specimen sizes with 75 × 150 × 9 mm were used for S6-cycles tests with 0.05% NaCl and 5% NaCl solutions. The differences of surface corrosion thicknesses and weight changes for different washing frequencies were evaluated.

3.3.1 Washing schedule and program

The specimen washing time interval of each test program is shown in **Table 3.4**. Total of seven specimens for both conventional and diluted S6-cycle tests. The specimen washing was taken in every week. Rust thickness, weight change, thickness change and surface salinity concentration measurements were taken after finishing every washing. The duration of washing proceeded till the surface salt concentration remains constant.

Initial data acquisition for the characteristics of each coupon were taken and registered before starting the accelerated test. All coupons were weighted, measured the dimensions (size and thickness) sand taken preliminary surface profiles of each coupon. Thickness was measured at the 14 selected points by using plastic template which can help to measure the thickness of a coupon in the same position every time.

The specimens were placed inside the chamber after all steps of the preliminary measurements were done. At every week of specimen conducting, the programmed coupons were withdrawn from the test chamber and performed physical observations

before power washing. The template of measurement points on the coupon is shown in **Figure 3.8**.

Table 3.4 Specimen washing schedule

Specimen	Week							
	01	02	03	04	05	06	07	08
A025	×	×	×	×	×	×	×	×
A025		×		×		×		×
A050			×			×		
A075				×				×
A100					×			
A125						×		
A000	No washing							

Note: (×) indicates a week to washing corresponding specimen

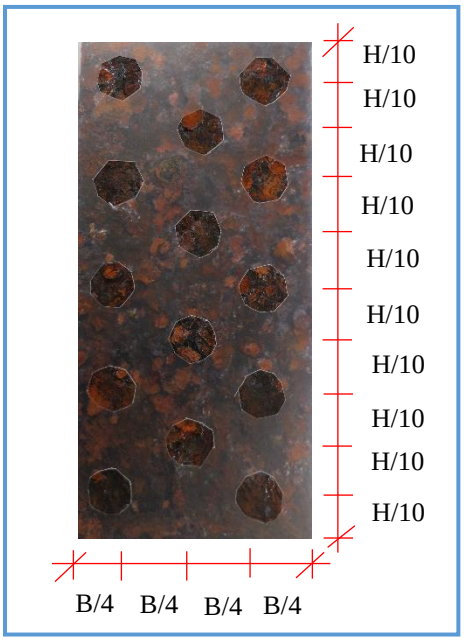

Figure 3.8 Location of thickness measurement points

The specimen washing program is described as shown in **Figure 3.9**. The specimens were washed as predefined wash interval and then drying with natural air for about 2 hours in room temperature. The weight and thickness measurements after washing are also recorded. The program is repeated at every wash interval.

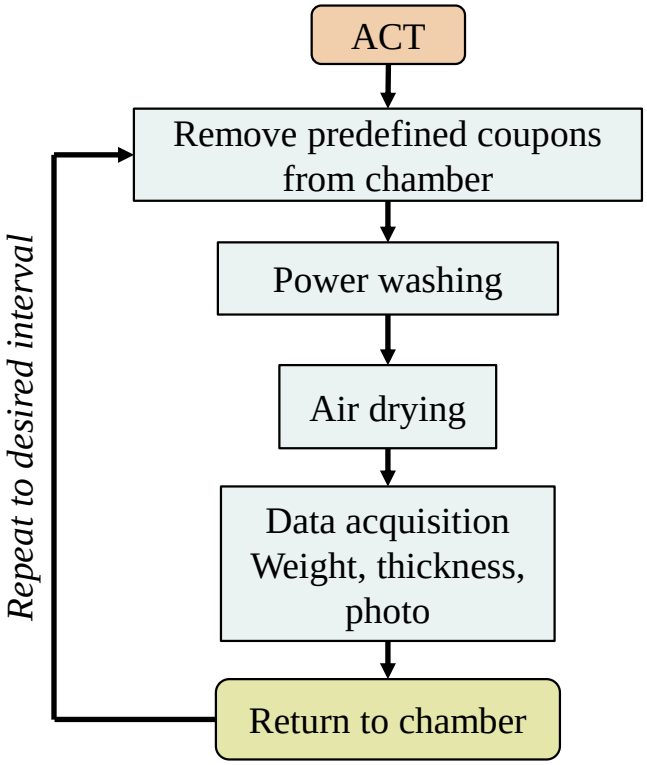

Figure 3.9 Steel washing program

The result of rust thickness value is defined as an average of 14 measurement points. The weight and thickness changes was registered to know the progress of corrosion at the end of every week exposure.

3.3.2 Equipment and its application

Rust removal from specimens were finished by using power washer with 15 MPa pressure capacity. The equipment takes water from a water source and ejects at a high pressure. This equipment is usually used to wash floor and wall surfaces. A strip pressure nozzle was applied to remove loose layer of rust and attached salt on the surfaces. **Figure 3.10** shows the power washer equipment used in this study.

The duration for power washing was varied on the amount of surface salt on the specimens. The selected coupons were taken out from the chamber and set up at the outside of the laboratory for washing. The coupons were washed with the power-washer machine in which water is ejecting at approximately 1450 psi (10 MPa). The distance between nozzle and specimen surface was kept at the constant value of 0.3 m to achieve constant pressure intensity in all specimens. **Figure 3.11** shows power washing of

coupon. The pressure water was applied till the surface salt content does not change by the repetitive surface salinity checking.

Figure 3.10 Power washer equipment

After finish power washing, the specimens were air-dried and returned back to the chamber to continue the accelerated test up to a more desired cycle numbers. The position of coupons inside the chamber were changed every week to reduce some possible error due to the effect of the location inside the chamber on the rate of corrosion.

Figure 3.11 Power washing steel coupons

Electronic balance and measured scale were used to measure weight changes and dimension changes. Corrosion penetration was measured by the corrosion thickness

meter as a similar device with the one in Chapter 2. The measurement of surface deposit salt was carried out by Handheld Surface Salinity Meter (SSM-14P by DKK-TOA CO-OPERATTION) which is shown in **Figure 3.12**. The operation of the salt meter is to attach measurement cell at the surface of measured specimen and inject pure water into the measured cell.

Figure 3.12 Surface salinity checker

During the measurement, the cell was attached to the middle part of specimen and stirring continuously for about 1 minute. The measurement range of the device is between 0 to 1999 mg/m^2 sodium chloride (NaCl). The data displayed on the screen only shows the average amount of adhesive sodium chloride in a diameter of 30 mm cell. After several measurements were finished till the salt percentages are stable on the surface, the specimens were positioned back inside the chamber again and run for another cycles.

3.4 Experimental results

3.4.1 ACT results for thickness loss measurement

The results of accelerated corrosion tests are presented in this section. The visual evaluation of surface condition is done by judging the color of rust products and the roughness of surface. The corrosion penetration on specimen surfaces were also discovered by measuring rust thickness through the chamber exposing time. Corrosion losses were calculated by differencing the weights between tested specimens and as-new specimens.

3.4.2 Rust appearance

Figure 3.13 shows the surface appearances passing through the exposure time. According to this figure, it can be seen that the color of the surface corrosion products change through exposure cycles (from the yellow orange to light brown). According to the figure, it can be seen that the corrosion propagate continuously till 300 cycles in conventional S6-cycles test. Moreover, it can also be observed that size of corrosion product is larger through the exposure. Severe corroded surfaces with loosely adherent rust layers were discovered on the specimens under 5% NaCl accelerated test. To evaluate the protective layer formation on weathering steel surfaces, 0.05% NaCl solution is made for S6-cycles test.

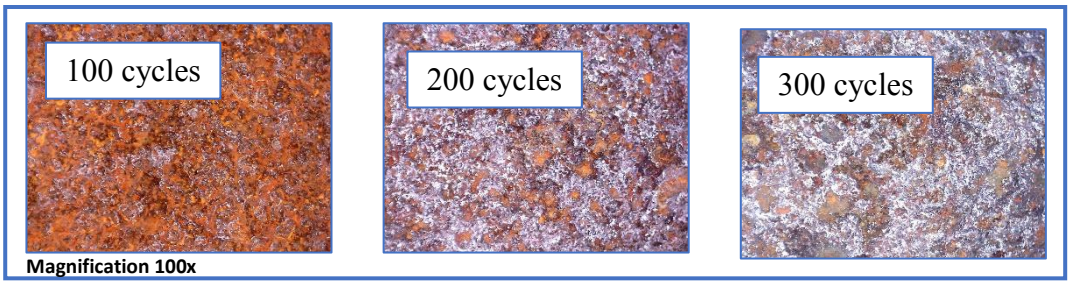

Figure 3.13 Rust color changes of SMAW steel in 5% salt solution test

The surface configuration of specimens in 0.05% salt concentration test are shown in **Figure 3.14**. In 0.05% NaCl test, compact layer of rust is observed on the specimens although poor platina performance results in an endless cycle of platina delamination under 5% NaCL test. On the other side, the diluted salt concentration test developed a dense well platina during the same exposure period.

Finer rust products are seen in diluted test than the conventional test. Moreover, the rust layer is more dense and compact in diluted test. According to this, S6-cycles test with 0.05% salt concentration which is referenced to Cebelcor cyclic test (M. Morcillo et. Al., 2013) for weathering steel is useful for simulation of protective rust layer in weathering steel.

The compactness of rust layer has been started after 200 cycles since the whole surface of specimen is covered by well-adhered protective rust layer. However, the protective patina is not fully formed on the specimen surface yet during this 300 cycles of exposure.

Figure 3.14 Rust color changes of SMAW steel in 0.05% salt solution test

According to R.J. Schmitt and W.P. Gallagher (1969), the formation of dense and well-adhering corrosion product layer of weathering steel is dependent upon the washing action of rain water and the drying action of the sun. The constant atmosphere inside the chamber where there is lack of rain and direct sunlight tented to retard the production of patina. However, the initiation of patina development will be determined in this 0.05% salt solution test.

3.4.3 Rust thickness and losses

The measurement of rust thickness on exposed specimens were taken after every 100 cycles of exposure. The purpose of this measurement is to discover rust layer development through the exposure period and to determine a law which is best fit the atmospheric corrosion of weathering steel in the chamber atmosphere. The correlation plots of rust thickness versus exposure time inside the chamber are as shown in **Figure 3.15**.

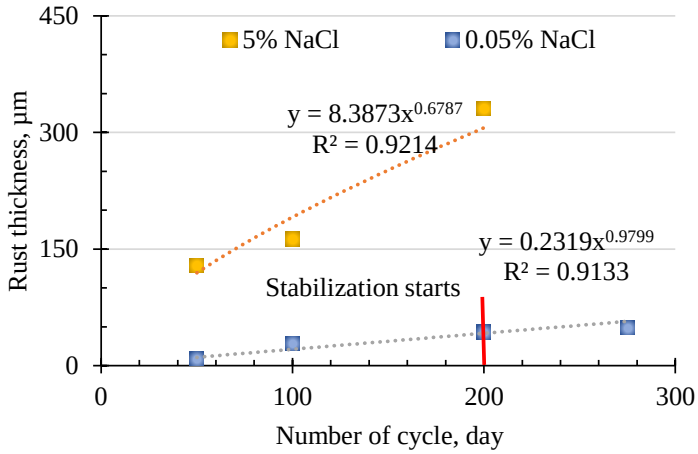

Figure 3.15 Rust thickness versus exposure time

The correlations between rust thickness and exposure time obey the power relation with high significant levels. Higher indexes of power equations show that the rust thickness develop with increased exposure time. According to this, it can be summarized that the development of rust layer in the chamber environment is same with outside atmosphere. The propagation of corrosion products on the specimen surfaces against testing time can also be seen in the figure.

The rust thickness propagation in 5% salt concentration continue to increase with testing time. The rust are so heavy after 200 cycles (50 days of exposure) and it was not be able to measure. The deviation in rust thickness was not so clear at the beginning of exposure, but, almost growing up to double of the rust thickness at 200 cycles (50 days of exposure). Both conventional and diluted tests can increase the rust thickness through exposure time, however, the propagation rate of rust thickness in diluted test deaccelerated after 50 days of exposure.

The stabilization of rust layer started during this period under 0.05% salt concentration S6-cycles test. This reveals that the diluted S6 cycle test with 0.05% NaCl solution is a useful test for determination of rust layer stabilization on weathering steel surface. The removal of rust has been done after every 100 cycles and calculated for thickness losses from the weight loss measurement by using Equation 3.1. After removing corrosion products from the specimens, the weights and thickness were measured and calculated for corrosion rates. The corrosion rates inside the chamber for test are shown in **Table 3.5**.

Table 3.5 Corrosion rate inside chamber

Test program	Corrosion rate (μm/yr.)
Diluted S6-cycles test	873.8
Conventional S6-cycles test	2621.5

The results are applicable to find for the acceleration coefficient of outdoor exposure test sites in other region and can able to extend for the prediction equations.

3.5 Accelerated corrosion test for steel washing evaluation

The results of accelerated test for the evaluation of steel washing program are presented in this section. The scheduled specimens were taken out from the chamber

and had done for washing and data recording. The program of washing were taken according to the **Table 3.1**. With the time inside the chamber, rough and flaky rust products grew on the specimens' surfaces. The rust propagation on the surfaces through the testing time are shown in **Figure 3.16**. The visualization of surface corrosion products configurations are identified that the surface changed from orange to brown color in contract to the steel gray color.

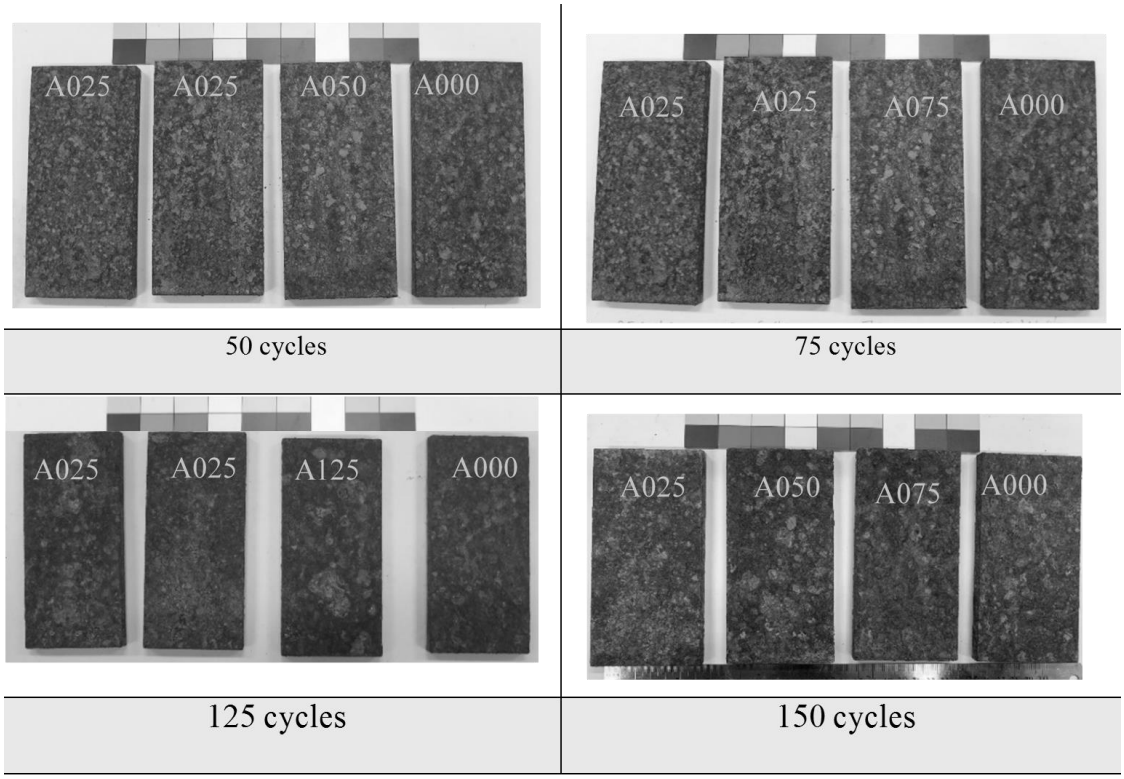

Figure 3.16 Wash specimen surface configuration

As compared to specimen wash frequency, more rough and flaky rust products can be observed in specimens with no wash in every cycles. Moreover, the degradation and blistering are also more intense.

The surface configuration for 75, 100 and 125 cycles wash specimens are seen that there have not so much differences with specimens without washing. The attached surface salt on the specimen was measured at every washing program. Measured surface salt results at each washing frequency are shown in **Table 3.6**. The maximum capacity of device is about 1999 mg/m^2 and it cannot be measured for the value higher than that.

Table 3.6 Measured surface attached salt

Wash program	Time inside chamber (days)	Surface attached salt (before wash) mg/m^2	Surface attached salt (after wash) mg/m^2
No wash	0	474	-
	6.25	1999	-
25 cycles	0	477	-
	6.25	1999	753
	18.75	-	1443
	31.25	-	1913
	43.75	-	1747
50 cycles	43.75	-	949
75 cycles	18.75	-	1809
	37.5	-	1397
100 cycles	25	-	1999
125 cycles	125	-	1999

As can be seen in table, power washing with natural water can reduce the amount of surface attached salt after frequent washing. The surface salt increase dramatically after 25 cycles of exposure (6.25 days) in which the values are very large to measure. It can only be measured after washing process. At 25 cycles, the surface salt content decreased up to 63% after washing. The amount of salt after washing also increased with exposure due to constant spraying of salt solution. However, the outside environment is very mild compared to simulated environment in which the salt can dump massively in a short period. It is expected that the washing reduce surface salt more effectively in real environment than the simulated one.

3.5.1 Weight change

The weight change normalized by the coupon area where corrosion is exposed through the testing time is shown in **Figure 3.17**. It can be seen that the weight change increased with time for all specimen.

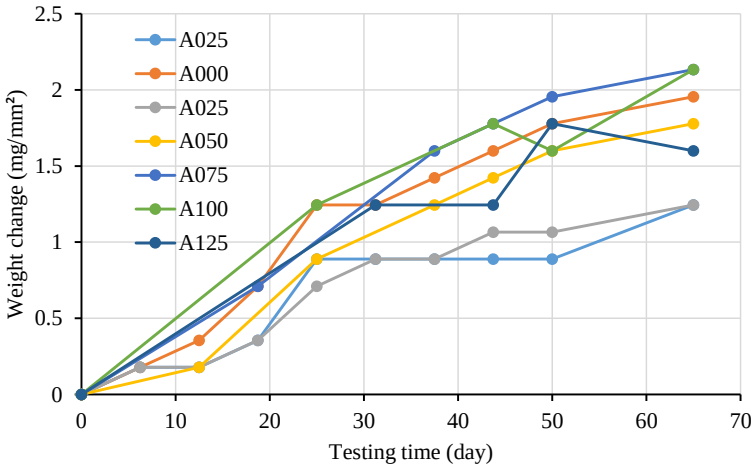

Figure **3.17** Weight change versus testing time

A slight increment of weight change is generated at the beginning of exposure, and it increased drastically after that. However, a significant relationship between the increments of weight with wash frequency was not clearly discovered. The pattern of increments are almost similar with specimen without washing expect A025 specimens. Therefore, the data from A100 and A125 were decided not to consider. The data from Groups A025 and A075 are combined and average, and plotted along with data corresponding to Group A000.

In **Figure 3.18**, a mean value of weight change for A025 and A070 shows more clear effect of steel washing on reducing the rate of weight increment. It can be seen that weight change in specimen without washing present higher rates of weight increment. The data for both groups are well fitted with the power functions with high correlation parameter R^2.

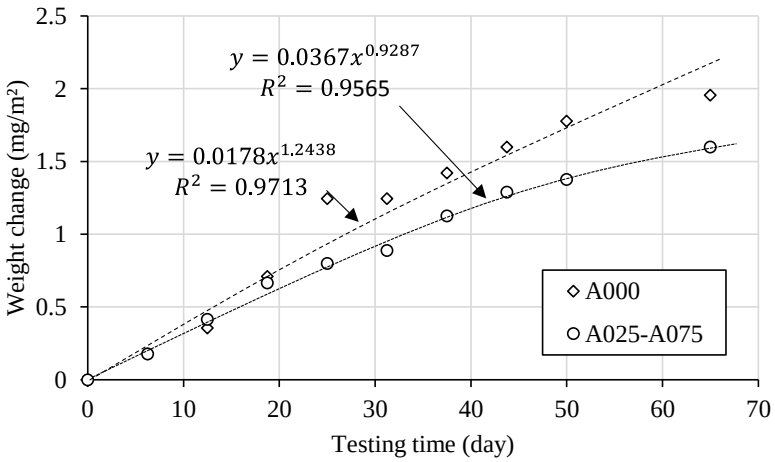

Figure 3.18 Mean value of weight change from A025-A075 and A000

3.5.2 Rust thickness increment

The rust thickness increment on the surface of specimen under an accelerated test are shown in **Figure 3.19**. Similar with weight change, rust thickness changes present an unclear pattern between wash frequency and rust thickness increment. The data for A025 and A075 are combined and averaged.

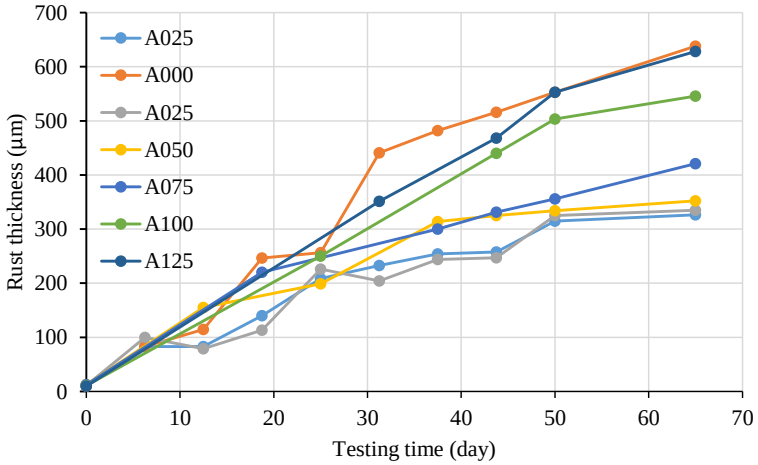

Figure 3.19 Rust thickness

The mean rust thickness of Groups A025 and A075 versus testing time with Group A000 are shown in **Figure 3.20**. The mean thickness loss from average data of A025 and A075 shows lower rust thickness than the specimen without washing.

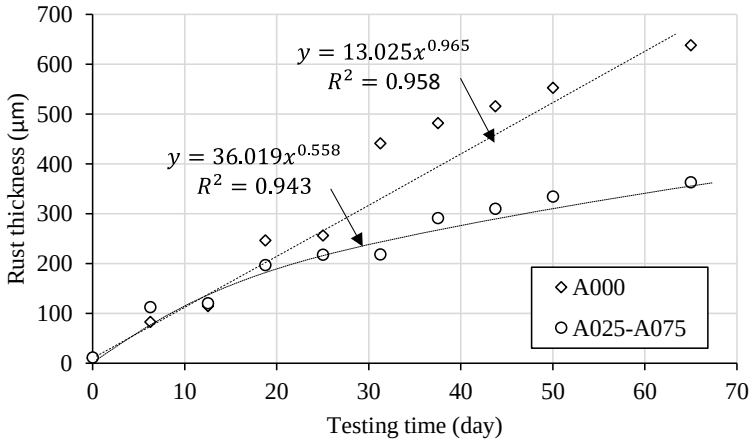

Figure 3.20 Mean value of rust thickness from A025-A075 and A000

The power relation with high correlation coefficients are also observed in relation between rust thickness and testing period inside the chamber. The rust thickness

propagation through the testing time under the S6-cycles chamber atmosphere can be predicted by using calculated correlation equations. There is a direct relation between rust thickness and corrosion losses. Therefore, the material degradation increased with increasing testing time inside the chamber.

3.6 Discussion and conclusions

The formation of compact rust layer grew easily in 0.05% salt solution S6-cycles test. Although the protective patina is not fully developed during these 300 cycles of exposure, dense and well-adhering corrosion product layer are discovered on weathering steel surface. The S6-cycles accelerated test with diluted salt concentration can simulate the protective patina on weathering steel surface.

The power function correlation is observed in the relation between rust thickness and exposure time inside the chamber. Lower penetration of corrosion is observed in the weathering steel specimens than the carbon steel in conventional S6-cycles test. According to this, weathering steel shows more or less protection than carbon steel in chamber atmosphere. To analyze the formation of protective patina of weathering steel, diluted S6-cycles test with 0.05% concentrated salt solution was performed. The result shows that dense rust layer formed after 200 cycles (50 days) in the diluted test. The equations in both test conditions are provided for prediction of carbon and weathering steels in simulated S6-cycles chamber atmosphere.

Steel washing program was conducted to evaluate the effect of steel washing on material degradation. The results show that specimen washing after 25 and 75 cycles reduce not only the weight change but also the rust thickness. Larger wash frequency cannot show any differences with specimen without washing. From the results obtained during the accelerated test, it can be concluded that subsequent washing with appropriate frequency can reduce corrosion degradation.

References

Albrecht, P., Coburn, S. ., Wattar, F. ., Tinklenberg, G. ., & Gallagher, W. . (1989). *Guidelines for the use of weathering steel in bridges*.

ASTM G1-03(2017)e1, Standard Practice for Preparing, Cleaning, and Evaluating Corrosion Test Specimens, ASTM International, West Conshohocken, PA, 2017, www.astm.org

ASTM B117-19, Standard Practice for Operating Salt Spray (Fog) Apparatus, ASTM International, West Conshohocken, PA, 2019, www.astm.org

Bowman, M. D., & Moran, L. M. (2015). Bridge preservation treatments and best practices (Joint Transportation Research Program Publication No. FHWA/IN/JTRP-2015/22). West Lafayette, IN: Purdue University. https://doi. org/10.5703/1288284316007

Cynthia L. Meade, Accelerated corrosion testing, *Metal Finishing*, **98**(6), 540(2000).

Fujiwara, H. and Tahara, Y. (1997), "Research on the correlativity of outdoor exposure test of painting test piece with corrosion test for steel bridge painting", Journal of Structural Mechanics and Earthquake Engineering, No. 570/I-40, 129-140.

Gu, H., Itoh, Y., & Kim, I.T. (2005). Accelerated exposure test studies for durability of steel bridge members. *1st international Conference on advances in experimental structural engineering 2005*, (July), 765–772.

https://www.toadkk.com/english/product/details/por/ssm-21p.html

https://www.directindustry.com/prod/kett-us/product-71402-1101391.html

International Organization for Standardization. (1985). *ISO 8407: Metals and alloys – procedures for removal of corrosion products from corrosion test specimens*. 1–7.

Itoh, Y., & Kim, I. T. (2006). Accelerated cyclic corrosion testing of structural steels and its application to assess steel bridge coatings. *Anti-Corrosion Methods and Materials*, *53*(6), 374–381.

JIS K8847. (1995). Hexamethylenetetramine (Reagent).

JIS K 5621, Anticorrosive Paint for General Use, Japanese standards Association, Japan, 2008. (in Japanese)

Kamimura, T., Doi, T., Kashima, K., Wagure, N., Hara, S., Nakahara, K., Miyuki, H. (2007). Investigation of rust layer formed on weathering steel coated with a surface treatment promoting protective rust formation. *Zairyo/Journal of the Society of Materials Science, Japan*, *56*(11), 1035–1041.

Lichti, K. A. (2008). Accelerated corrosion testing. *48th Annual Conference of the Australasian Corrosion Association 2008: Corrosion and Prevention 2008*, (February), 71–80.

Montoya, P., Díaz, I., Granizo, N., De La Fuente, D., & Morcillo, M. (2013). An study on accelerated corrosion testing of weathering steel. *Materials Chemistry and Physics*, *142*(1), 220–228. https://doi.org/10.1016/j.matchemphys.2013.07.009

Morcillo, M., Chico, B., Díaz, I., Cano, H., & de la Fuente, D. (2013). Atmospheric corrosion data of weathering steels. A review. *Corrosion Science*, *77*, 6–24.

Public Works Research Institute. (1988). Nationwide survey on airborne chloride. *PWRI Technical Memorandum No. 2678*, 1988 (in Japanese).

Qian, Y., Xu, J., & Li, M. (2015). An accelerated testing method for the evaluation of atmospheric corrosion resistance of weathering steels. *Anti-Corrosion Methods and Materials*, *62*(2), 77–82. https://doi.org/10.1108/ACMM-11-2013-1319

Raymund Singleton, Accelerated corrosion testing, *Metal Finishing*, 108(11), 366(2010).

Sun Zheming. (2017). *Evaluation of time of wetness and salinity and their effect on steel corrosion*. Kyoto University.

Chapter 4

TIME-SCALED CORRELATION BETWEEN ACCELERATED CORROSION VERSUS FIELD TESTS

4.1 Introduction

An accelerated corrosion test (ACT) is a controlled test to simulate the atmospheric corrosion at the laboratory in a short time. Atmospheric corrosion process is a combination of several environmental factors. However, an ACT is based on controlling of few factors in the laboratory. Based on this considerations, the results from ACT should be used by the appropriate judgement compared with the outdoor initial measurement. A relationship should be determined to obtain the actual level of corrosion corresponding to the level of corrosion of coupons inside the chamber. A time scaled correlation between a unit time in the chamber during ACT and the corresponding time for a real environment can be useful to correlate the results obtained from ACT to real problems. The extrapolation of results from the ACT during a short period of time to real problems of larger periods of time can help to predict the long-term degradation of steel in real structures, such as in a bridge.

In this chapter, the time scaled correlation between the corrosion in the accelerated laboratory test and outdoor exposure test was calculated to determine the time necessary to the equivalent corrosion degradation of steel in the real environments. The calculation is based on the outdoor corrosion measurement in **Chapter 2** and the accelerated corrosion test results from **Chapter 3**. The objectives of this chapter are to determine the acceleration factor (Ac) of the studied areas and to define the corrosion stabilization period in their respective environments. The effectiveness of steel washing was also considered to maintain the weathering steel bridge performance till its tentative service life by deciding an appropriate frequency of washing period. Prediction equation for long-term thickness loss was formulated by applying the relationship between Ac

and the site related environmental parameter, such as salt concentration in the atmosphere.

4.2 Acceleration coefficient (Ac)

The acceleration coefficient is an index to show how fast the accelerated test is comparing to atmospheric exposure tests. The coefficient can be calculated by dividing time scale of outdoor exposure test and time scale of accelerated exposure test. The present study calculated Ac of weathering steel in the proposed test sites.

4.2.1 Determination of acceleration coefficient

The calculation of acceleration coefficient is based on the measured corrosion data in the outdoor exposure test and the accelerated test results. To determine the acceleration coefficient of weathering steel, S6-cycles accelerated test results (**Chapter 3**) were used. The example calculation of acceleration coefficients are shown in **Figure 4.1**. In the calculation, the results of 7 test sites in Myanmar for about 3 years exposure and the accelerated test results for 200 cycles (about 34 days inside the chamber) are compared, and then the acceleration coefficient (Ac) is obtained by dividing the time scale in the real environment and unit time scale inside the chamber. The calculated Ac are based on the diluted S6 cycles tests with 0.05% NaCl solution.

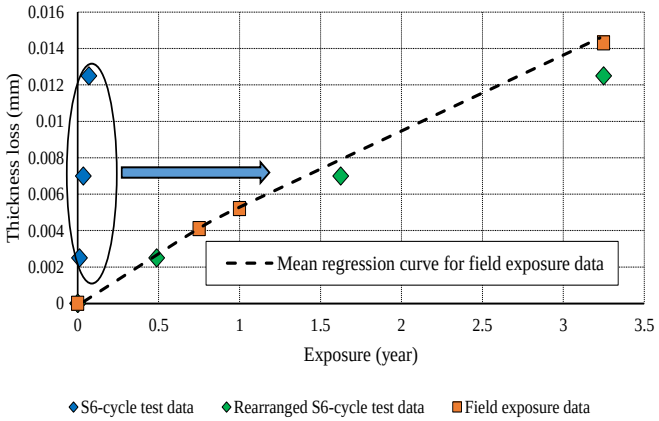

Figure 4.1 Calculation of acceleration coefficient

The calculated acceleration coefficients for the test sites are as shown in **Table 4.1**. As can be seen in the table that, the coefficients are accompanied with the off-shore distances of test site locations and flying salt contents (**Chapter 2**), although there has

one test site in low Ac for urban environment than others due to unconsidered environmental parameter; sulfur dioxide. The calculation of Ac are also taken for the Asia's environment by using referenced data of corrosion rate (test sites are same as in Chapter 2). The Ac are calculated by using the corrosion rate inside the chamber as described in (Chapter 3) and it is shown in Appendix C. The results of Ac at the Asia test sites are within 41-104 at the test sites with low flying salt content (i.e., salt amount is lower than 0.5 mdd) and the ranges are in between 7-35 at the test sites which are closer to the sea sand (i.e., salt content is more than or equal to 0.5 mdd).

Table 4.1 Calculated Ac of test sites in Myanmar

Test site	Distance from Costal line	Ac 0.05% NaCl Test
Sittwe	1.4	8
Dawei	13	16
Pathein	37	21
Yangon	51	19
Maubin	63	18
Hinthada	88	20
Mandalay	342	43

The accuracy of correlation equation is checked by using Ac at 31 test sites in Japan by Itoh (2006) as prescribed in **Figure 4.2**. The researcher calculated an acceleration coefficient (Ac) based on the weight loss in conventional S6 cycles accelerated corrosion tests and the outdoor exposure test results in Japan.

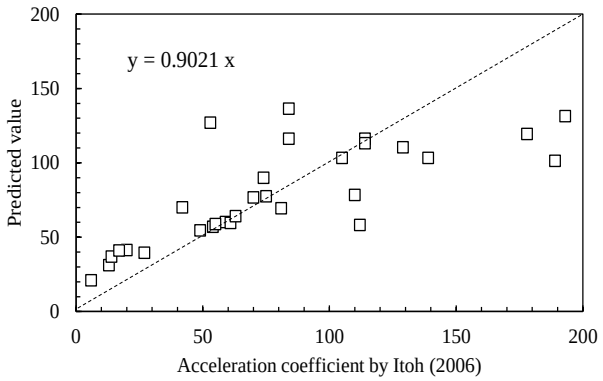

Figure 4.2 Comparison of acceleration coefficients

In **Figure 4.2**, the calculated Ac have good agreement with Itoh's results with small error percentages (i.e., negative 10%) in this calculation. However, the data shows some agreement with the previous, the range of values are quite large. Therefore, it is suggested to define the region into separate with similar weather condition within Asia region.

4.3 Prediction equation by the application of Ac and flying salt in Asia

The corrosion on the surface of specimens inside the accelerated test are uniform at the beginning, and the corrosion products formed more heavily in the regions where the salt water remained the longest on the panel surface after that. According to the characteristics of the environment inside the chamber, the repeated hourly spraying caused the corrosion product to form aggressively especially where the largest droplets formed on the surface. The area of penetration was wider against the number of exposure time, and finally the whole surface is fully covered by the blistering at the end of the intended cycles as show in **Figure 4.3**.

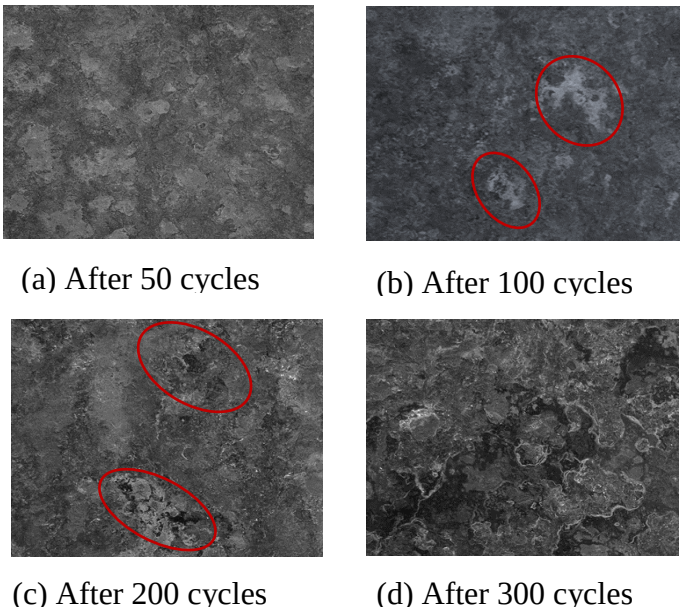

(a) After 50 cycles (b) After 100 cycles

(c) After 200 cycles (d) After 300 cycles

Figure 4.3 Surface configurations in combined cycle test

A mean regression curve for length of exposure time and thickness loss in **Figure 4.4** shows that a correlation is fitted with power series with correlation coefficient of 0.775. The relationship between thickness loss and testing time can be described by **Equation 4.1**.

$$T_1 = 0.024 t_d^{0.626} \qquad R = 0.88 \qquad \textbf{(4.1)}$$

where: T_1 = mean thickness loss (mm)

t_d = testing time (day)

The corrosion rate of 2064 µm/year is calculated after 300 cycles of exposure inside the S6-cycles chamber environment.

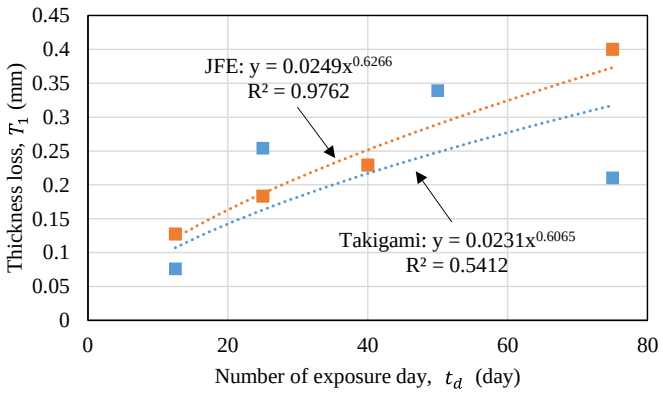

Figure 4.4. Correlation of thickness loss vs time

The prediction equation is driven by using the correlation between acceleration coefficient and amount of flying slat. No complete data for all the test locations' flying airborne salt contents are available in all Myanmar test sites. Therefore, the amount of airborne salt at some exposure test sites are calculated based on the PWRI equation (1988) formulated by the measured flying salt at 266 sites in Japan. The relation of calculated Ac and amount of flying salt in the Asia test sites were determined.

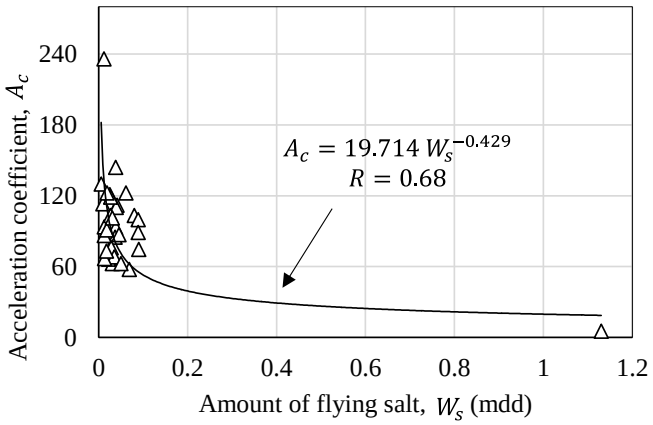

Figure 4.5 The relation between amounts of flying salt and Ac

Negative power correlation is observed in relationship between calculated Ac and amount of flying salt in Asia atmosphere as can be seen in **Figure 4.5**. The correlation equation is shown in **Equation 4.2**.

$$A_c = 19.71\, W_s^{-0.429} \qquad R = 0.68 \qquad \textbf{(4.2)}$$

where, W_s is the amount of flying salt (mg/m^2/day, mdd) and A_c is the acceleration coefficient.

In order to check the relation between acceleration coefficient and temperature and relative humidity (as in the combination form of time of wetness), the correlation of these two parameters is shown in **Figure 4.6**. According to this figure, no strong relation between acceleration coefficient and time of wetness is observed. The prediction equations for current studied areas are driven based on the amount of flying slat and exposure period on sites.

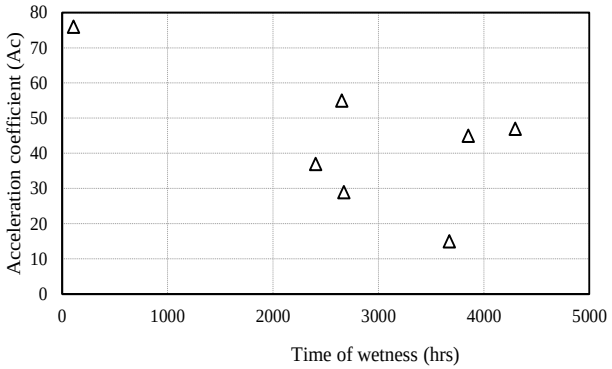

Figure 4.6 The relation between TOW and Ac

Long-term prediction equation is formulated based on Equations 2 and 3. The flying slat deposition rate is considered as the major environmental factor for prediction because a strong relation is observed in corrosion rates and flying salt contents of test sites. The driven prediction equation is shown in **Equation 4.3**.

$$T_1 = 0.154\, (W_s^{0.429} \times t_y)^{0.626} \qquad \textbf{(4.3)}$$

where: $T_1 =$ thickness loss (mm)

$W_s =$ amount of flying salt (mdd)

t_y = exposure time (year)

The formulated prediction equation by the accelerated test results and the amount of flying salt is able to calculate the future mean thickness loss from the measured amount of flying salt at the test sites. This prediction equation is based on the Asia's environment and the S6 cycles accelerated test. The variables in the equation can be different at the different environments and different accelerated tests.

4.4 Calculation of equivalent time for weathering steel bridge washing

The following part defines the appropriate time interval for the bridge washing in the real structures relevant with the steel washing results from **Chapter 3**. To obtain this correlation, the averaging results from the frequency which shows clear effectiveness of steel washing. In **Chapter 3**, it can be seen that the wash frequencies of 25 cycles, 50 cycles and 75 cycles can reduce the penetration of corrosion. To achieve economical wash frequency, 25 cycles interval is removed from consideration because of the reduction rate is not so much difference with 50 cycles and 75 cycles. For practical implementation of the results, the mean value for the frequency of the two combined groups resulted in an average frequency of washing was considered as the suitable time for the real structure. The corresponding time interval of averaged time interval for the washing is 3 weeks. From the acceleration coefficients from the **Table 4.1** and the relevant time appropriate for the steel washing, the results of the effective time interval for weathering steel bridge washing in real environment is calculated as shown in **Table 4.2**.

Table 4.2 Time for weathering steel bridge washing

Years at real environments		
Weeks at ACT	Coastal	Urban
3	1.8	5.5

According to the calculated results, the weathering steel bridges located in the coastal environment in Myanmar need to wash in every one and half years. For the urban environment, the bridge washing in every five and half years will be effectively reduced the corrosion penetration.

Moreover, the stabilization of corrosion on the weathering steel at the accelerated test was found out after 200 cycles. This rust stabilization time is equivalent to 5 years in the outside urban environment. According to the results from the Ac and the calculated rust stabilization time, it can be concluded that the weathering steel bridge washing should be performed right after the rust stabilization on the members of bridge.

The development of weathering steel protectiveness layer formation inside the chamber with or without washing was also examined to know whether or not the steel washing can help on faster development of patina formation. The surface unevenness and thickness variation were measured by 3D laser scanner machine as shown in **Figure 4.7**.

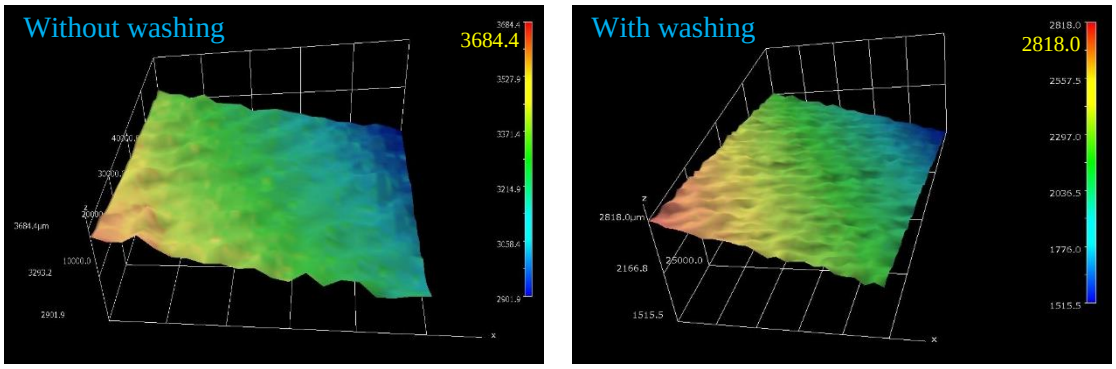

(a) Surface at 200 cycles in 0.05% NaCl test (b) Surface at 100 cycles in 0.05% NaCl test

Figure 4.7 3D scanner results

As presented in **Chapter 3**, the formation of protectiveness on weathering steel started at 200 cycles in 0.05% NaCl test with no washing program. However, a similar rust thickness and surface uniformity was observed at 100 cycles in 0.05% NaCl test with frequent washing program. The result of comparison shows that steel washing can not only reduce the corrosion propagation rate but also introduce the rapid formation of protective patina on weathering steel surface.

4.5 Discussion and conclusions

This chapter discusses about the calculation of acceleration coefficients at the several test sites in Myanmar and formulation of prediction equation has been carried out by using calculated coefficients. The results of the calculated Ac show that the values decrease with increasing distance from the seashore of test sites. The corrosion rates in the accelerated test are well fitted with power series against the length of exposure. The

surface configuration of specimens through the testing time show that the chamber atmosphere create corrosion penetration stared in small region where the salt water contact and it emerges to the whole surface. The corrosion rate decrease after reaching the peak at the specific cycles as in outdoor atmosphere. Following with this Ac calculation, the application of Ac in the formulation of prediction equation is proposed. By doing this, the prediction of long-term corrosion in any test sites can be calculated by knowing only one parameter, such as salinity.

Steel washing evaluation proved that the corrosion penetration can be effectively reduced by the water washing when the frequency is appropriate. This research find out that the period for the bridge washing in the real environment to reduce the corrosion penetration in effective way. Moreover, steel washing also promotes the formation of protective rust layer of weathering steel. The time interval for bridge washing in coastal and urban environments can be specified as 1.8 years and 5.5 year respectively. This proposed subsequent frequency of bridge washing can help in the maintenance of weathering steel bridges to their intended service lives.

References

ASTM B117-19, Standard Practice for Operating Salt Spray (Fog) Apparatus, ASTM International, West Conshohocken, PA, 2019, www.astm.org

Belen, C., Daniel, de la F., Ivan, D., Joaquin, S., & Manuel, M. (2017). Annual Atmospheric Corrosion of Carbon Steel Worldwide. An Integration of ISOCORRAG, ICP/UNECE and MICAT Databases. *Materials*, *10*(6), 601. https://doi.org/10.3390/ma10060601

Cynthia L. Meade, Accelerated corrosion testing, *Metal Finishing*, **98**(6), 540(2000).

FUJIWARA Hiroshi; Research on the correlativity of outdoor exposure test of painting test piece with corrosion test for steel bridge painting, Proceedings of JSCE 570, 129-140, 1997-07-21

Gu, H., Itoh, Y., & Kim, I.T. (2005). Accelerated exposure test studies for durability of steel bridge members. *1st international Conference on advances in experimental structural engineering 2005*, (July), 765–772.

Itoh, Y., & Kim, I. T. (2006). Accelerated cyclic corrosion testing of structural steels and its application to assess steel bridge coatings. *Anti-Corrosion Methods and Materials*, *53*(6), 374–381.

Japan Weathering Test Centre (2006). *Research on Long-Term Durability and Standardization of Life Prediction of Elemental Equipment Related to New Power Generation*, Research Project for Standardization of Development Result, Consignment of New Energy and Industrial Technology Development Organization Result Report, 100007184 (in Japanese).

L. T. H. Lien, P. T. San, & H. L. Hong (2007). Results of studying atmospheric corrosion in Vietnam 1995-2005. *Science and Technology of Advanced Materials*, *8*(7–8), 552–558. https://doi.org/10.1016/j.stam.2007.08.011

M. Morcillo, "Atmospheric Corrosion in Ibero-America: The MICAT Project," in *Atmospheric Corrosion*, ed. W. Kirk and H. Lawson (West Conshohocken, PA: ASTM International, 1995), 257-275. https://doi.org/10.1520/STP14924S

Tadashi Shinohara, et al. (2012). E-Asia joint research program final report: *Corrosion mapping of structural materials in Asia area with understanding effects of environmental factors* (Version 1).

Chapter 5

SYSTEM RELIABILITY ANALYSIS OF CORRODED WEATHERING STEEL GIRDER BRIDGE

5.1 Introduction

Bridges in Myanmar are at risk from aging and lack of periodical maintenance which is leading to structural deterioration from the environmental attacks and from increasing traffic. Most of the bridges in Myanmar were built in 1988, and bridges during this periods were absolutely aged without any intermittent maintenances. Furthermore, almost all of the bridges were constructed in the delta and coastal regions due to the present of several rivers. Since these regions are very close to the sea, the corrosion of bridge due to the airborne salt carried out by the wind becomes a vital issue in bridge maintenance.

According to the investigation by the research team in collaboration of YTU and JICA (2012), the deterioration of long span bridges in Myanmar were mainly caused by chloride attack. A survey conducted in 2012 by Japan Infrastructure Partners (JIP) mentioned that many bridges in Myanmar have recently occurred in severe deteriorations and requires countermeasures (Japan Infrastructure Partners, 2012). On the first of April 2018, Myaungmya Suspension Bridge located in Ayeyawaddy region in the southern part of Myanmar collapsed. The main reason of this bridge collapse is still questionable. However, a JICA survey in 2012 reported that the abutment of the bridge moved forward and the traffic was restricted from two lanes to single lane flow at that time. Furthermore, some damages in the cable are also discovered during that survey. **Figure 5.1** shows Myaungmya Bridge after the collapse. The failure of the Myaungmya Bridge is showing the necessities of condition assessment and safety measurement on existing bridges in Myanmar to reduce the cost and social impact of bridge falling.

Figure 5.1 Myaungmya Bridge after collapse

Corrosion of bridges is a major problem as they age which requires replacement, which costs billions. According to CHBDC (2003), total annual costs of corrosion is much more than the costs of floods, hurricanes, tornadoes, fires, lighting, and earthquake. Corrosion can be occurred in structures when the materials exposes to the corrosive environment, named as atmospheric corrosion. By the nature of this type of corrosion, it can be reported to account for more failures in terms of cost and tonnage than any other form of corrosion. The possible types of bridge corrosion have been studied by Kayser and Nowak (2001). In addition, excessive rust accumulation over the years can be serious enough to disconnect the girder web from the flange, which poses significant concerns for structural capacity especially at girder ends (ENC 1991-6; 1994, A.S. Nowak; 2002, R.L. Brockenbrough; 1983, J.R, Kayser & A.S. Nowak; 1987).

The major effect of corrosion is the loss of metal section resulting in a considerable reduction of resistance. It can cause not only fracture but also yielding and buckling of members. Changes in member stresses and geometric properties are associated with loss of material. A reduction in the net area of a member will cause an overall increase in member stresses for a given load. A consequence of surface corrosion is the reduction in member cross sectional properties, such as the section modulus or the slenderness ratio. Moreover, corrosion product buildup may also affect structural performance. Accumulated rust can act as desiccant, retaining moisture may further promote corrosion. Also, growing ‘pack rust’ can exert a considerable pressure on adjacent elements (G. Konig & A.S. Nowak, 1992).

Weathering steel has been used nationwide in the construction of bridges because of its advantages in performing protective oxide coating without requiring painting when the structural details are properly designed and the bridge exposed in the suitable environment. Under these conditions, it offers the potential for considerable savings in life-cycle costs by the elimination of the need for maintenance painting. The initial cost of an unpainted weathering steel bridge is said to be about the same as the cost of a painted regular steel bridge. Furthermore, by eliminating the need for maintenance painting, paint jobs of bridges over difficult terrains, electrified railways, and bodies of water can be avoided; heavy traffic lanes need not be closed; and safety hazards to motorists and painters alike are prevented. Otherwise, under some environmental conditions corrosion has continued at a rate more rapid than anticipated, and there is concern about the long-term performance of this material under field environment where weathering bridges are constructed. The present research bases on the real field measurement results of the weathering steel corrosion rates and develop the long-term corrosion losses prediction to apply the real bridge structure.

The major factors of structure deficiencies are contributed by the age, inadequate maintenance, increasing load spectra and environmental contamination. In order to make the decision about deficient members to repair or replace, it is essential to evaluate the level of structure performance. The most accurate data of bridge evaluation tends to propose advance diagnosis procedures for structure repair with minimum time and cost. In this matter, it is important to evaluate the structural performances under time dependent levels of corrosion. The major effect of thickness losses by corrosion results in reduction of structural load-carrying capacity and reliability. Therefore, it is important to develop a procedure in order to accurate prediction of load-carrying capacity of existing bridges. The statistical data of corrosion for evaluation of bridge performances are developed by using the on-site measurement based long-term atmospheric corrosion thickness losses prediction equation. Finite Element model is performed to get the structural responses of bridge members. Load and resistance data are generated as random variables to evaluate the reliability of bridge system by probabilistic approach. The probabilistic methods are mostly applied in the development of a new generation of design codes in bridge engineering (such as AASHTO LRFD 2004; CHBDC 2003; Eurocodes; 1994). These codes were based on the ultimate limit states for individual components. However, Eamon

and Nowak (1990) found that the interaction of typical secondary elements such as end-stiffening elements and diaphragms has a varying effect on system reliability, depending on element stiffness, bridge span and girder spacing.

The objective of this chapter is to establish the relationship between system reliability and degree of deterioration, especially by corrosion. The deterioration rate was defined by time dependent corrosion levels predicted by field measurement. Uniform corrosion loss was considered to define girder resistance model. A finite element method (FEM) is used to calculate deflections and bridge system responses under different levels of corrosion attack. Ultimate and serviceability limit states are considered as limit state functions for reliability analysis. Monte Carlo Simulation is employed for system reliability approach (A. S. Nowak; 2000). In this chapter, the main focus is on the variation of system reliabilities of girder-bridge as a function of time under uniform corrosion deterioration. The obtained reliability spectra can serve as a basis for the development of rational criteria for the evaluation of existing girder bridge structures under predefined corrosion patterns.

5.2 Target bridge and corrosion model

Thakan Chaung Bridge, situated in Bogale city in the south of Myanmar, was constructed in 2018. The bridge was built crossing through the Thakan River. The bridge is plate girder type and total of 704 m in length. **Figure 5.2** shows an over view of bridge. The bridge was made by the carbon steel at middle spans and the weathering steel at two approach spans at both sides as shown in **Figure 5.3**.

The configuration of the bridge is two lanes slab on steel I- Girder Bridge, which has a clear roadway width of 7.315 m. The bridge consists of four steel I girders as shown in Figure 5.4 with equal spacing of 2.438m and a 200 mm thick reinforce concrete slab. A 50 mm thick asphalt is used for the weathering surface. The weathering steel bridge was made by the weathering steel with yield strength (f_y) of 365 MPa and specified concrete strength (f'_c) of 25 MPa. The geometrical data of bridge is given in **Table 5.1**.

Figure 5.2 Thakan Chaung Bridge

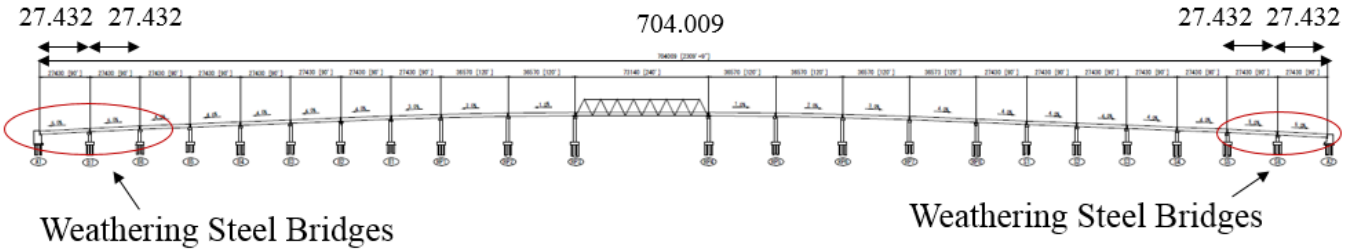

Figure 5.3 Position of weathering steel bridges (Unit: m)

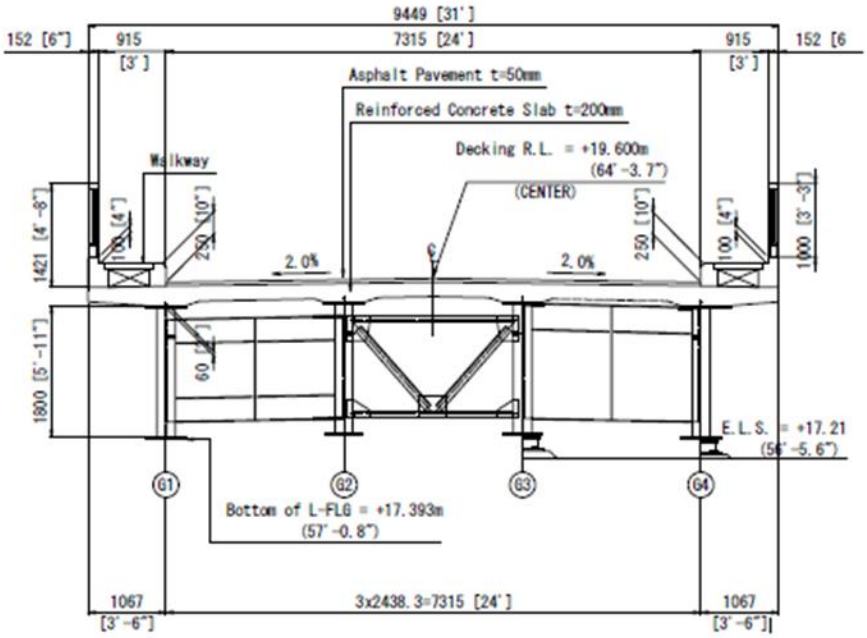

Unit: mm (ft)

Figure 5.4 Steel bridge configuration

Table 5.1 Geometric data of bridge

Flange thickness (mm)		Flange width (mm)				Web thickness (mm)	Stringer spacing (mm)
G1, G4	G2, G3	G1,4-1	G1,4-2	G2,3-1	G2,3-2		
24	23	470	550	440	530	9	2438

The bridge is located in the southern delta region in Myanmar and calculation of corrosion losses are determined by using the measured data from three nearby test sites. The prediction of thickness loss was made by the measured data and accelerated test results as described in **Chapter 4**. Uniform corrosion loss is applied to the whole area of main girder as shown in **Figure 5.5**.

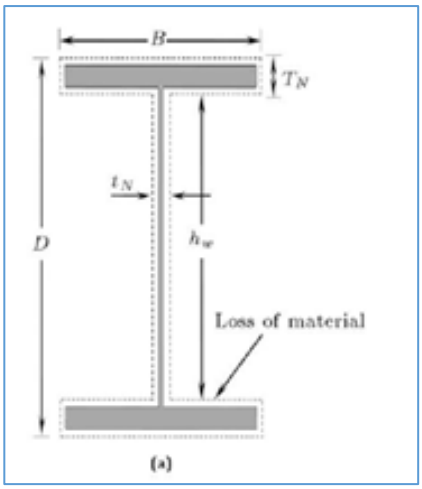

Figure 5.5 Girder corrosion pattern

The calculation of thickness reduction has been carried out by using the equation defined in **Chapter 4** where the equations are driven by the relation between laboratory and exposure tests. Corrosion losses for both specimens with and without regular pressure washing were examined by performing different washing frequencies. Long-term corrosion are predicted based on the environmental parameters (airborne salt concentration in atmosphere is major parameter in this study).

The calculated time variant thickness loss values for washing and no washing alternatives is shown in **Figure 5.6**. The steel washing alternative produces lower

thickness loss value than no washing. The maximum girder thickness loss is 2 mm after the 100 years of exposure period under the condition without any maintenance activities.

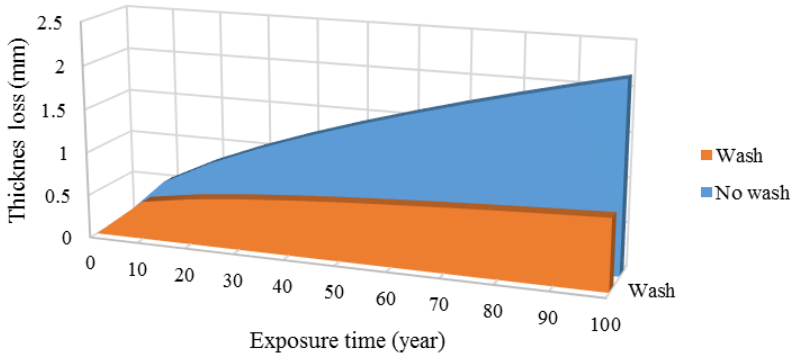

Figure 5.6 Girder thickness reduction

The corrosion loss in specimen with washing alternative is almost three times lower than that in specimen without washing. The thickness reduction through exposure time for both scenarios are applied as a uniform pattern to the main girders of bridge.

5.3 Time variant reliability analysis

Bridge reliability is a time-dependent phenomenon, because bridge materials deteriorate with time and the bridge loading process varies with time. The evaluation of steel bridge structures under the environment is the most important process in the bridge management system. In most modern structural design codes, the safety of a structure is measured (either directly or indirectly) in terms of its reliability index.

The study of time dependent becomes an essential under the variation of environmental effects consideration, such as corrosion effects. Studying the reliability of bridges under such conditions requires a throughout understanding of the long-term behaviour of bridge materials under the effect of various types of loads. The remaining life of bridges are determined based on the level of target reliability. According to the calibration of AASHTO 1994, the target reliability is selected as 3.07. This study also take this value as target value for proposed bridge.

5.4 Probability of failure and reliability

The structural reliability is a concept of the limit states design process (Walbridge 2005). ASSHTO LRFD Bridge Design Specifications (2007), have adopted the reliability index, β, as a measure of reliability instead of probability of failure (P_f). The reliability index in the range of 2 to 4.5 is specified for typical structural engineering situations. The target reliability index of 3.5 for new bridge structures was determined by AASHTO LRFD specifications from the calibration results of a spectrum of traditional bridge design situations (1985 and earlier) including steel, reinforced and pre-stressed concrete construction. The target reliability index of 3.5 was adopted for capacity checking at design load level in this study.

Limit states are defined as the conditions of a structure or component beyond which it ceases to fulfill the function for which it was designed. Three types of limit states are defined according to the AASHTO design standard, namely fatigue, serviceability, and ultimate limit states. Fatigue cracking of a structure occurs at the fatigue limit state, while the serviceability limit state coincides with the occurrence of excessive vibrations or static deformations, sufficient to effect the usability or durability of the structure. Total failure of the structure by any suitable mechanism (i.e. fracture, buckling, overturning) is considered to be an ultimate limit state. Limit states may be described by limit state functions; $G(\bar{z})$, which is a form of:

$G(\bar{z}) > 0$, means that the limit state is satisfied, so failure does not occur,
$G(\bar{z}) < 0$, means that the limit state is surpassed and failure occurs, and
$G(\bar{z}) = 0$, is the so-called "failure surface".

where $\bar{z}$ is the vector of statistical variables, z_i, which take into account the various sources of uncertainty associated with the limit state function.

The safety philosophy of the CAN/CSA S6-06 is to have a consistent level of risk to life for each bridge element. The level of risk is equal, by definition, to the probability of failure multiplied by the cost of failure. The cost of failure of a bridge element is related to the likelihood of the element failure leading to loss of life. A consistent level of risk is maintained if a higher probability of failure is accepted in the elements whose failure will

not result in a loss of life, or a lower probability of failure is accepted in the elements whose failure might result in a loss of life. Likewise, a structural element that receive frequent inspections, shows warning signs if approaching failure, or is capable of redistributing its load to other elements will be less likely to cause loss of life.

5.4.1 Failure mechanisms in bridges

A failure of structure occurs when the structure can no longer perform its function. The function includes not only structural aspects such as to carry traffic loads safely traffic loads for expected periods of time and to provide a comfortable passage (minimize deflections and vibrations), but also to provide aesthetic values to the users. The structural performance can usually be expressed in terms of mathematical equations and limit state functions, involving various parameters of material properties, dimensions and geometry (Nowak 1990).

In practice, a simple formulation of the limit state function is often impossible. Both resistance, R and load effect, Q, are functions of multiple parameters. These parameters vary randomly, some are difficult to quantify (e.g. geometric configuration), and they are often time-variant (e.g. live load or effect of corrosion) and/or correlated. For a typical bridge girder, the limit state functions can be formulated for various conditions, including:

1. Bending moment capacity; R can be defined as the moment-carrying capacity for the girder, and Q as the maximum load resisted by the girder. Q is a joint effect of dead load, live load, environmental effects, and so on.
2. Shear capacity
3. Buckling capacity; overall and local
4. Deflection; excessive deformations may affect the user's comfort or cause some structural problems (e.g. increased dynamic truck load)
5. Vibrations; may affect the user's comfort
6. Accumulated damage conditions, including rebar corrosion in reinforced concrete beams and slabs, pre-stressing tendons, structural steel sections), fatigue (mostly affects steel sections, pre-stressing tendons and rebar), cracking (concrete) and other forms of material deterioration.

5.4.2 Limit state functions and reliability index

A limit state function is a boundary between desired and undesired performance of a structure. There are three types of limit sates in the reliability of structures, as presented below:

1. Ultimate limit states (ULSs) represent the collapse of the structure due to loss of structural capacity.
2. Serviceability limit states (SLSs) represent the failure states for normal operation in service condition.
3. Fatigue limit states (FLSs) represent the loss of strength for a structural component under the condition of repeated loading.

The ultimate limit state of moment and shear (ULS_M and ULS_S) and the serviceability limit state (SLS) are considered in this study.

The design formula in AASHTO LRFD code 2012 is shown in the following equation:

$$1.25\,DL + 1.5\,DW + 1.75\,LL\,(1 + IM) < \emptyset R \qquad \textbf{(5.1)}$$

where, DL, DW and LL are nominal values of load components and $IM = 0.33$. $\emptyset$ is the resistance factor, and R is the nominal value of resistance, which is either the moment strength or shear strength. The deterministic values (1.25, 1.5 and 1.75) are load factors of LRFD design code due to uncertainties.

Probabilistic models of load and resistance are established for each time point to calculate the system reliability of deteriorated bridge by corrosion. Limit state for the current analysis considers as ultimate limit state (ULS) refers to flexural or shear failure of the critical section among the girders and serviceability limit state (SLS) which is associated with the maximum allowable deflection specified by the AASHTO. The structural performance is expressed in term of limit state functions, considering parameters of material properties, dimensions and geometries (A.S. Nowak & K. R. Collins, 2000). A simple limit state is considered in this study and structure failure is corresponding to R being less than Q. The corresponding limit state function, g, is

$$g = R - Q \qquad \textbf{(5.2)}$$

If $g > 0$, the structure is safe, otherwise it fails. The probability of failure, P_F, is equal to,

$$P_F = Prob\ (R - Q < 0) = Prob\ (g < 0) \quad \textbf{(5.3)}$$

In general, the limit state function can be a function of many variables such as load components, influence factors, resistance parameters, material properties, dimensions and analysis factors. A direct calculation of P_F may be very difficult, and it is not possible. Therefore, it is convenient to measure structural safety in terms of a reliability index, β. Reliability index is related to probability of failure:

$$\beta = -\Phi^{-1}(P_F) \quad \textbf{(5.4)}$$

where Φ^{-1} = inverse standard normal distribution function.

The reliability index is calculated using the iterative procedure developed by Rackwitz and Fiessler based on normal approximation to non-normal distributions at the design-point.

This procedure starts with the resistance, R, let F_R is the probability cumulative distribution function (CDF) and f_R is the probability density function (PDF) for R. The initial value for R, at the design point is guesses as R^*. Later, F_R is approximated by a normal distribution, $F_{R\prime}$, such that

$$F_{R\prime} = F_R(R^*), \text{ and}$$
$$f_{R'}(R^*) = f_R(R^*) \quad \textbf{(5.5)}$$

The standard deviation of R' is

$$\sigma_{R\prime} = \varphi\{\Phi^{-1}[F_R(R^*)]\}/f_R(R^*) \quad \textbf{(5.6)}$$

where $\varphi\ (R)$ = PDF of the standard normal random variable and φ_R = CDF of the standard normal random variable.

The mean of R' is,

$$m_{R\prime} = R^* - \sigma_{R'}\ \Phi^{-1}[F_R(R^*)] \quad \textbf{(5.7)}$$

The similar procedure is carried out for all random variables in the limit state function (in this case, Q).

A reliability index β is computed by:

$$\beta = (m_{R'} - m_{Q'})/(\sigma_{R'}^2 + \sigma_{Q'}^2)^{1/2} \quad \textbf{(5.8)}$$

Then, a new design point is calculated by:

$$R^* = m_{R'} - \beta\sigma_{R'}^2/(\sigma_{R'}^2 + \sigma_{Q'}^2)^{1/2} \quad \textbf{(5.9)}$$

The second iteration begins; the approximating normal distributions are found for F_R and F_Q at the new design point. Calculations are continued until R^* does not change in consecutive iterations.

5.4.3 Load models

According to Nowak (2004), even the load in a critical components reach the ultimate value, other components can take additional loads and prevent a failure of the structure. The qualification of load sharing for this type of load sharing requires a special approach using system reliability models. The bridge load and resistance models for ultimate limit state of selected bridge are defined as follows.

The statistical parameter of the total load, Q, are determined as a function in terms of statistical parameters for load components. The mean of Q, is denoted by μQ, which is determined by the sum of the mean values of load components as show in the following equation:

$$\mu Q = \mu DL + \mu DL + \mu LL + \mu IM \quad \textbf{(5.10)}$$

Where, μDL is the mean dead load; μDW is the mean dead load for wearing surface; μLL is the mean live load, and μIM is the mean dynamic load.

Bridge load model includes dead and live load (truck traffic) based on those developed for the calibration of the AASHTO LRFD Code (2004). For dead load model, it includes the weight of girders, deck slab, wearing surface, barriers, and sidewalks. The

basis statistical parameters bias factor and coefficient of variation of dead load are 1.03 and 0.08 for factory-made components (girders and diaphragms), and 1.05 and 0.1 for cast-in-place components (deck, barriers and sidewalks) respectively. For the asphalt wearing surface, it is taken as the coefficient of variation as 0.25 to have a mean value of 90 mm.

Live load statistical parameters are adopted from the recorded data measured by the survey of heavily-loaded trucks from Michigan highways. The simulation from this research give the results for statistical parameters for traffic load. The axel spacing and weight distribution of HL 93 truck specified by AASHTO (2004) are shown in **Figure 5.7**. The position of the truck is decided by constructing influenced line diagram to maximize the bending moment effect on the bridge. The position of loading considered in present study is shown in **Figure 5.8**. The mean dynamic load factor is taken as 0.1 while the coefficient of variation is 0.8.

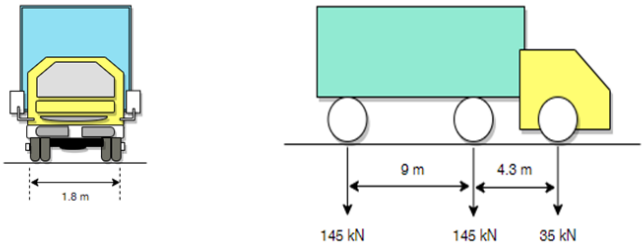

Figure. 5.7 Load configuration of HL-93 Truck

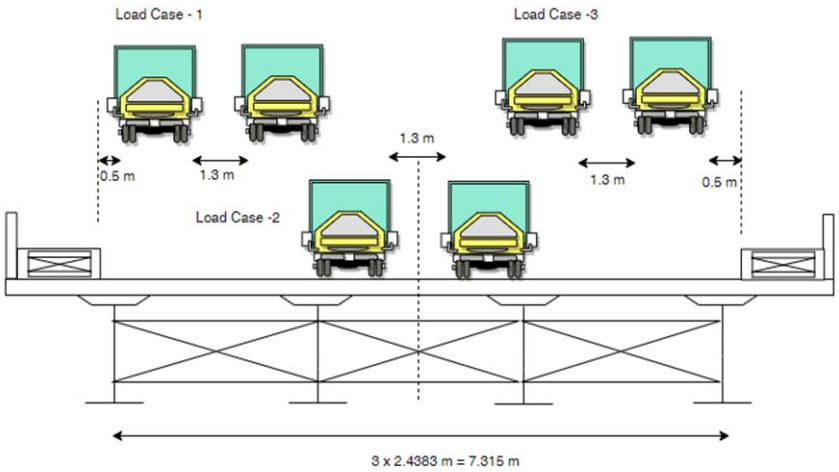

Figure. 5.8 Positions of load on the bridge

For single lane loaded case, bias factor (ration of actual moment to AASHTO LRFD HL-93 design moment) for a single truck varies from 1.3 for the shortest span (10 m) to 1.2 for longer spans (50 m), while coefficient of variation V is 0.11 for all spans. For the two-lane loaded case, λ for each truck varies from 1.2 at 10 m to 1.0 at 50 m, while V for each truck varies from 0.14 at 10 m to 0.18 at 50 m.

5.4.4 Resistance models

Sami and Nowak (1991) presented that a resistance model can be considered as a product of three factors: material properties (strength), fabrication (dimension), and professional (analysis). The statistical parameters used in the probabilistic analysis of bridge are given in **Table 5.2**. This table shows the parameters influencing flexural and deflection of bridge. The derivation of statistical parameters were taken on the basis of available data by Nowak et al. (1991). Monte Carlo simulation will be used to generate the random numbers of variables. The generated material and load random numbers are input to ABAQUS model simulations to get the statistical parameter of system resistance. The distribution of bridge resistance is considered as lognormal.

Table 5.2 Statistical parameters used in the probability analysis

	Variables	Mean to nominal	Coefficient of variation	Distribution	References
Material properties	f_y	1.115	0.1	Lognormal	Nowak,1991
	f_c'	0.805	0.15	Lognormal	Nowak,1991
Dead load	Factory made	1.03	0.08	Normal	Nowak,2011
	Cast-in-place	1.05	0.1	Normal	Nowak,2011
	Asphalt	*250 mm	0.15	Normal	Nowak,2011
	Miscellaneous	1.03-1.05	0.08-0.1	Normal	Nowak,2011
Live load	30m span, Moment	1.15	0.1	Normal	Nowak,2011

*Mean thickness

The capacity of bridge in terms of ultimate truck weight carried by the structure as the system resistance. The maximum load effect is assumed due to multiple trucks. Two trucks side by side load case is applied in present study. Nonlinear analysis of Girder Bridge was performed by modelling 3 dimensional bridge in Commercial Finite Element Software ABAQUS. The system resistance is a random variable. The variation is determined by variation in material properties and load parameters. The statistical parameters of system resistance are obtained by simulating multiple nonlinear analysis with different material properties and loading.

5.4.5 System reliability

In considering structural reliability, it is important to recognize that the failure of a single component may or may not mean failure of the structure (A. S.Nowak & K. R. Collins, 2000). Conventionally, the reliability of structure considered in AASTO considered on member reliability without considering the effect of secondary members effects. Therefore, it is important to realize whether the reliability of an individual member may or may not be representative of the reliability of the entire structural system.

From each girder reliability index, the corresponding system reliability index can be calculated. An important consideration in the system reliability analysis is degree of correlation between the components. It can have a large effect on the reliability of the system; however, it is very hard to assess this correlation. Therefore, two extreme cases: series system (full relation with coefficient of correlation, $\rho=1$), and parallel system (no correlation with coefficient of correlation, $\rho=0$) are considered as idealized systems in this study.

In series system, the failure of one member leads to immediate failure of the entire system. In contrast, parallel system considers as all of the members must fail before the system fails. These two systems as shown in **Figures 5.9 and 5.10** are taken into consideration in this study. With the assumption that the strengths of the elements are all statistically independent, the probability of failure of series and parallel systems are calculated as shown in **Equations 5.11 and 5.12** respectively.

Independent components

$\rho = 1$

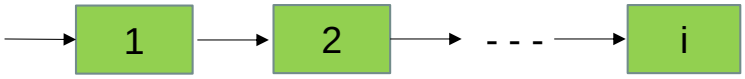

Figure. 5.9 Series system

Probability of failure of series system; $$P_f = 1 - \prod_{i=1}^{n}[1 - P_{f_i}] \quad \textbf{(5.11)}$$

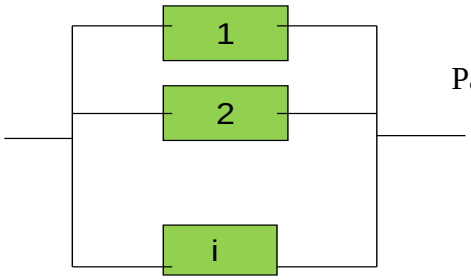

Parallel system

$\rho = 0$

Figure. 5.10 Parallel system

Probability of failure of parallel system; $$P_f = \prod_{i=1}^{n} P_{f_i} \quad \textbf{(5.12)}$$

Where: P_{f_i} is the probability of failure of the ith element.

5.5 Finite element modelling and system resistance

Finite element analysis by using ABAQUS was adopted for the computation of the resistance of bridge at system level. Probabilistic system reliability analysis was proceeded based on the results from ABAQUS outputs. Multiple nonlinear models are developed to simulate the system behavior under time dependent corrosion attacks. Two types of nonlinearities (i.e. material and geometric) are taken into account in ABAQUS for the nonlinear finite element analysis (Abaqus User Guide, 2016). S4R element with six degree of freedoms is used for modelling of girders and cross frame and concrete desk slab. Truss element is used for cross frame and lateral bracing of proposed bridge finite element modelling. The same material properties were used for the flanges and webs of the models. To express the material nonlinearity effect, the ABAQUS metal plasticity

model with kinematic hardening was utilized. An elastic-perfect plastic model based on a simplified bilinear stress-strain curve without strain hardening was assumed in the finite element model.

The nominal yield stress, modulus of Elasticity and Poisson's ratio of 365 MPa, 210000 MPa and 0.3 were used for steel and compressive concrete strength of 25 MPa and Poisson's ration of 0.2 were assigned for concrete material, respectively. Residual stresses were not considered in this study. In boundary conditions, one end fixed (i.e. rotation at perpendicular to bridge axis is free) and one end moveable (i.e. displacement along the bridge axis and rotation perpendicular to bridge axis are free) were set up to get the similar boundary conditions with real structure. The constructed FE model is shown in **Figure 5.11**.

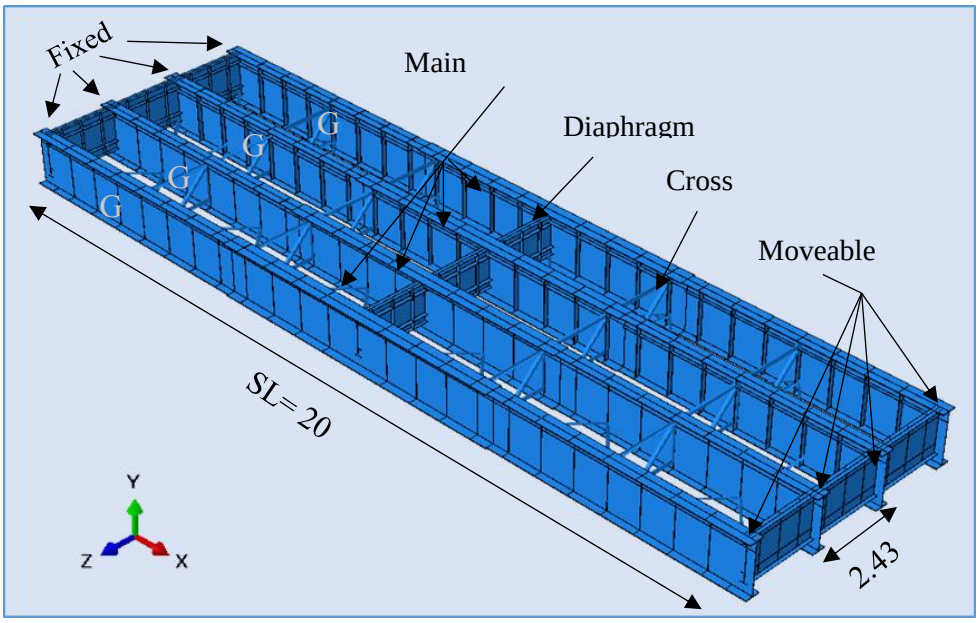

Figure 5.11 FE modelling

The basis load combination includes dead load and live load (statistic and dynamic). Dead load is associated with the self-weight of the girder, deck, barriers, side walk and, wearing surface and so on. Two side by side HL 93 were applied on the bridge as nominal load model and the load is gradually increased until the predefined limit states are reached. The truck position in longitudinal direction is determined by using influence line analysis, the worst loading scenario for the maximum bending moment is observed at where the middle wheel location is 4.501 m from the mid-span of girder. The dynamic

effect of live load is considered using dynamic load amplification factor. The nonlinear analysis solution was achieved using the Newton-Rhapson method in conjunction with the modified RIKS method and the large displacement theory. Geometric nonlinearities are also accounted for the analysis.

The normalized live load is generalized with respect to the nominal live load model such as HL-93 truck by a load factor, LF. The first member fail under ductile failure is defined as LF1 (t) at time t, whereas the bridge system can still sustain the extra live load until the ultimate limit state (ULS) is approached at LF_u (t), which is usually corresponds to the flexural failure of one or several girders that disables the functionality of the bridge system. In addition, there has another limit sate under the ultimate limit state called service limit state (SLS) according to the excessive maximum deflection specified by AASHTO that is L/1000. The performance of the bridge under that limit state is defined as LFS (t) at the time of t. System resistance is expressed as the multiples associated with nominal live-load model, that is, the ratio between the weight of the maximum live load that includes the predefined limit state (i.e., ULS and SLS) and that of the nominal live load model.

The analysis model was verified by using a variety of simplified methods. In this study, the total applied load uniformly to the entire structure is checked with sum of the reaction forces from the analysis model. Theoretically, the total applied load can be calculated and should equal the sum of the reactions from the analysis model.
Check reactions for FWS load versus applied load:

Weight of FWS=1 KN/m²
Area over which FWS applied= 7.315 m × 27.432 m = 200.665 m²
Total weight of FWS= 1 KN/m² × 200.665 m² = 200.665 KN

Table 5.3 Reaction of bridge model (FE model outputs)

Location	Exterior G1	Interior G2	Interior G3	Exterior G4
Left hand support	17.134	21.568	21.934	17.145
Right hand support	25.564	35.735	35.306	25.495
			Total	199.884

The calculated total weight is equal to the sum of the reactions from the model. Additionally, since the structure is symmetric the reactions should also be symmetric. The reactions are symmetric as would be expected. After verifying the results from the Analysis Software, the model was updated to perform probabilistic nonlinear analysis. A million of Monte Carlo simulation for random numbers generation were conducted for the considered random parameters and input to the ABAQUS analysis. An example Monte Carlo simulation of random variables for yield stresses of flange and web are showing in **Figure 5.12**.

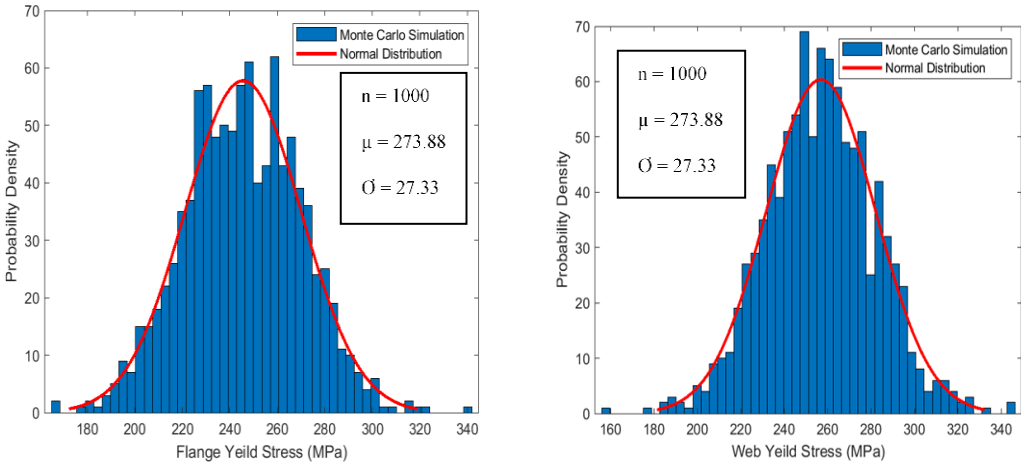

(a) Yield stress of flange (b) Yield stress of web

Figure 5.12 Monte Carlo simulation of yield strength

The system resistance is evaluated using the FEM outputs in a probabilistic way by giving the model to associated random variables. Twenty models of each thickness reduction in girders were generated to capture the system resistance and recorded the statistical parameters (mean and standard deviation) for further reliability analysis. The gross vehicle weight (GVW) of the truck is proportionally increased till the distribution factors of per axle are kept constant which is noted as system ultimate resistance in terms of LF, which is the ratio between the GVW of the applied live load at the failure (i.e., defined limit state).

Two failure patterns such as shear and bending are taken into considers. The LF at the allowable deflection is defined as system resistance at serviceability limit state. The allowable deflection for serviceability limit state specified by AASHTO 1996 is L/1000 is used in this model. The live load deflection at each girders are shown in **Figure 5.13**.

The presented vertical deflections are the values of mid span section of each girder of intact bridge.

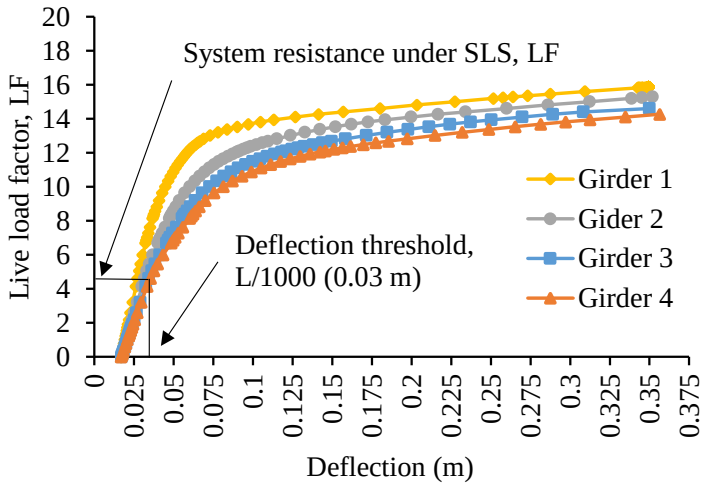

Figure 5.13 Load-structural response curves: live load deflection

Girder G4 reached the allowable deflection for serviceability limit state firstly. The deflection differences between the girders are seen in the figure. This is due to the fact that the loading cases 1 and 3 (closer to the edge girders) are more critical than transverse symmetric load. This unsymmetrical loading can cause G4 and G3 to deform fist. Several finite element models with different material and load random variables were generated to get the statistical parameters of system resistance under serviceability limit state level (LFs) for each time-dependent thickness loss intensity.

The ultimate shear capacity of plate girder under pure shear is calculated as:

$$V_n = CV_p \tag{5.13}$$

$$V_p = \frac{A_v f_{yw}}{\sqrt{3}} \tag{5.14}$$

Where, A_v = shear area

$$\frac{D}{t_w} \leq 1.12\sqrt{\frac{Ek}{F_{yw}}}\ ; \qquad C = 1 \tag{5.15}$$

Where, E = modulus of elasticity, k = shear buckling coefficient, F_{yw} = yield strength of web member

The calculation of ultimate moment resistance is calculated by considering on web thickness ratio of girder. The dimension of girder sections are shown in **Figure 5.14**.

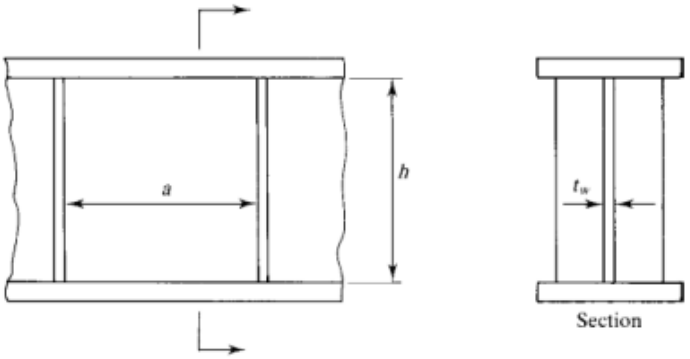

Figure 5.14 Girder cross section

Since $\frac{h}{t_w} > 5.7\sqrt{\frac{E}{F_y}}$ and $\lambda < \lambda_p$, girder web is considered as slender web with compact flange. Therefore, the yielding of compression flange is controlled and moment resistance of girder is defined as:

$$\phi M_n = \phi\ R_{pg} F_y S_{xc} \qquad \textbf{(5.16)}$$

Where, strength factor; $R_{pg} = 1 - \left[\frac{a_w}{1200+300\ a_w}\right]\left[\frac{h_c}{t_w} - 5.7\sqrt{\frac{E}{F_y}}\right]$ and section modulus; $S_{xc} = \frac{I_x}{y_c}$.

Figure 5.15 represents a figure regarding the stress distribution at near the girder ends. The maximum stress was observed near the girder ends. The maximum stress in the main girder was observed in the web plate of I-girder in the location around the support. A yielding of Girder 4 occurred firstly and then successive failures are discovered in all girders as can be seen in **Figure 5.16**. Finally, Girder 1 and Girder 2 reach their ultimate capacity and the LF at this state is defined as the load carrying capacity of bridge system at the ultimate limit state. Both shear and moment carrying capacities of system are extracted from the analysis.

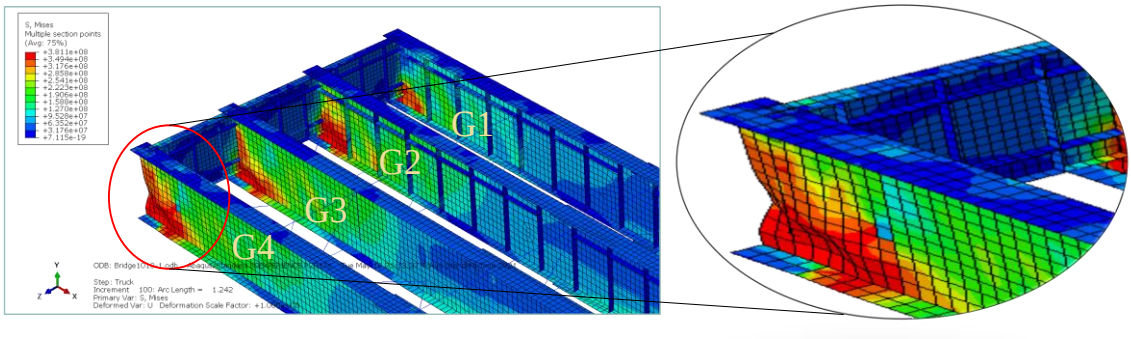

Figure 5.15 Stress distribution near the girder end

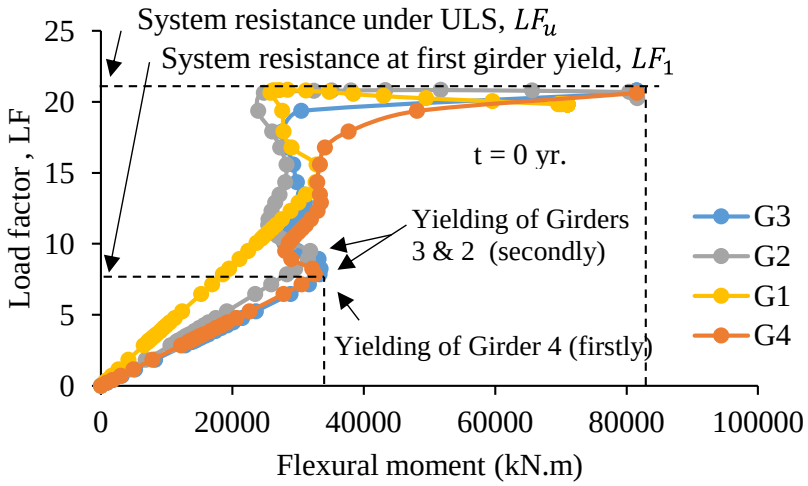

Figure 5.16 Load-structural response: ultimate moment carrying capacity

The simulated load factor at the failure of first girder is considered as LF1 and the one at all members reach at maximum shear capacity is assumed as ultimate LF for shear and at maximum moment capacity is considered as LF for moment carrying capacity of the system. Failure of bridge is occurred due to the web local buckling at the girder ends. The ultimate shear capacity of bridge is lower than the moment carrying capacity. The reduction of bridge system in shear and moment capacities against the amount of thickness losses at the varying time frame is shown in **Figure 5.17**.

The figures show that corrosion has reduced the system resistance capacity through the passage of time. The system shear capacity decreased about 50% after reducing girder thickness value at 100 years and system moment carrying capacity decreased about 30% after 100 years of exposure. It can be said that corrosion has reduced the safety factor against shear force more than against flexural moment.

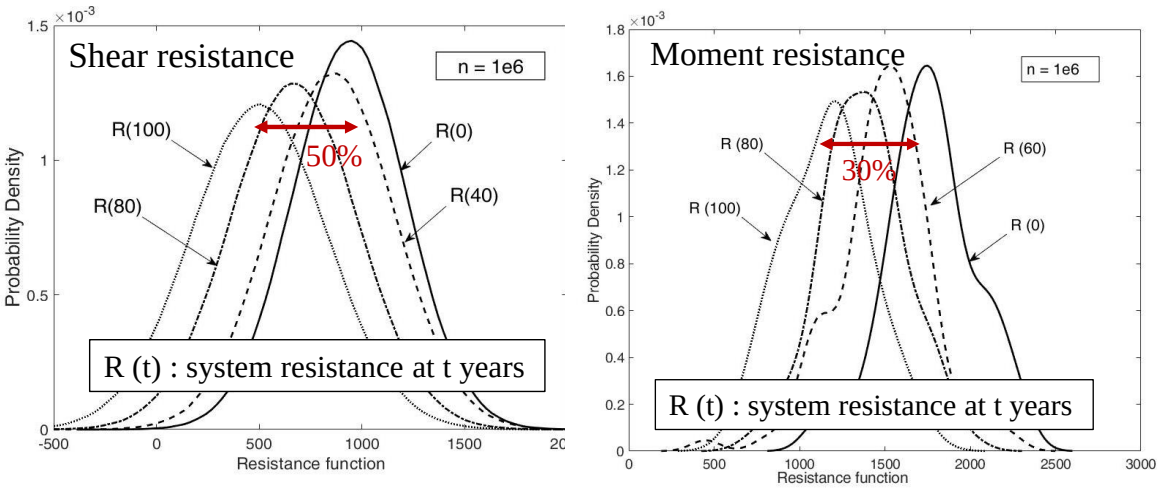

Figure. 5.17 System resistance reduction against time

5.6 Results of system reliability analysis

By applying the calculated thickness loss to the girders of bridge and using generated data from the Monte Carlo simulation, the system resistance under different time variant corrosion level are generated as the load carrying capacity from the ABAQUS outputs. The measurement of individual girder ultimate load carrying capacity is measured at the mid span of tension flange under the failure state where the first yielding occurs at the girder. Probability density function for generated load and resistance by Monte Carlo simulation are as shown in **Figure 5.18**.

The failure of system is calculated based on generated load and resistance models. The probability of failure is defined as the probability that the load is greater than the resistance as shown in **Figure 5.19**.

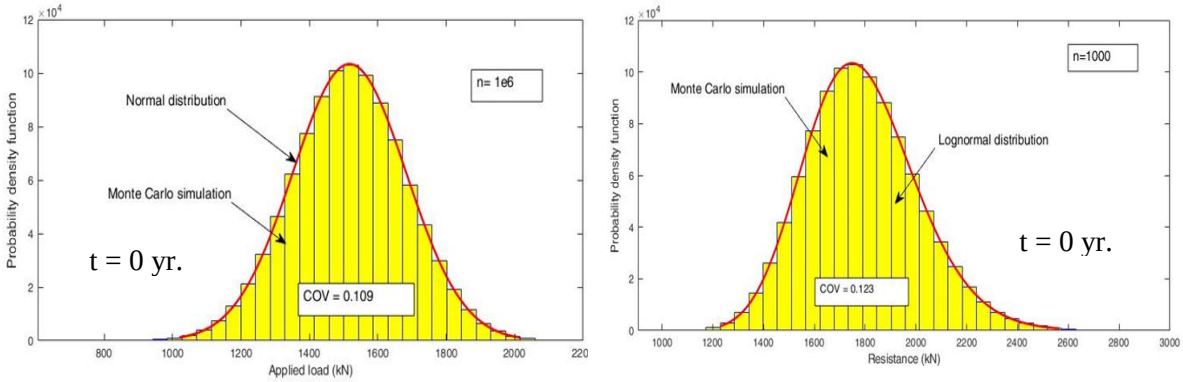

Figure 5.18 Generation of load and resistance models by Monte Carlo simulation

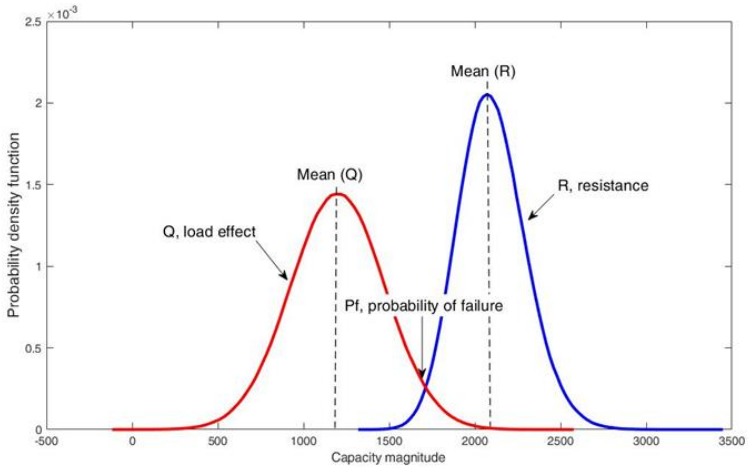

Figure 5.19 Load versus resistance probability density function

The results of the reliability indexes are shown in **Figure 5.20**. According to the figure, the system resistance decreased with corrosion propagation. The reliability indices of the bridge system are much larger than the reliability index of each individual girder which is indicating the benefit of redundancy and ductility on structural safety. The resistance decreased about 23% and 42% in moment and shear capacity in ULS and 43% in SLS of intact at 100 years of exposure.

Considering the effect of corrosion, the reliability index of the most critical girder degrades to the threshold value by AASHTO (i.e., 3.07) at about 60 years, whereas the three others system reliability indices remain above the threshold value through the design service life.

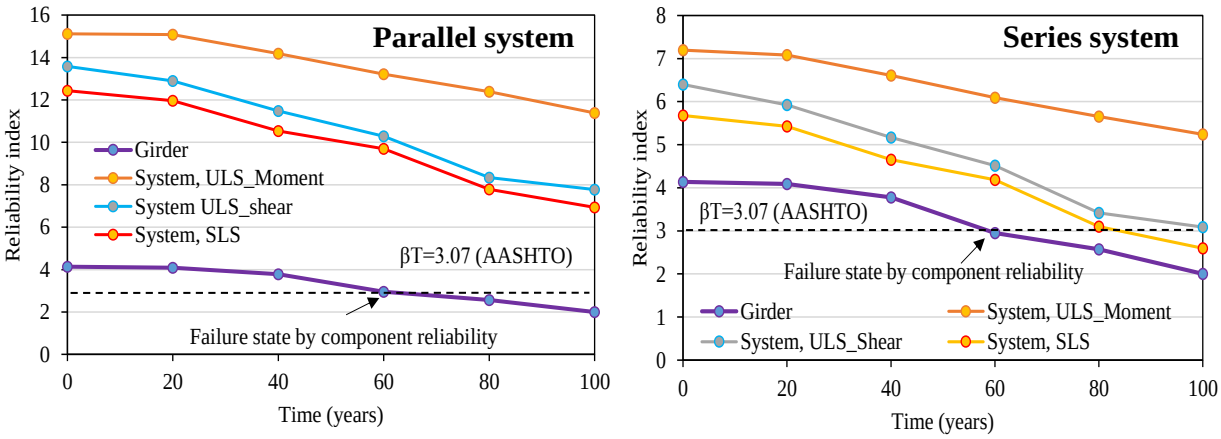

Figure 5.20 Reliability indices of parallel and series systems

The figures also describe that parallel systems produce higher reliability indices than series systems. The results show reliability indices of parallel system are almost twice higher than the one in series system.

An evaluation of series and parallel systems are carried out by comparing the indexes calculated by tow extreme degree of correlation. The results are shown in **Figure 5.21**. The figure shows that the coefficient of correlation, ρ, can decrease system reliability index. The reliability index determined by parallel system is much larger than the series system in all failure modes (moment, shear, serviceability and yielding of first girder). It is also observed that the index calculated by series system got lower than girder reliability index as described in Figure 5.16. This might be the common characteristic of a series system. Moreover, higher deviations are observed in series than parallel. These data tell us that the series system is less reliable than either of its components and series system in the girder bridge. Moses 1997 mentioned that several components in the girder bridge must fail simultaneously for an overall system failure. According to this, calculation of bridge reliability by using parallel system can prevent the evaluating of the structural performance of the girder bridge from by being too low by using other systems.

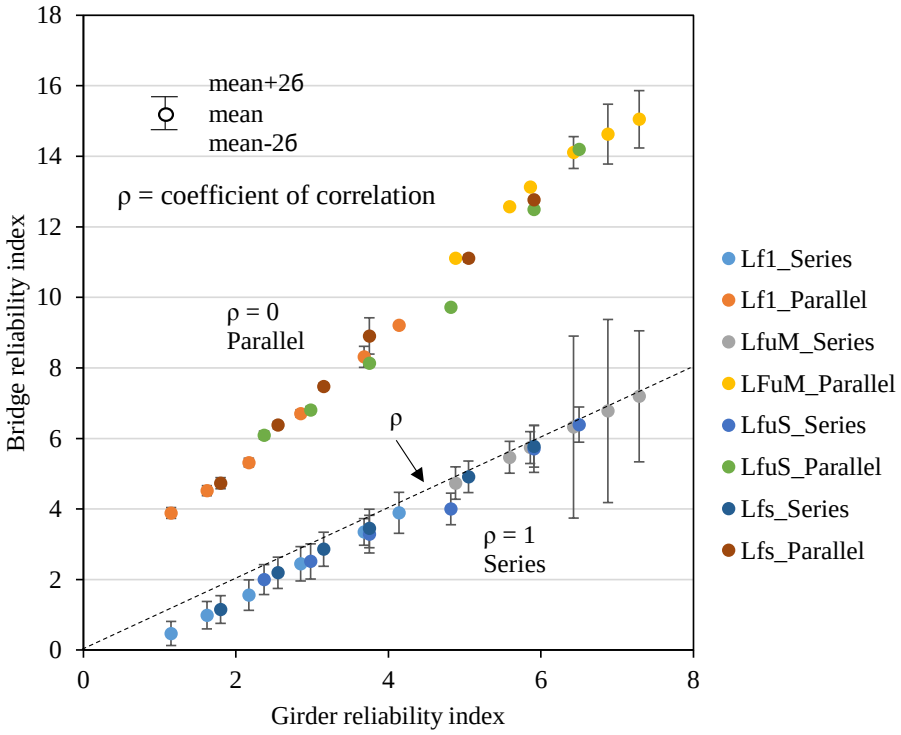

Lf1 = yielding, LfuM = ultimate moment, LfuS= ultimate shear, Lfs = service

Figure 5.21 Series and parallel system reliability indices

Reliability indexes of bridge with or without steel washing is shown in **Figure 5.22**. The positive effectiveness of steel washing on bridge reliability can be seen in the figure. The bridge reliability at serviceability and ultimate shear states with no washing (i.e., Lfs-N & Lfu_SN) fall under the threshold value by AASHTO at 60 and 78 years respectively.

In contrast, the bridge reliability with regular washing in all limit states (ultimate shear, moment and serviceability) symbolled in the figure as Lfu_MW, Lfu_SW and Lfs_W remain over the target value till the end of service life. The results from the figure supports the statement that steel washing is an effective bridge maintenance to enhance structural degradation of steel girder highway bridges due to corrosion problem. The steel bridge washing alternative resulted in a better option by reducing the rate of structural capacity degradation when compared to the no washing option.

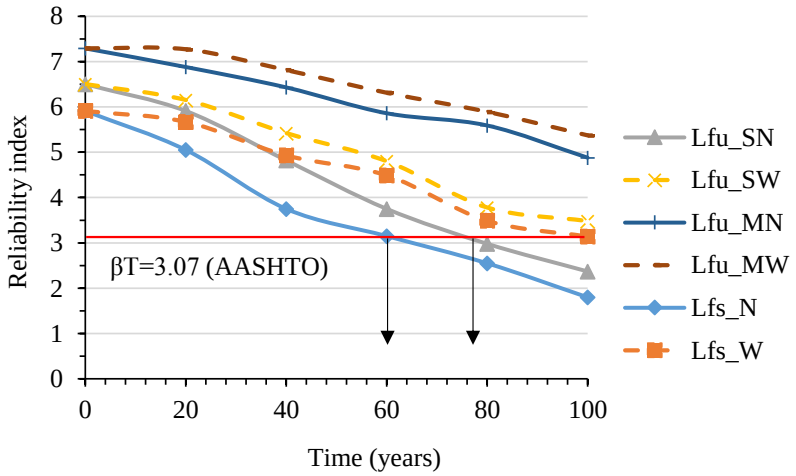

Figure 5.22 Reliability indexes of bridge with and without washing

The time-dependent deterministic system redundancy is also considered as the parameter changed under the corrosion attack. The redundancy value is quantified by the ratios between the load factor at system limit states of serviceability, ultimate moment and shear, (LFs (t), LFu_M (t) and LFu_S (t)) and load factor at the fist girder failure (LF1 (t)) (Ghosn and Moses 1998). The formulae used in the calculation is described as follows:

$$R_u\,(t) = \frac{LF_u\,(t)}{LF_1\,(t)} \quad \textbf{(5.17)}$$

$$R_s\,(t) = \frac{LF_s\,(t)}{LF_1\,(t)} \quad \textbf{(5.18)}$$

where: $R_u\,(t)\ and\ R_s\,(t)$ = system reverse ratio at time with respect to ULS and SLS

The results of calculated time variant redundancy indices are shown in **Figure 5.23**. The system redundancy indicators in ULS decreases in accordance with the corrosion process (from 2.7 at t= 0 year to 2.4 at t= 100 years in moment and from 1.95 at t= 0 year to 1.38 at t= 100 years in shear). The deterministic regarding to SLS also decrease obviously from 1.85 at initial state to 1.38 at 100 years of corrosion propagates. The maximum redundancy reduction is observed in service limit state and it is about 25%. Moses & Ghosn (1998) suggested a minimum value of 1.3 and 1.1 for ultimate limit state, Ru and serviceability limit state, Rs to ensure a redundant super-structure system.

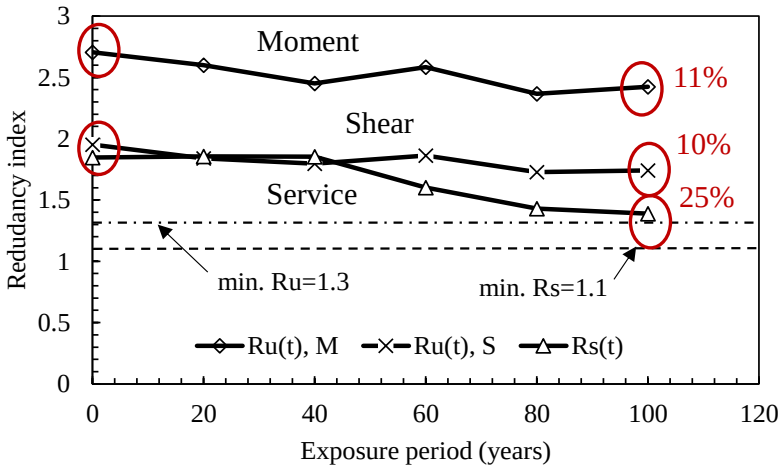

Figure 5.23 Redundancy at limit states

As indicated in the figure, the system reverse ratios regarding with ULS of moment; Ru(t), M, ULS of shear; Ru(t), S and SLS; Rs(t) are larger than 1.3 and 1.1 throughout the service life, describing a satisfactory redundancy performance. Therefore, the assumption for reliability calculation as parallel system found an agreement with this redundancy validation. The quantification of redundancy urges that the corrosion can downgraded the performances of system redundancy.

5.7 Discussion and conclusions

Reliability evaluation under corrosion attack is performed in this chapter. The finite element analysis results show that the shear reliability reduces more than moment reliability after passage of time. System reliability indexes are higher than member reliability indexes. The system reliability indexes for the studied bridge are higher than the target index defined by the AASHTO standard, however, the section reliability index falls under the limit value after the 60 years of exposure. The negative effects of atmospheric corrosion on system redundancy is observed in this study. The results from calculation of system reliability show the benefits of secondary member in reliability calculation. Parallel system produced higher reliability indices than series system. Therefore, the consideration of system reliability of the girder bridge in parallel system can prevent the structure performance in judging low value.

The benefits of bridge washing on structural performances under the passage of time is evaluated. This section points out that steel pressure washing with water can prevent the progression of rust layer on the member surface and should be considered as an appropriate maintenance measure of atmospheric corrosion in bridges.

The system resistance decreased about 23% and 42% of intact model in moment and shear and 43% in serviceability state at 100 years of service. The redundancies of representative bridge indicate satisfactory redundancy performances at 100 years' service life. The negative effect of steel corrosion on system reliability and redundancy can be seen in this section.

References

ABAQUS, *Standard User's Manual*, Hibbitt, Karlsson and Soren-son, Inc., 2008.

AASHTO LRFD Bride Design Specifications, Washington, D.C., 2004.

Andrzej S. Nowak and Jianhua Zhou, *System reliability models for bridges*, Structural safety, 7 (1990) 247-254.

Andrzej S. Nowak, "Load model for bridge design code", Canadian Journal of Engineering, 2011. DOI: 10.1139/l94-004

A. S. Nowak, "System reliability models for bridge structures", Bulletin of the Polish Academy of Sciences Technical Sciences, Vol. 52, No. 4, 2004.

A.S. Nowak and M. M. Szerszen, Reliability Profiles for Steel Girder Bridges with regard to Corrosion and Fatigue, Ernst & Sohn, Berlin, Germany, 2001.

A. S. Nowak and Kevin R. Collins, Reliability of Structures, Mc Graw Hill, Singapore, 2000.

A. S. Nowak and K. R. Collins, "Reliability of Structures", pp. 184-195; 302-311, McGraw Hill, Boston, 2000.

Bing Tu, You dong, A.M.ASCE and Zhi Fang, "Time-dependent reliability and redundancy of corroded prestressed concrete bridges at material, component, and system level", Bridge Eng., ASCE, 24 (9), 2019.

C. D. Eamon and A. S. Nowak, "Effects of edge-stiffening elements and diaphragms on bridge resistance and load distribution", ASCE Journal of Bridge Engineering 7(5), 258-266 (September/October 2002).

CHBDC, Canadian Highway Bridge Design Code, Canadian Standard Association, Toronto, 2003.

ENC 1991-3 Eurocode 1: Basis of Design and Actions on Structures. Part 3: Traffic loads on Bridges, 1994.

Galambos, T. V., Ed., Guide to Stability Design Criteria for Metal Structures, 5th ed., John Wiley & Sons, New York, 1998.

Ghosn, M., F. Moses, 1998. "Redundancy in highway bridge superstructures", NCHRP Rep. No. 406. Washington, DC: National Cooperative Highway Research Program.

G. Konig and A. S. Nowak, (ed.), Bridge Rehabilitation, Ernst & Sohn, Berlin, Germany, 1992.

JICA, Research Study on Review and Application of the Bridge Engineering Training Center Project in Myanmar, Final Report, Japan Internationa Cooperation Agency, September 2012.

Japan Infrastructure Partners. Current Situation and Issues of Myanmar's Bridge Work; Japan Infrastructure Partners: Tokyo, Japan, 2012.

J. R. Kayser, The effects of corrosion on the reliability of steel girder bridges, Ph.D., Thesis, Dept. of Civil Eng., University of Michigan, Ann Arbor, MI, 1988.

Moses, F., "Problems and prospects of reliability-based optimization", Engineering Structures, Vol. 19, No. 4, pp. 293-301, 1997.

P. Albrecht and A.H. Naeemi, "Performance of weathering steel in bridges", National Cooperative Highway Research Program Report 272, 1985.

R. Rackwitz and B. Fiessler, "Structural reliability under combined random load sequences", Computer and Structures 9, 489-494 (1978).

Sami W. Tabsh and Andrzej S. Nowak, "Reliability of highway girder bridges", Journal of Structural Engineering, Vol. 117, No. 8, Pg. 2372-2388, 1991. DOI: 10.1061/(ASCE)0733-9445(1991)117:8(2372)

Source: https://www.iis.u-tokyo.ac.jp/en/news/2920/

Walbridge, S. *A Probabilistic Study of Fatigue in Post-Weld Treated Tubular Bridge Structures*. EPFL Thesis No. 3330. École Polytechnique Fédérale de Lausanne, 2005

Chapter 6

PROPORSAL OF STEEL BRIDGE MAINTENANCE PLAN BASED ON LIFE-CYCLE COST ANALYSIS

6.1 Introduction

The usage of weathering steel in infrastructure construction is popular in the recent era due to its minimum maintenance cost. The appropriate use of weathering steels can be effectively reduce charges cost by corrosion problem which occurs as usual in carbon steel. The constructive quantity of weathering steel bridges has increased in Japan (Japan Association of Steel Bridge Construction, 2001) as shown in **Figure 6.1**. The use of proportion of weathering steel in bridge construction increased remarkably after 1999.

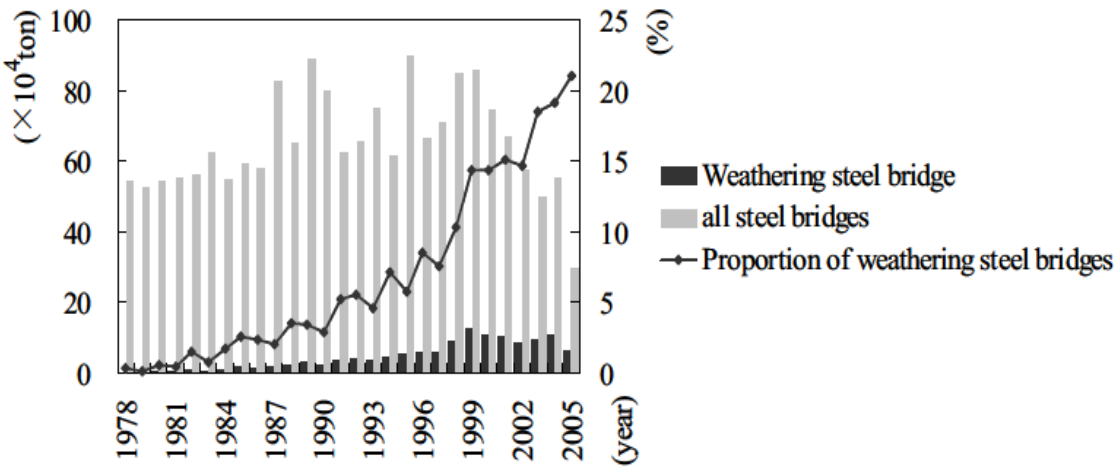

Figure 6.1 Constructive quantity of weathering steel bridges in Japan
(Japan Association of Steel Bridge Construction, 2001)

According to the technical report published by JFE engineering (2005), the number of steel bridges being built by WS has approximately trebled in the last ten years throughout the world and now it accounts for more than 15% of the market. The advantage of WS usage is potential for savings in life cycle cost by eliminating the need for the initial painting and periodic repainting of the entire superstructure, as it is required for the ordinary steels that do not resist atmospheric corrosion. WS forms its protective oxide layer that inhibits the steel from rusting in the atmosphere in a suitable environment. The NCHRP report (1990) describes the accumulation of much debris become wet from condensation, leaky joints and spray are mostly experienced in highway bridges. Different combination of these factors can cause exposure conditions under which the weathering steels cannot form a protective oxide coating. Therefore, WS is not a maintenance-free material and the bridge built by WS must be maintained properly.

The ability of weathering steel to resist atmospheric corrosion is vital to its being successfully used. According to the National Cooperative Highway Research Program Report (1990), the weathering steel can only give satisfactory performance while the environment provides an adequate period of drying, must not provide excessive periods of wetting, and must not contain excessive amounts of corrosive contaminants. The anti-corrosive performance of weathering steel in bridge is a combination of factors related to the general climate of the region plus factors related to the specific bridge site. The report also mentioned that it is necessary to understand the behaviors of local climatic environments, called microenvironments. Atmospheric corrosion data are also useful for the determination effects of environments on weathering steel corrosion. However, these data cannot perfectly match the corrosion rates in the real bridge because the test data are obtained from the small coupons test. In contract, structural bridge members have grater mass and possess different thermal effect than small test pieces. Therefore, the effective inspection and maintenance program is essential to ensure for weathering steel bridge to reach its design service life. According to the guidelines for the use of weathering steel in bridges, the regular inspection of bridge should be done every 2 years as is required for the painted bridge.

The appearance of the oxide film (color and texture) indicates the degree of protectiveness of weathering steel. A visual inspection and photographing can only deceptive for that kind of appearance inspection. The condition of oxide film should be

trapped with hammer and vigorously wire brushes to determine whether the film adheres to the underlying steel base or has de-bonded as flakes or laminar sheets. The purpose of this section is to show the inspected appearance of the oxide film which refers to the weathering steel's protectiveness. The assessment of these bridge inspection can provide a helpful information in determining whether the bridge satisfies in sound condition or it is necessary for remedial paint to protect a high degree of uniform or local corrosion.

The true cost of a bridge structure is the cost to build, inspect and maintain the bridge over the entire lifespan of the bridge. This is often specified as the "life-cycle" cost, and it is a better measure of the real cost of a bridge, rather than an initial, or first cost. The consideration whether WS is suitable to use to a bridge or not depends on the LCC reduction effect of bridge through its service life with respective to the corrosion severity of bridge site. This chapter describes the significant effect in LCC reduction of WS application in bridges for two different environments (coastal and urban environments). Three alternative systems involve bare weathering steel with periodical edge paint, bare weathering steel washed after every 1.8 years by high pressure hosing and weathering steel washed after every 5.5 years by high pressure hosing are considered in this economic analysis. The comparison of LCC of bridges with painting and use of bare WS with or without periodic washing are taken into consideration in determining the least expensive alternative maintenance systems. This chapter propose an economical maintenance plan of steel bridge in Myanmar based on practical measures in real weathering steel bridge in Myanmar and life-cycle calculation.

6.2 Visual inspection based condition assessment

The visual inspection of oxide film color and texture can determine the degree to the oxide film that helps weathering steel to be protective. The color may vary from maroon to black, in contrast to the bright orange color of new rust on ordinary steel. The texture may be smooth or may provide small particles of rust when rubbed with the hand. The normal protective oxide will adhere to the underlying steel and will not separate in flakes or sheets. When the appearance indicates that the oxide film is non-protective, the measurement of uniform corrosion penetration and pit depth should also be measured with ultrasonic thickness gauge on a member. Japan Association of Steel Bridge

Construction and Japan Iron and Steel Federation proposed the visual inspection based criterion for condition assessment of weathering steel. The condition states are categorized into 5 levels ranging from 5 to 1 as shown in **Table 6.1**. In the table, the condition states are classified by the rust flake grain sizes. The patina layer is defined at the grain size within 1 mm and 5 mm in diameter (rust thickness of less than 400 μm) and the condition is acceptable level with high index ranging from 5 to 3. The level 2 is specified as the state of required in detail inspection and it granule size is in between 5 to 25 mm in diameter (rust thickness is within 400 and 800 μm). The poorest condition state, i.e. level 1 implies the area observed having thick and loose laminar sheets and appears very severe corrosion.

Table 6.1 Rating criterion based on visual inspection and rust thickness measurement

Condition state	Attribute	Description of rust patina	Rust thickness
5	Acceptable	Very thin protective oxide film	< 200μm
4		Average granule size: <1mm diameter	< 400μm
3		Average granule size: 1~5mm diameter	
2	Require detail inspection	Granule size: 5~25mm diameter Having rust flakes	> 400μm < 800μm
1	Failed	Thick and loose laminar sheets, very severe corrosion	> 800μm

Rating: 5 Rating: 4 Rating: 3

Rating: 2 Rating: 1 Rating: 1

Figure 6.2 Appearance of 9 years' exposure test (Japan Iron and Steel Federation)

Moreover, the variation of color and texture of oxide layer are also highlight as the grading of condition by the Japan Iron and Steel Federation. **Figure 6.2** shows the

grading of condition with respective surface configuration. The variations of the steel surface can be clearly displayed the rating. As similar with the condition statement, the ratings are differ through the size of surface grain and the grading can be determined easily by visual observation in comparison with the specification. Thickness measurement is also necessary to specify the condition of rust when the surface seems oxide layer does not develop.

6.2.1 Field inspection of weathering steel bridge in Myanmar

The visual field inspection and rust thickness measurement were performed at the real bridge same with reliability evaluated bridge named the Thankan Chaung Bridge (the first weathering steel bridge in Myanmar). The bridge is plate girder type and measurements were carried out at each girder (such as exterior and interior girders) and joint. Corrosion thickness gauge was used for the rust thickness measurement on the different members such as cross frame, main girder, joints close to the drainage and bracing.

The bridge inspection at 22 point on the different bridge members were conducted. The lists of inspection points are shown in **Table 6.2**. Similar measurements were taken at the same points at each girder.

Table 6.2 Inspection points

Member	No. of points	Location
Flange	6	Lower flange (top and bottom)
Web	8	Both sides
Joint	4	Interior and exterior
Cross frame	4	Middle

The inspection was conducted in February, 2020 while over 2 years after the public opening. The bridge was constructed in combine with carbon steel at the middle spans of bridge and four end panels (on each side) are made by weathering steel. The rust thickness measurements were taken at the side span where weathering steels are used.

The repetitive measurements at the same point were done for the accuracy of data. The rust thickness measurement and photographing of oxide surface in both ordinary and close-up were taken during the survey period.

6.2.2 Surface appearance

The inspection photos and measured data are described in this section. The overall views of the bridge are shown in **Figure 6.3**.

(a) Overall view of bridge underneath (b) Exterior girder

Figure 6.3 Surface configuration of weathering steel bridge

As can be seen in figure that the dumping of dust and other foreign matter are observed at the top surface of lower flange. According to the photos, the rust layer is more emerge at the lower flange than the other parts. The close-up pictures of lower flange at the bottom surface is shown in **Figure 6.4**.

(a) Girder (close up) (b) Bottom flange (close up)

Figure 6.4 Close-up view of lower flange

Figure 6.4 (a) shows the surface condition at the middle of the end span and Figure 6.4 (b) shows the surface condition of lower flange bottom surface near the end panels

closer to the abutment. According to the photos, the bottom surface has flaky and granular rust. The location of this place can easily access by the people and the effect of human behaviors interfere the steel performances. By the visual inspection guided by the Japan Iron and Steel Federation, the grading of the corroded surface at the present bridge can be identified as in grading between 3 and 4 at the girder web. However, the rust is flakier at the bottom surface of lower flange near the abutment. The grading 2 is observed for that area. It is noted that the potential problems related to weathering steel with extended periods of wetness which is caused by the excessive dumping of dirt and debris on the surfaces was seen at the current bridge. This condition create chloride to attach easily attached and it is leading to corrosion process more severe. The main reason of this situation may cause by the inadequate management of water at the drainage. Additional measurement for the maintenance activity is advisable.

6.2.3 Color and texture

The NCHRP 314 report (1990) described that the guidelines for the color of oxide layer and its appearance. The definition of each color and texture by the guideline is described in Table 6.3. According to the guideline, the color of rust layer in yellow orange at the current bridge describes that the rust layer is at the initial state of formation and no protective layer is forming yet. Furthermore, the texture of rust layer was discovered as dusty at the web and top flanges. It means that the exposure at the initial stage and it might change after a few years. However, the partial granular rust layer was observed at the bottom of lower flange.

Table 6.3. Appearance of rust layer (NCHRP) (a) Color condition

Color	Condition
Yellow orange	Initial stage of exposure
Light brown	Early stage of exposure
Chocolate brown to purple brown	Development of protective oxide
Black	Non-protective oxide

Table 6.3. Appearance of rust layer (NCHRP) (b) Texture condition

Texture	Condition
Tightly adherent, capable of withstanding hammering or vigorous wire brushing	Protective oxide
Dusty	Early stages of exposure, should change after a few years
Granular	Possible indication of problem depending on length of exposure and location of structure
Small flakes, 6 mm in diameter or greater	Initial condition of non-protective oxide
Large flakes, 12 mm in diameter or greater	Non-protective oxide
Laminar sheets or nodules	Non-protective oxide, severe corrosion

The condition in present situation describes that it is possible to the initiation of problem depending on the length of exposure and location of structure. In accordance with this, the measurement will be taken again after a few years later. The decision for suitable surface treatment (such as painting or high pressure washing) to the bridge should be taken on the further measurement.

6.2.4 Rust thickness measurement

The position of the bridge is seen as one side of the bridge is close by the seashore as shown in **Figure 6.5**. It is located at 28.15 km far away from the sea shore.

The measurements were taken on the weathering steel bridge at both sides. Rust thicknesses were measured at different members such as lower flange, cross frame, joint and web. The thickness of rusts are varied according to the location of the member. The measurement results are shown in **Figure 6.6** for the test site near the sea and **Figure 6.7** for the opposite test site.

(a) Bridge location on google map

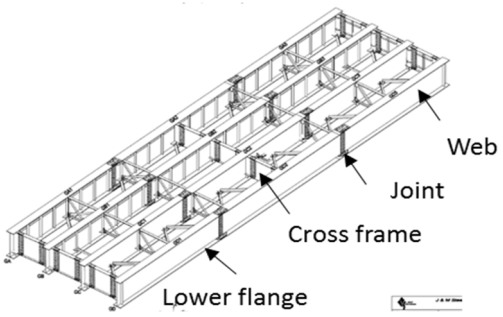

(b) Bridge structural composition

Figure 6.5 Location of bridge and components

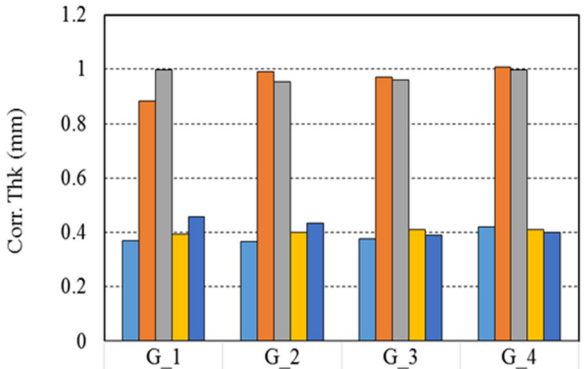

	G_1	G_2	G_3	G_4
Web	0.370625	0.36625	0.37813	0.4196
Lower Flange_top surf	0.8825	0.990375	0.971375	1.00825
Lower Flange_bot. surf	0.9965	0.9525	0.961	0.9975
Joint	0.394	0.3995	0.4095	0.409
Cross Frame	0.4585	0.435	0.391	0.399

Figure 6.6 Rust thickness at close to the sea site

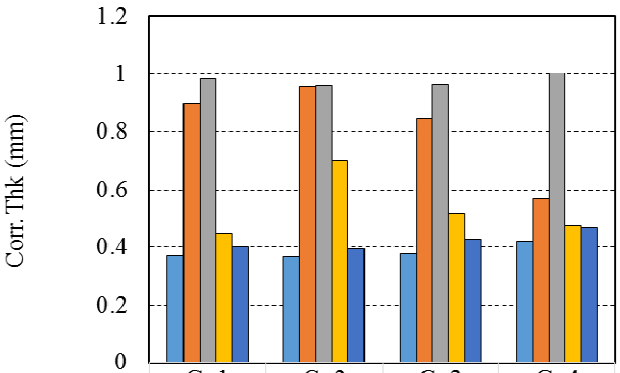

	G_1	G_2	G_3	G_4
Web	0.370625	0.36625	0.37813	0.4196
Lower Flange_top surf	0.895625	0.958625	0.84625	0.567875
Lower Flange_bot. surf	0.98275	0.96175	0.96325	1.00425
Joint	0.446	0.7005	0.5175	0.474
Cross Frame	0.4015	0.3955	0.426	0.4685

Figure 6.7 Rust thickness at opposite to the sea site

The highest rust thickness was measured at bottom surface of lower flange. The maximum is about 1 mm. The penetration of rust layer is more intense at the test site which is closer to the sea as expected. A measured rust thickness is higher than the acceptable level specified by the Japan Iron and Steel Federation although the visual observation makes the grading between 3 and 4 in acceptable range. Measurement error during the survey time is also considerable. Further measurement should be taken to determine the appropriate maintenance activities on the bridge.

6.3 Life-cycle cost analysis

Life-cycle cost (LCC) is a method used to assess the total cost of a project. LCCA is particularly useful when a single project has different alternatives that fulfill the original requirements. Different alternatives could vary in initial investment or cost, operational costs, maintenance costs, or other long-term costs (Stefan L. L. M & Mark D.B, 2019). This kind of analysis, when applied to bridge infrastructure projects, is called as bridge life-cycle cost analysis (BLCCA). The American Society of Civil Engineers and ENO Center of Transportation (2014) mentioned that an examination of the full life-cycle costs help an agency in determining the appropriate investment in an asset given current and future constraints.

The cost of keeping a bridge in a safe and good condition is not a one-time expenditure based on the initial cost of construction (Bowman and Moran, 2015). The cost of operating a bridge in a good condition requires a long-term investment during the entire expected service life (Hema et al., 2004). Scheduled preventive bridge maintenance activities are more efficient and cost-effective than reactionary maintenance activities (NYSDOT, 2008; FHWA, 2011; Yanev, 2011).

The purpose of LCCA is to specify an economically efficient set of actions and their timing during the bridge's life cycle to achieve the 50-to-100 year service life that many bridge-management professionals feel is an appropriate target for this major public investment [NCHR report 483, 2002]. Life-Cycle Cost Analysis (LCCA) can assist in making a decision oriented by showing the benefits from different alternatives to achieve the same expected results (Azizinamini et al., 2013). A bridge represents a long-term, multi-year investment. Following its planning, design, and construction, a bridge requires

periodic maintenance and possibly repair or rehabilitation actions to ensure its continued function and safety.

A LCCA is performed typically in the following sequential steps:

- Identifying alternative systems
- Defining time frame of bridge service life
- Defining cost for each alternative
- Comparing expenditures from different alternatives, and
- Making final decision.

6.3.1 Alternative maintenance systems and costs

Painting and frequent bridge washing with suitable time interval are determined as alternative systems in present study. Six types of paint systems are adopted from the former researcher from YTU (Yu Y. K. W, 2017). The initial and repainting costs of painting systems are also adopted.

The composition of painting systems are described in **Table 6.4**. The costs, repair interval and number of intervention for maintenance and inspection are presented in **Table 6.5**. The expenditure of steel bridge washing with 1.8 years interval in coastal and 5.5 years interval in urban environments are examined. The unit cost for steel bridge superstructure washing considered in this study was conducted by Sobanjo (2001) and Hearn (2012). The cost of girder washing was estimated as $ 10 per linear foot. The condition of girder is assumed as no corrosion on the surface at the time of washing. Life span of bridge is considered as 100 years in this study.

The time of first maintenance and repair for painting system used in this study are referred to ISO 12944. Repainting time interval for series 2A and 2C are determined by Japan Paint Manufacturers Association. Paint system 1B has the least maintenance interval which is necessary to repaint after 2 years. The maximum service life of paint is observed in paint system 2A which needs to repaint only once in 100 life span although the initial paint cost is higher than paint system 1B.

Table 6.4 Paint systems and compositions

Type of paint	Series name					
	1			2		
	1A	1B	1C	2A	2B	2C
1st coat	Epoxy	Lead-based	Epoxy	Inorganic zinc-rich	Inorganic zinc-rich	Inorganic zinc-rich
2nd coat	Epoxy	Lead-based	Epoxy	Epoxy	Epoxy	Epoxy
3rd coat	Fluororesin	Alkyd	Epoxy	Fluororesin	Silicon-acrylic	Polyurethane
4th coat	Fluororesin	Alkyd	Epoxy	Fluororesin	Silicon-acrylic	Polyurethane

Table 6.5 Painting cost and maintenance intervention during lifespan (100 years)

Paint type		Unit cost (¥/m^2)	Maintenance (Years)	Intervention / 100 years life
1A	Initial cost	1,263	15	7
	Repainting cost	1,290		
1B	Initial cost	4,00	2	50
	Repainting cost	427		
1C	Initial cost	2,715	5	20
	Repainting cost	1,656		
2A	Initial cost	3,088	60	1
	Repainting cost	3,115		
2B	Initial cost	2,828	15	6
	Repainting cost	2,855		
2C	Initial cost	2,603	18	7
	Repainting cost	2,629		
JIS SMA surface treatment	Initial treatment cost	1200	30	3
	Edge repaint	100		
	Pressure washing	120	1.8/5.5	56/19

The cost of weathering steel surface treatments with periodical edge repainting are adopted from a LCC calculation by the Japan Association of Steel Bridge Construction (2000).

6.3.2 Results from LCCA

A LCCA is performed in this section by considering different maintenance scenarios applied during the bridge service life. For simplicity, the LCCA only emphasized on the expenditures related to the bridge maintenance activities. The maintenance activities include surface treatments with different paint systems and JIS SMA Steel with surface weathering preparation. The life-cycle cost calculation is performed by using paint and repainting costs of considered paint systems and frequent bridge washing with their expected durability and washing time interval.

Figure 6.8 shows the calculated LCC for maintenance activities considered. The use of WS in bridge does not require painting at intervals of several years, and is economically superior to the painted bridges as can be seen in figure. Different painting systems are considered as surface treatment on conventional steel. Among different kinds of paint systems, paint system 1C is commonly used in Myanmar recently. Reduction in LCC for paint system 1A and paint system 2A are obviously seen in figure. Although the initial cost of paint system 1B is the lowest among considered paint systems, it prone to higher LCC than other paint systems. Paint system 1C has the highest LCC at the end of considered service life even though the initial cost is low.

A frequent bridge washing with proper time interval was considered as regular maintenance activities for its visible benefits on structural performance as described in Chapter 5. The maintenance programs consisted in regular steel girder washing at each 1.8 years and 5.5 years are proposed for coastal and urban environments respectively. As presented in figure, LCC under 5.5 years washing program promotes saving in LCC more than seven times than the conventional surface painting which is usually done in Myanmar. Moreover, application of WS with 5.5 years washing interval in urban environment cost lower expenditure than all kinds of paint systems at the end of service life.

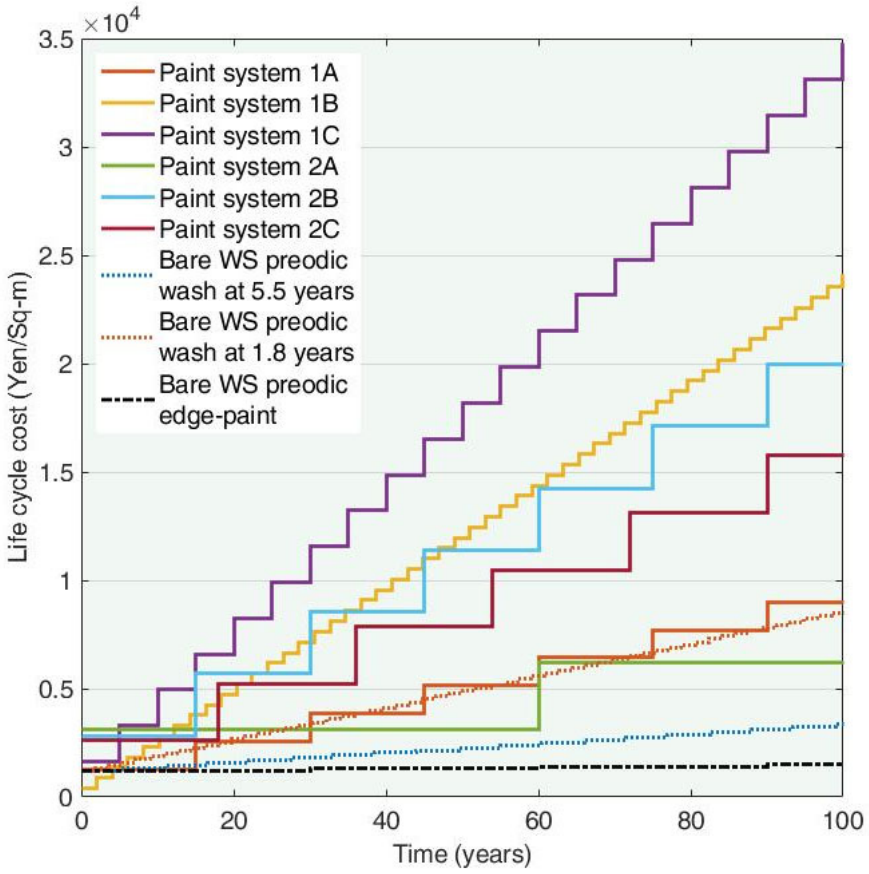

Figure 6.8 Life cycle cost based on the expected service life

The use of WS with narrow washing time interval in coastal environment is worth more cost than paint system 2A. In compare to the costs of paint system 2A and WS with intermittent washing in coastal region, the judgement will be needed based on the engineers' practices. However, WS costs lesser than the cost for commonly used paint system in Myanmar. The surface preparation with series 2A paint system will be a little more economical than WS in the coastal region.

6.4 Discussion and conclusions

A visual inspection of weathering steel bridge at the site has been taken. According to the visual inspection guideline, the oxide layer color and texture at the bridge is in rust layer initiation stage. Protective layer of weathering steel has not been formed yet. An abnormal rust development is found at the lower flanges for some

unfavorable reasons such as blocking of drainage, long-term deposition of foreign matters (e.g. dirt, debris and soot) and water leakage from the deck expansion joint. A specific reason for this severe rust formation could not inspected and pointed out during that time of measurement. Considering on skill of measured person and other environmental issues, the measurement should be retaken after a few time later. The author would like to recommend for the making surface treatment to the bridge before the rust layer is growing seriously on the surface. Bridge washing with power hosting for the removal of dirt and loose rust layer is one of the acceptable maintenance activities at present test site. Further investigation will be conducted in the near future to provide the information about suitability of weathering steel for infrastructure construction in Myanmar.

The economic study focuses on comparative costs of six different paint systems which were exposed to the environment in Myanmar and calculated the deterioration rate for repainting. The calculation of life cycle cost for each paint system has done and chose the proper paint system through the structure's life span. Three alternative systems involved bare weathering steel with different levels maintenance are considered as compared with paint systems in previous paint systems study. According to the finding, the use of bare weathering steel with proper periodical maintenance activities can effectively increase the bridge reliability. In Chapter 4, the effectiveness of steel washing is simulated in consideration with different environment conditions. The suitable time frame for bridge washing in coastal environment and urban environment with mild atmospheric concentration are about 1.8 years and 5.5 years respectively. The cost of each maintenance action shows that the use of bare weathering steel with frequent washing can achieve more economic approach against conventional paint. In Myanmar, paint system 1C is commonly used recently. The evaluation of maintenance actions prove that the life cycle cost can be reduced up to ten times when weathering steel is applied with periodical hosting than the application of conventional paint system. Moreover, bare weathering steel washed after every 1.8 years in coastal region worth more cost than paint system 2A. It is noted that use of bare weathering steel in coastal region is still controversial. If the painting system 2A is applied in that region, the maintenance cost could be kept below the cost of weathering steel. However, in compare with paint system 1C, the cost will be still less worth in the use of weathering steel with periodic hosting. The significant effect of reduction in LCC by using WS with regular washing in bridge is presented.

References

Albrecht, P., Coburn, S. ., Wattar, F. ., Tinklenberg, G. ., & Gallagher, W. . (1989). *Guidelines for the use of weathering steel in bridges*.

Bridges, W. S. (n.d.). *A PROPOSAL FOR MAINTENANCE MANUAL OF WEATHERING STEEL BRIDGES Eiki Yamaguchi 1*.

Crampton, D. D., Holloway, K. P., & Fraczek, J. (2013). Assessment of Weathering Steel Bridge Performance in Iowa and Development of Inspection and Maintenance Techniques (Final Report). In *Iowa Department of Transportation Office - Federal Highway Administration*.

Goto, S., Aso, T., & Miyamoto, A. (2008). Development of an advanced inspection system for weathering steel bridges based on digital image recognition. *Bridge Maintenance, Safety, Management, Health Monitoring and Informatics - Proceedings of the 4th International Conference on Bridge Maintenance, Safety and Management*, 349. https://doi.org/10.1201/9781439828434.ch198

Hsu, C. W., Chang, C.C. & Lin, C.J. 2003. A practical guide to support vector classification.

National Cooperative Highway Research Program Report 314, *Guidelines for the use of weathering steel in bridges*, Transportation research board, National research council, 1990.

National Cooperative Highway Research Program Report 272, *Performance of Weathering Steel in Bridges*, Transportation Research Board Executive Committee, 1984.

The Kozai Club (Iron and Steel Mill Products Association) and Japan Association of Steel Bridge Construction. 2001. Application of Weathering Steel to Highway Bridges (Explanation).

Albrecht, P., Coburn, S. ., Wattar, F. ., Tinklenberg, G. ., & Gallagher, W. . (1989). *Guidelines for the use of weathering steel in bridges*.

Albrecht, P., Coburn, S. ., Wattar, F. ., Tinklenberg, G. ., & Gallagher, W. . (1989). *Guidelines for the use of weathering steel in bridges*.

American Society of Civil Engineers & ENO Center of Transportation (2014). Maximizing the Value of Investments using Life Cycle Cost Analysis. Washington,

DC: American Society of Civil Engineers. Retrieved from https://www.enotrans.org/wp-content/uploads/LCCA.pdf

Azizinamini, A., Power, E., Meyers, G., Ozyildirim, H., Kline, E., Whitmore, D., and Mertz, D., (2013). "Design Guide for Bridges for Service Life." Strategic Highway Research Program, Transportation Research Board, SHRP 2 Renewal Project R19A.

D. C. Cook, "Spectroscopic identification of protective and non-protective corrosion coatings on steel structures in marine environments," Corrosion Science, vol. 47, no. 10, pp. 2550–2570, 2005.

FHWA, (2011). "Bridge Preservation Guide – Maintaining a State of Good Repair Using Cost Effective Investment Strategies." FHWA Publication Number: FHWA-HIF-11042.

Albrecht, P., Coburn, S. ., Wattar, F. ., Tinklenberg, G. ., & Gallagher, W. . (1989). *Guidelines for the use of weathering steel in bridges*.

Hawk, H. (2002). Bridge life-cycle cost Analysis, NCHRP Report 483. In *(No. 483) Transportation Research Board*.

Hema, J., Guthrie, W., Fonseca, F., (2004). "Concrete Bridge Deck Condition Assessment and Improvement Strategies." Utah Department of Transportation. Report UT-04-16

Hearn, G., (2012). "Deterioration and Cost Information for Bridge Management." Colorado Department of Transportation. DTD Applied Research and Innovation Branch. Report No. CDOT-2012-4. Final Report.

ISO 12944: Paints and varnishes-Corrosion protection of steel structures by protective paint systems - Part 5: Protective paint systems.

Kage, K. Matsui, and F. Kawabata, "Minimum maintenance steel plates and their application technologies for bridge life cycle cost reduction technologies with environmental safeguards for preserving social infrastructure assets," JFE Technical Report, no. 5, pp. 37–44, 2005.

NYSDOT, (2008). "Fundamentals of Bridge Maintenance and Inspection". New York State Department of Transportation. Office of Transportation Maintenance.

Sobanjo, J., Thompson, P., (2001). "Development of Agency Maintenance, Repair & Rehabilitation (MR&R) Cost Data for Florida's Bridge Management System." Final

Report. Contract No. BB-879. State Maintenance Office. Florida Department of Transportation.

Soliman, M., & Frangopol, D. M. (2015). Life-Cycle Cost Evaluation of Conventional and Corrosion-Resistant Steel for Bridges. Journal of Bridge Engineering, 20(1), 06014005.

Steel, J. F. E., Type, J., & Coat, C. (2005). Minimum Maintenance Steel Plates and Their Application Technologies for Bridge Life Cycle Cost Reduction Technologies with Environmental Safeguards for Preserving Social Infrastructure Assets, *JFE Technical Report*, *5*(5), 37–44.

Stefan L. Leiva Maldonado & Mark D. Bowman, *Life-cycle cost analysis for short and medium-span bridges, Joint transportation research program*, Indiana Department of Transportation and Purdue University, 2019.

The Japan Association of Steel Bridge Construction. Seisakukenky-iinkai. Kokyo no Bosei-to-bosyoku Tokusyu (Kokyo no. 62,63), 2000.

Yanev, B., Richards, G., (2011). "Bridge Maintenance in New York City. Network- and Project-Level Interaction." Transportation Research Record: Journal of the Transportation Research Board, No. 2220. Transportation Research Board of the National Academies, Washington, D.C.

Yu Yu Kyi Win (2017). *Assessment of Corrosion-induced Deterioration and Protection of Structural Steel Elements in Myanmar*. Thesis Submitted in Partial Fulfilment of of the Degree of Doctor of Philosophy in Civil Engineering, Department of Civil Engineering, Yangon Technological University, Yangon, Myanmar.

Chapter 7

SUMMARY AND RECOMMENDATION

7.1 Summary of research outcomes

This research intends to understand the corrosion of structural steels in Myanmar and its effect on structural degradation in bridges. Experimental assessments were performed outdoor and laboratory atmospheres. Future prediction model was formulated based on the time-scaled correlation between field exposure and laboratory tests. A structural degradation of bridge under time varying corrosion losses were examined by approaching probabilistic reliability analysis. Economic analysis of bridge maintenance programs are also discussed based on the bridge maintenance practice at real environment. The study proposes the beneficial use of weathering steel in bridge construction in Myanmar.

In **Chapter 2**, outdoor exposure test results for 3 years period are shown. According to the measurement results, low and medium levels of corrosion were defined at the present exposure sites in Myanmar. The formation of weathering steel patina in outdoor exposure was faster than in shelter. Long-term prediction equations are proposed for future corrosion loss in Myanmar. The behaviors of corrosion in Asia's environment is mainly influenced by temperature and salt concentration. The effects of temperature vary depending on the period of time condensation. Temperature threshold value in Asia's atmosphere is determined as 20°C. Based on nature of atmosphere in Asia, an appropriate dose-response function is approved by varying on sulfur dioxide and temperature factors in ISO 9223 functions which is proposed by previous researcher.

In **Chapter 3**, an accelerated cyclic corrosion test with S6 cycles program with two different salt concentrations were performed to understand the performance of weathering steel (SMA) protective layer formation. The outcomes from the test show that rust layer stabilization of SMA steel is observed at 200 cycles (50 days) in 0.05%

salt solution test. This experiment result declares that the S6 cycles test with diluted salt concentration can simulate weathering steel patina. The accelerated corrosion test was also performed to evaluate the steel coupons under a washing program. The periodical washing with different frequencies were conducted and it showed that steel washing with suitable time frame can reduce corrosion rate.

Chapter 4 is about to find the correlation with accelerated test and corrosion penetration at real environments to determine the time correlation between outdoor and chamber atmosphere. By using this coefficient and amount of flying salt in the test site's atmosphere, the prediction equations were proposed. The optimum frequency of a steel bridge washing period was also calculated Ac and effective time interval of washing inside chamber. The equivalent time for effective bridge washing in real environment was found that regular washing with 1.8 years and 5.5 years interval are needed in coastal and urban environments respectively. Moreover, it can also said that the steel washing can assist for the faster development of protective rust layer of weathering steel than no washing.

The evaluation bridge reliability under corrosion attack was conducted in **Chapter 5** to find out the degradation of bridge performance by understanding the variation of corrosion effects. The finite element analysis results show that the shear capacity decreased more than moment capacity after corrosion was applied. The maximum degradation of shear capacity was occurred at the girder ends and found the maximum flexural stress at the center of span. The system can perform its reliability above the target value specified by AASHTO at the end of service life, however, the individual member reliability index falls under the target value after the 60 years of corrosion intensity. According to the finding, 23% and 42% in moment and shear of the bridge performances were reduced after 100 years of exposure time. The calculation of reliability on system is more economical rather than the member approach.

The benefits of bridge washing was also confirmed by checking the reliability calculation in both wash and no wash scenarios. The performance of bridge under regular wash program show higher value than the target one till the end of predefined service life. In contrast, reliability in serviceability and ultimate shear state without washing maintenance show lower value at 60 years and 80 years respectively. The redundancy was also considered as a parameter which can tolerate by the corrosion effect. The system redundancy indicators in ULS decrease with corrosion propagation. The value decrease from 2.7 in moment and 1.9 in shear at the initial state to 2.4 in

moment and 1.38 in shear at 100 years of service life. The deterministic regarding to SLS also decrease obviously from 1.85 at initial state to 1.38 at 100 years. The calculated values for all systems are above safety margin defined by Moses (1998). Therefore, the studied bridge performed its redundancy very well till the end of bridge service life.

In **Chapter 6**, field measurement results of weathering steel bridge are shown and the results declares that corrosion simulated by the small coupon test may not fully describe the performance in real structure. The corrosion development in studied bridge was more severe than the description by the use of weathering steel bridge guide. The dumping of foreign matter at the girder lower flange cause the dense rust layer at the time of measurement. Further investigation and measurement should be taken to the weathering steel bridge in Myanmar and maintenance will be recommended.

The economic analysis of carbon steel with paint and weathering steel with regular maintenance activities had been carried out. Comparing of costs for different painting systems (as a referenced to past study of painting system in Myanmar) and bare weathering steel with regular washing program, the results show that the cost of weathering steel with wash frequency 1.8 years in costal environment is equivalent to the high quality paint system. By this, it is controversial for using weathering steel in coastal regions. The reducing in expenditures in urban environment with 5.5 years wash interval save enormous amount at 100 years of bridge life. The present study recommend for the use of weathering steel in inland region for life time economic benefits.

7.2 Recommendations for the future research

The corrosion measurements in field exposure site should be extended at the different geographical locations such as mountainous regions and the marine. The prediction equation in the present study considered on the flaying slat and the acceleration coefficients. The future research should be added more environmental parameters. The parametric study of bridge reliability considered on span length and boundary conditions are also recommended for the more reliable results.

The on-site measurement of rust thickness on weathering steel bridge should also be proceeded for the evaluation of rust stabilization in real environment. The author

also provide recommendations on bridge washing practice in the real structure for the maintenance of weathering steel bridge.

APPENDIX

A. Experimental data in Myanmar

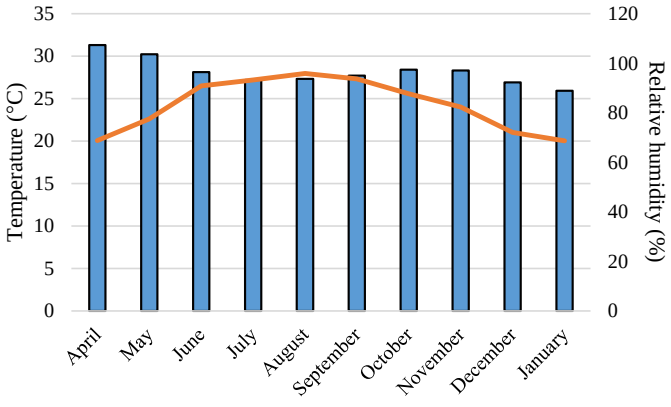

Figure A.1 Temperature and RH in Yangon

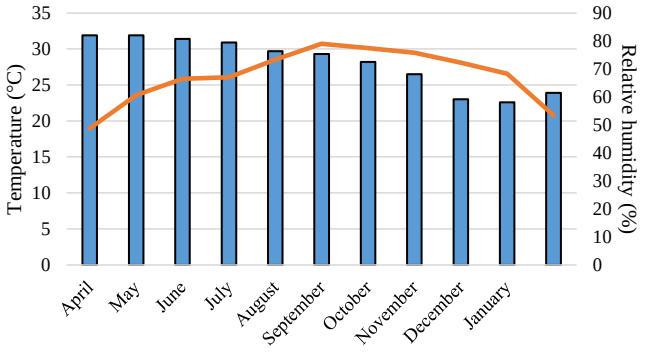

Figure A.2 Temperature and RH in Mandalay

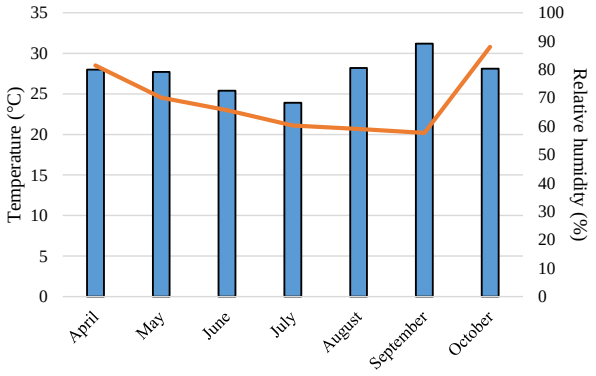

Figure A.3 Temperature and RH in Hinthada

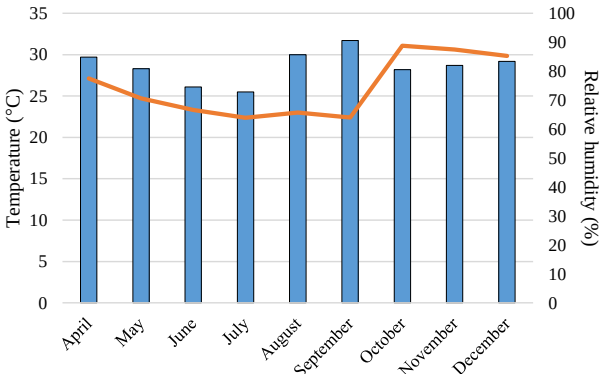

Figure. A.4 Temperature and RH in Pathein

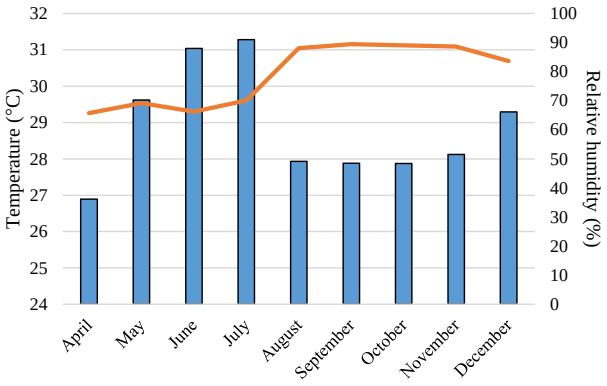

Figure A.5 Temperature and RH in Maubin

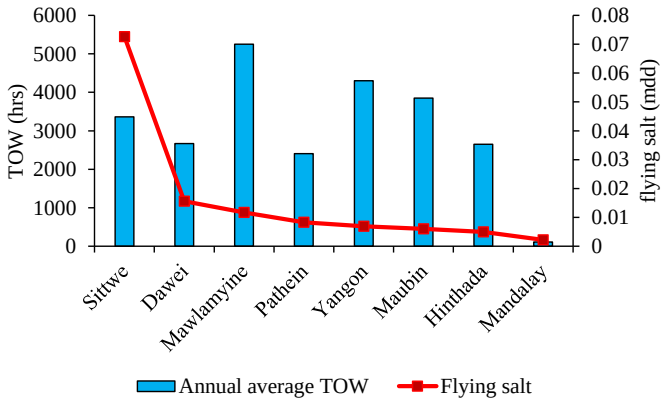

Figure A.6 Time of wetness and flying salt

Table A.1 Measured corrosion data of carbon steel in Myanmar

Carbon Steel / SM													
Mark	Intial weight (g)	Weight after pickling (g)	Corrosion loss (g)	Ave. corrosion loss (g)	Corrosion loss (g/m2)	Ave. corrosion loss (g/m2)	Corrosion depth (μm)	Ave. corrosion depth (μm)	Corrosion rate (mm/y)	Ave. corroison rate (μm/y)	Start date	End date	Site
SM62	39.0417	38.7465	0.2952	0.2905	101.4228	99.79650469	12.9201	12.7129	0.0126	12.4403	8/26/2014	9/3/2015	Sittwe
SM63	39.2181	38.9352	0.2829		97.1968		12.3818		0.0121				
SM64	39.1963	38.9030	0.2933		100.7700		12.8369		0.0126				
SM71	39.3018	39.1400	0.1618	0.1698	55.3752	58.10170554	7.0542	7.4015	0.0069	7.2427	8/28/2014	9/5/2015	Dawei
SM72	39.2903	39.1180	0.1723		58.9687		7.5119		0.0074				
SM73	39.3208	39.1456	0.1752		59.9612		7.6384		0.0075				
S889	38.7999	38.6948	0.1051	0.1099	36.1245	37.7858	4.6018	4.8135	0.0045	4.6976	9/10/2015	9/18/2016	Mawlamyine
S890	38.8163	38.7062	0.1101		37.8430		4.8208		0.0047				
S891	38.7506	38.6360	0.1146		39.3898		5.0178		0.0049				
SM44	39.1769	39.0342	0.1427	0.1387	49.0177	47.63228717	6.2443	6.0678	0.0062	6.0678	3/18/2014	2015/3/18	Yangon
SM45	39.3102	39.1773	0.1329		45.6514		5.8155		0.0058				
SM46	39.2922	39.1518	0.1404		48.2277		6.1437		0.0061				
S892	38.9225	38.8059	0.1166	0.1175	39.9679	40.3348	5.1000	5.2000	0.0051	5.1526	10/13/2015	10/13/2016	Pathein
S893	39.7939	38.6729	0.121		41.5483		5.3000		0.0053				
S894	38.7383	38.6233	0.115		39.4881		5.1000		0.0051				
S937	38.6881	38.56	0.1281	0.1282	44.0930	44.1274	5.6418	5.6462	0.0056	5.6462	10/20/2015	10/19/2016	Maubin
S938	38.423	38.295	0.128		44.0586		5.6374		0.0056				
S939	38.626	38.4975	0.1285		44.2307		5.6594		0.0057				
S916	38.7856	38.6878	0.0978	0.0977	33.6038	33.5808	4.3065	4.30356667	0.0043	4.2918	7/10/2015	7/10/2016	Hinthada
S917	38.9688	38.8712	0.0976		33.5350		4.2977		0.0043				
S918	38.7589	38.6611	0.0978		33.6038		4.3065		0.0043				
SM53	38.9359	38.8735	0.0624	0.0567	21.4305	19.47294801	2.7300	2.4806	0.0027	2.4874	3/20/2014	2015/3/19	Mandalay
SM54	38.9071	38.8518	0.0553		18.9921		2.4194		0.0024				
SM55	39.0877	39.0353	0.0524		17.9962		2.2925		0.0023				

Table A.2 Measured corrosion data of weathering steel in Myanmar

Weathering Steel / SMA													
Mark	Intial weight (g)	Weight after pickling (g)	Corrosion loss (g)	Ave. corrosion loss (g)	Corrosion loss (g/m2)	Ave. corrosion loss (g/m2)	Corrosion depth (μm)	Ave. corrosion depth (μm)	Corrosion rate (mm/y)	Ave. corroison rate (μm/y)	Start date	End date	Site
A59	38.997	38.688	0.3090	0.3143	106.1378	107.9697	13.5207	13.7541	0.0132	13.4591	8/26/2014	9/3/2015	Sittwe
A60	38.648	38.337	0.3110		106.8247		13.6082		0.0133				
A61	38.947	38.624	0.3230		110.9466		14.1333		0.0138				
A68	38.649	38.492	0.1570	0.1657	53.9558	56.934269	6.8734	7.2528	0.0067	7.0972	8/28/2014	9/5/2015	Dawei
A69	38.613	38.446	0.1670		57.3925		7.3111		0.0072				
A70	38.692	38.519	0.1730		59.4545		7.5738		0.0074				
A1160	38.216	38.091	0.1250	0.1210	42.9298	41.5560	5.4688	5.2938	0.0053	5.1664	9/10/2015	9/18/2016	Mawlamyine
A1161	38.214	38.098	0.1160		39.8388		5.0750		0.0050				
A1162	38.135	38.013	0.1220		41.8995		5.3375		0.0052				
A041	39.187	39.044	0.1430	0.1493	49.1208	51.2963	6.2574	6.5346	0.0063	6.5346	3/18/2014	2015/3/18	Yangon
A042	39.112	38.962	0.1500		51.5253		6.5637		0.0066				
A043	39.112	38.957	0.1550		53.2428		6.7825		0.0068				
A1163	38.247	38.119	0.1283	0.1190	43.9784	40.8246	5.6023	5.2006	0.0056	5.1864	10/13/2015	10/13/2016	Pathein
A1164	38.285	38.163	0.1217		41.7887		5.3234		0.0053				
A1165	37.990	37.883	0.1069		36.7067		4.6760		0.0047				
A1208	38.5383	38.3944	0.1439	0.144633	49.5315	49.7839	6.336	6.368433	0.0063	6.3684	10/20/2015	10/19/2016	Maubin
A1209	38.4445	38.2981	0.1464		50.3920		6.4461		0.0064				
A1210	38.6532	38.5096	0.1436		49.4282		6.3232		0.0063				
A1187	38.2205	38.115	0.1055	0.106833	36.2494	36.7076	4.6564	4.715267	0.0046	4.7024	7/10/2015	7/10/2016	Hinthada
A1188	38.1268	38.0164	0.1104		37.9331		4.8727		0.0049				
A1189	37.9859	37.8813	0.1046		35.9402		4.6167		0.0046				
A050	39.376	39.325	0.0510	0.0447	17.4817	15.310742	2.2270	1.9504	0.0022	1.9558	3/20/2014	2015/3/19	Mandalay
A051	39.214	39.173	0.0410		14.0539		1.7903		0.0018				
A052	39.143	39.101	0.0420		14.3967		1.8340		0.0018				

B. Corrosion severity map

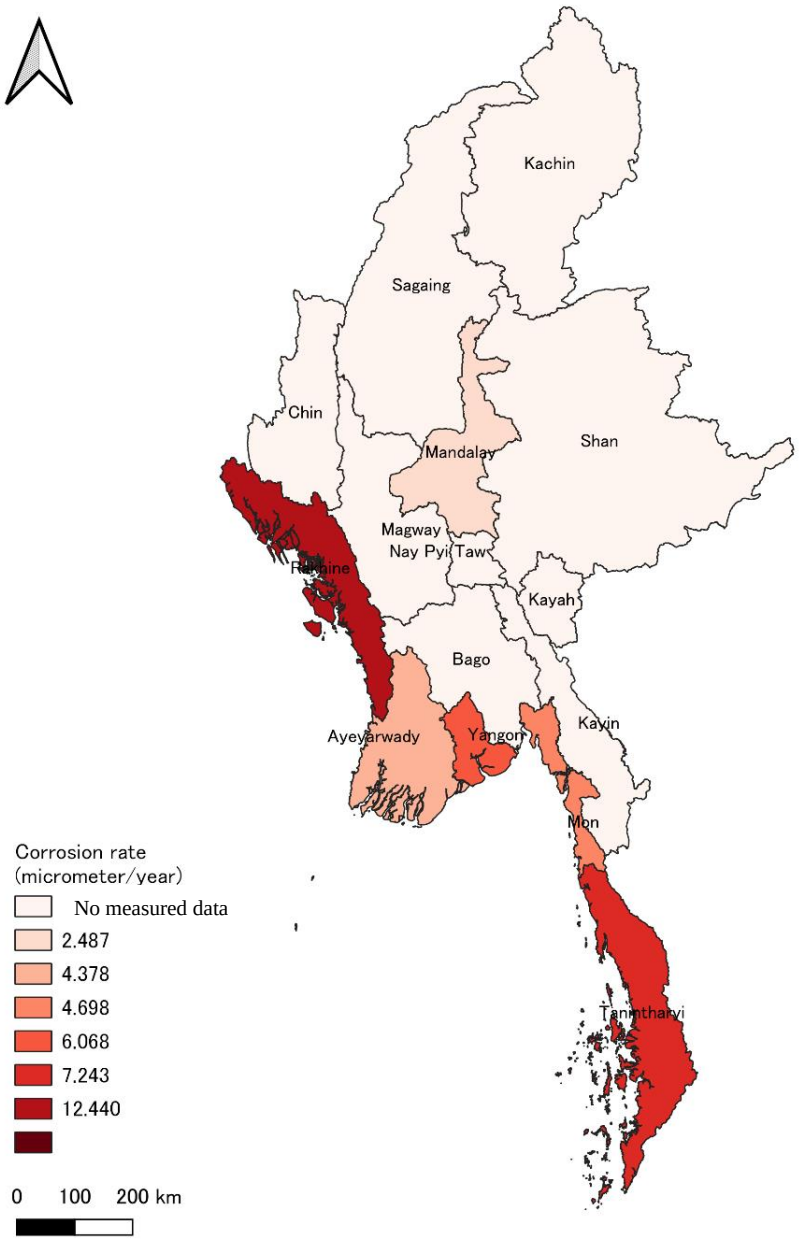

Figure B.1 Visual presentation of corrosion severity in Myanmar

C. Referenced data in Asia and calculated Ac

Table C.1 References data in Japan

Prefecture	Corrosion rate		T	RH	TOW	SO_2	CL^-	Corrosion rate Japan
	$g/m^2/year$	µm/year	(°C)	(%)	h/year	$mg/m^2/day$	$mg/m^2/day$	Ac
Asahikawa	127.7	16.2	6.9	77	3658	3.12	0.56	127.41
Kushiro	272.5	34.7	6.6	75	3359	1095	18.02	59.48
Sapporo	155.9	19.8	9.1	68	2635	7.7	13.65	104.24
Akita	252.1	32.1	12.1	73	3744	4.05	51.01	64.30
Yamagata	137	17.4	12	75	4093	2.32	2.5	118.62
Niigata	200.5	25.5	14.2	69	3194	4.92	24.8	80.94
Takaoa	221.3	28.2	14.4	73	3887	3.3	8.98	73.19
Kyoto	114.6	14.6	16.3	63	2363	3.82	3.82	141.37
Yonago	203.4	25.9	15.5	72	3632	2.74	12.53	79.69
Morioka	135	17.2	10.4	72	3233	2.16	6.1	120.00
Sendai	177.4	22.6	12.5	72	3402	1.72	3.79	91.33
Tsukuba	176.8	22.5	15.9	76	4370	3.22	1.23	91.73
Choshi	316.2	40.2	14.4	78	4629	4.6	14.96	51.34
Tokyo	147.6	18.8	16.6	59	1841	6.03	4.13	109.79
Yamanakako	146.3	18.6	11.1	72	3402	2.01	0.91	110.97
Shimizu	247.9	31.5	16.9	69	2758	5.15	2.46	65.52
Kariya	150.5	19.1	16.3	66	2654	4	3.94	108.06
Izumi	160.4	20.4	17.4	63	2411	3.43	2.69	101.18
Kochi	194.8	24.8	17.5	68	3020	5.34	3.68	83.23
Fukuyama	159.1	202	15.9	69	3284	4.45	1.14	10.22
Omura	160.5	20.4	17.5	68	3020	3.7	8.02	101.18
Hayato-Cho	217.7	27.7	18.9	67	3020	3.7	2.79	74.51
Nishibara-Machi	376.6	47.9	23.2	70	3444	2.83	23.46	43.09
Miyakochima	981.9	124.9	23.7	79	5409	3.29	34.4	16.53
Miyakochima kaigan	3221.2	409.8	23.7	79	5409	15.68	113.05	5.04

Table C.2 References data in Vietnam

Prefecture	Corrosion rate		T	RH	TOW	CL^-	Exposure	Corrosion rate Vietnam
Province	g/m^2/year	µm/year	(°C)	(%)	h/year	mg/m^2/day	Test	Ac
Hanoi	240.36	30.6	24.1	81.3	4697	0.64	1995	67.45
Do Son	290.7	37	23.6	86.1	6359	30.5	1995	55.78
Da Nang	264.64	33.7	25.9	83.1	5672	3.08	1995	61.25
Nha Trang	254.23	32.3	26.7	80.8	4651	19.3	1995	63.90
HCM City	191.92	24.4	27.7	75.6	4205	1.22	1995	84.59
Vong Tau	191.23	24.3	27.5	79.3	4495	13.58	1995	84.94
Son Tay	287.74	36.9	23.4	86.3	6451	0.56	1995	55.93
Do Son	297.74	37.9	23.3	86.1	6081	17.51	2003	54.46
Hai Duong	287.52	36.6	23.5	85.9	6226	6.89	2003	56.39
Hanoi	249.71	31.8	24.1	79.8	4917	2.24	2003	64.91
Thanh Hoa	242.95	30.9	23.9	84.7	6158	3.48	2003	66.80
Quang Ninh	255.76	32.5	24.8	82.6	5604	10.28	2003	63.51
Hue	247.567	31.5	24.6	85.89	6001	1.33	2003	65.52
Da Nang	264.65	33.7	25.8	83.3	5701	4.99	2003	61.25
HCM City	190.53	24.2	27.7	75.6	4205	4.58	2003	85.29
Vong Tau	205.77	26.2	27.4	79.4	4400	16.5	2003	78.78
Tieng Giang	166.05	21.1	27	81	5086	8.9	2002	97.82
Tieng Gaing	186.35	23.7	27	83	5543	8.9	2002	87.09
Hanoi	181.85	23.1	24.7	79	4661	1.8	2002	89.35
Hanoi	226.75	28.8	24.5	78	4435	1.76	2005	71.67
CHM city	163.65	20.8	28.3	74	3467	3.06	2002	99.23
CHM city	138.75	17.7	28	77	4157	2.66	2005	116.61

Table C.3 Measured data in Myanmar

Prefecture	Corrosion rate	T	RH	TOW	SO_2	CL^-	Myanmar
	µm/year	(°C)	(%)	h/year	mg/m^2/day	mg/m^2/day	Ac
Yangon	15.5	30	89.2	5183	2.41	3.7	133.1613
Mandalay	8.92	32	75	1175	2.4	1.2	231.3901
Mawlamyine	17.2	27.7	92	5253	–	1.89	120